

CHAPTER 5

SENSORLESS CONTROLLER DESIGN FOR THE NINE-PHASE IPM

5.1 Introduction

In this chapter a controller is designed for the nine-phase IPM machine. The controller is designed based on the main component of the machine circuit. After modelling the nine phase converter the controller is designed using the minimum copper loss strategy. The current regulators are also designed using the regular dynamic equations of the machine in the rotor reference frame. To implement the precise control to the machine the rotor position is needed, therefore the position estimation method is presented in the following sections of this chapter. The position estimation presented in this chapter, is based on the high frequency injection method. In this method a high frequency voltage is injected to a non-torque producing channel of the machine and the position of the rotor is extracted from the high frequency currents due to the high frequency voltages. The general form of the high frequency currents is obtained using the harmonic balance technique and the essential signal processing method is presented to extract the position data from the currents. The presentation of the new position estimation method based on the high frequency voltage injection in the non-torque producing channel of the machine in stationary reference frame is the novel part of this chapter. The controller is simulated and tested using the full order model of the machine that was generated in the chapter 3. After confirming the performance of the controller and estimator with MATLAB simulation the controller and estimator are discretized and translated to C++ language to be implemented in DSP. Finally, the performance of the method is verified with experimental results. The steady state analyses of the machine are also presented in this

chapter in which the nine phase machine capability is obtained for different operation modes using FEMM.

5.2 Controller Design

In this section a speed controller is designed for the nine-phase IPM machine. The controller is based on minimum copper loss strategy. After deriving the equations of the nine-phase inverter in the rotor reference frame the controller equations are derived for the fundamental components of the machine.

5.2.1 Converter Model

The nine-phase converter is shown in the Figure 5.1.

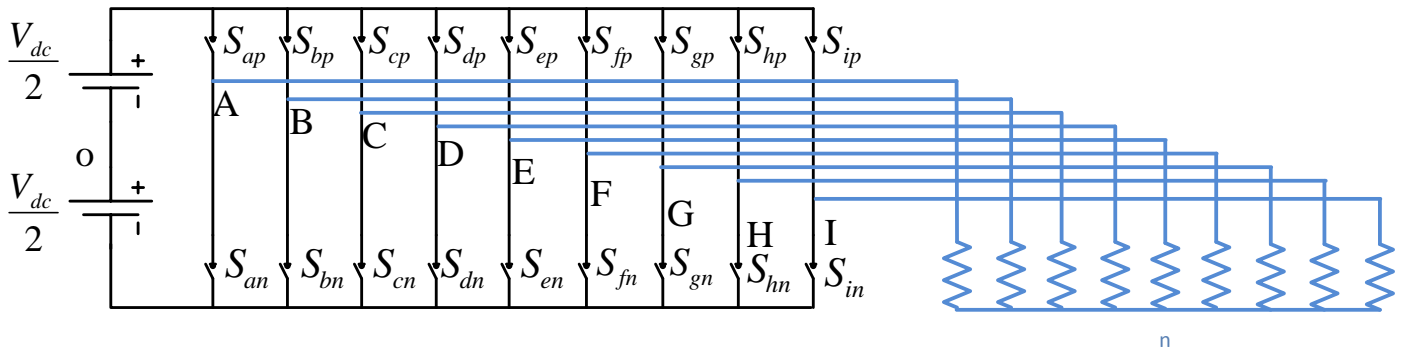


Figure 5.1: The nine phase inverter.

The switches of each leg of the inverter are complementary therefore:

$$\begin{aligned}
S_{ap} + S_{an} &= 1 \\
S_{bp} + S_{bn} &= 1 \\
S_{cp} + S_{cn} &= 1 \\
S_{dp} + S_{dn} &= 1 \\
S_{ep} + S_{en} &= 1 \\
S_{fp} + S_{fn} &= 1 \\
S_{gp} + S_{gn} &= 1 \\
S_{hp} + S_{hn} &= 1 \\
S_{ip} + S_{in} &= 1
\end{aligned} \tag{5.1}$$

Where: ‘ S_{xp} ’ and ‘ S_{xn} ’ are the switching functions of the top and bottom switches of leg ‘x’ of the inverter. Also output voltages of the inverter can be expressed as:

$$\begin{aligned}
V_{AO} &= \frac{V_{dc}}{2}(S_{ap} - S_{an}) & V_{DO} &= \frac{V_{dc}}{2}(S_{dp} - S_{dn}) & V_{GO} &= \frac{V_{dc}}{2}(S_{gp} - S_{gn}) \\
V_{BO} &= \frac{V_{dc}}{2}(S_{bp} - S_{bn}) & V_{EO} &= \frac{V_{dc}}{2}(S_{ep} - S_{en}) & V_{HO} &= \frac{V_{dc}}{2}(S_{hp} - S_{hn}), \\
V_{CO} &= \frac{V_{dc}}{2}(S_{cp} - S_{cn}) & V_{FO} &= \frac{V_{dc}}{2}(S_{fp} - S_{fn}) & V_{IO} &= \frac{V_{dc}}{2}(S_{ip} - S_{in})
\end{aligned} \tag{5.2}$$

$$V_{dc} = 200V$$

Using equation (5.1), the voltage equations can be rewritten as:

$$\begin{aligned}
V_{AO} &= \frac{V_{dc}}{2}(2S_{ap} - 1) & V_{DO} &= \frac{V_{dc}}{2}(2S_{dp} - 1) & V_{GO} &= \frac{V_{dc}}{2}(2S_{gp} - 1) \\
V_{BO} &= \frac{V_{dc}}{2}(2S_{bp} - 1) & V_{EO} &= \frac{V_{dc}}{2}(2S_{ep} - 1) & V_{HO} &= \frac{V_{dc}}{2}(2S_{hp} - 1) \\
V_{CO} &= \frac{V_{dc}}{2}(2S_{cp} - 1) & V_{FO} &= \frac{V_{dc}}{2}(2S_{fp} - 1) & V_{IO} &= \frac{V_{dc}}{2}(2S_{ip} - 1)
\end{aligned} \tag{5.3}$$

Where: the switching function of the top switch of each phase ‘ S_{xp} ’ and the expression for the modulation index can be written as:

$$S_{xp} = 0.5(1 + M_{xp}), \quad x = a, b, c, d, e, f, g, h, i \quad (5.4)$$

$$M_{xp} = \frac{2(V_{xp} + V_{no})}{V_{dc}}, \quad V_{no} = \frac{V_{dc}}{2}(1 - 2\alpha) - \alpha V_{\min} - (1 - \alpha)V_{\max}$$

Where: ' V_{xp} ' presents the reference voltage for phase 'x', ' V_{\min} ' is the minimum value of the nine phase set, ' V_{\max} ' is the maximum value of the nine phase set and ' α ' is also given in equation (5.5).

$$\alpha = \frac{1}{2}[1 + \text{sgn}[\cos(9\omega_s t + \delta)]] \quad (5.5)$$

Where ' ω_s ' is the frequency of the command voltages and ' δ ' is the initial angle of the modulation index.

Substituting the switching function of equation (5.4) in to the voltages of equation (5.3) results in equation (5.6).

$$\begin{aligned}
V_{An} &= V_{dc} \frac{M_a}{2} \\
V_{Bn} &= V_{dc} \frac{M_b}{2} \\
V_{Cn} &= V_{dc} \frac{M_c}{2} \\
V_{Dn} &= V_{dc} \frac{M_d}{2} \\
V_{En} &= V_{dc} \frac{M_e}{2} \\
V_{Fn} &= V_{dc} \frac{M_f}{2} \\
V_{Gn} &= V_{dc} \frac{M_g}{2} \\
V_{Hn} &= V_{dc} \frac{M_h}{2} \\
V_{In} &= V_{dc} \frac{M_i}{2}
\end{aligned} \tag{5.6}$$

Since the machine is controlled in the rotor reference frame the inverter, voltages also should be transformed to the rotor reference frame.

$$\begin{bmatrix} V_{q1} \\ V_{d1} \\ V_{q3} \\ V_{d3} \\ V_{q5} \\ V_{d5} \\ V_{q7} \\ V_{d7} \\ V_o \end{bmatrix} = \tag{5.7}$$

$$\frac{V_{dc}}{9} \begin{bmatrix} c(\theta) & c(\theta - \alpha) & c(\theta - 2\alpha) & c(\theta - 3\alpha) & c(\theta - 4\alpha) & c(\theta - 5\alpha) & c(\theta - 6\alpha) & c(\theta - 7\alpha) & c(\theta - 8\alpha) \\ s(\theta) & s(\theta - \alpha) & s(\theta - 2\alpha) & s(\theta - 3\alpha) & s(\theta - 4\alpha) & s(\theta - 5\alpha) & s(\theta - 6\alpha) & s(\theta - 7\alpha) & s(\theta - 8\alpha) \\ c(3\theta) & c3(\theta - \alpha) & c3(\theta - 2\alpha) & c3(\theta - 3\alpha) & c3(\theta - 4\alpha) & c3(\theta - 5\alpha) & c3(\theta - 6\alpha) & c3(\theta - 7\alpha) & c3(\theta - 8\alpha) \\ s(3\theta) & s3(\theta - \alpha) & s3(\theta - 2\alpha) & s3(\theta - 3\alpha) & s3(\theta - 4\alpha) & s3(\theta - 5\alpha) & s3(\theta - 6\alpha) & s3(\theta - 7\alpha) & s3(\theta - 8\alpha) \\ c(5\theta) & c5(\theta - \alpha) & c5(\theta - 2\alpha) & c5(\theta - 3\alpha) & c5(\theta - 4\alpha) & c5(\theta - 5\alpha) & c5(\theta - 6\alpha) & c5(\theta - 7\alpha) & c5(\theta - 8\alpha) \\ s(5\theta) & s5(\theta - \alpha) & s5(\theta - 2\alpha) & s5(\theta - 3\alpha) & s5(\theta - 4\alpha) & s5(\theta - 5\alpha) & s5(\theta - 6\alpha) & s5(\theta - 7\alpha) & s5(\theta - 8\alpha) \\ c(7\theta) & c7(\theta - \alpha) & c7(\theta - 2\alpha) & c7(\theta - 3\alpha) & c7(\theta - 4\alpha) & c7(\theta - 5\alpha) & c7(\theta - 6\alpha) & c7(\theta - 7\alpha) & c7(\theta - 8\alpha) \\ s(7\theta) & s7(\theta - \alpha) & s7(\theta - 2\alpha) & s7(\theta - 3\alpha) & s7(\theta - 4\alpha) & s7(\theta - 5\alpha) & s7(\theta - 6\alpha) & s7(\theta - 7\alpha) & s7(\theta - 8\alpha) \\ 1/2 & 1/2 & 1/2 & 1/2 & 1/2 & 1/2 & 1/2 & 1/2 & 1/2 \end{bmatrix} \begin{bmatrix} M_{ap} \\ M_{bp} \\ M_{cp} \\ M_{dp} \\ M_{ep} \\ M_{fp} \\ M_{gp} \\ M_{hp} \\ M_{ip} \end{bmatrix}$$

, $\alpha = \frac{2\pi}{9}$, $S = \sin$, $C = \cos$, $\theta = \text{reference angle}$

Equation (5.7) can be represented as equation (5.8).

$$\begin{bmatrix} V_{q1} \\ V_{d1} \\ V_{q3} \\ V_{d3} \\ V_{q5} \\ V_{d5} \\ V_{q7} \\ V_{d7} \\ V_o \end{bmatrix} = V_{dc} \begin{bmatrix} M_{q1} \\ M_{d1} \\ M_{q3} \\ M_{d3} \\ M_{q5} \\ M_{d5} \\ M_{q7} \\ M_{d7} \\ M_o \end{bmatrix} \quad (5.8)$$

Where:

$$\begin{bmatrix} M_{q1} \\ M_{d1} \\ M_{q3} \\ M_{d3} \\ M_{q5} \\ M_{d5} \\ M_{q7} \\ M_{d7} \\ M_o \end{bmatrix} = \frac{2}{9} \begin{bmatrix} c(\theta) & c(\theta - \alpha) & c(\theta - 2\alpha) & c(\theta - 3\alpha) & c(\theta - 4\alpha) & c(\theta - 5\alpha) & c(\theta - 6\alpha) & c(\theta - 7\alpha) & c(\theta - 8\alpha) \\ s(\theta) & s(\theta - \alpha) & s(\theta - 2\alpha) & s(\theta - 3\alpha) & s(\theta - 4\alpha) & s(\theta - 5\alpha) & s(\theta - 6\alpha) & s(\theta - 7\alpha) & s(\theta - 8\alpha) \\ c(3\theta) & c3(\theta - \alpha) & c3(\theta - 2\alpha) & c3(\theta - 3\alpha) & c3(\theta - 4\alpha) & c3(\theta - 5\alpha) & c3(\theta - 6\alpha) & c3(\theta - 7\alpha) & c3(\theta - 8\alpha) \\ s(3\theta) & s3(\theta - \alpha) & s3(\theta - 2\alpha) & s3(\theta - 3\alpha) & s3(\theta - 4\alpha) & s3(\theta - 5\alpha) & s3(\theta - 6\alpha) & s3(\theta - 7\alpha) & s3(\theta - 8\alpha) \\ c(5\theta) & c5(\theta - \alpha) & c5(\theta - 2\alpha) & c5(\theta - 3\alpha) & c5(\theta - 4\alpha) & c5(\theta - 5\alpha) & c5(\theta - 6\alpha) & c5(\theta - 7\alpha) & c5(\theta - 8\alpha) \\ s(5\theta) & s5(\theta - \alpha) & s5(\theta - 2\alpha) & s5(\theta - 3\alpha) & s5(\theta - 4\alpha) & s5(\theta - 5\alpha) & s5(\theta - 6\alpha) & s5(\theta - 7\alpha) & s5(\theta - 8\alpha) \\ c(7\theta) & c7(\theta - \alpha) & c7(\theta - 2\alpha) & c7(\theta - 3\alpha) & c7(\theta - 4\alpha) & c7(\theta - 5\alpha) & c7(\theta - 6\alpha) & c7(\theta - 7\alpha) & c7(\theta - 8\alpha) \\ s(7\theta) & s7(\theta - \alpha) & s7(\theta - 2\alpha) & s7(\theta - 3\alpha) & s7(\theta - 4\alpha) & s7(\theta - 5\alpha) & s7(\theta - 6\alpha) & s7(\theta - 7\alpha) & s7(\theta - 8\alpha) \\ 1/2 & 1/2 & 1/2 & 1/2 & 1/2 & 1/2 & 1/2 & 1/2 & 1/2 \end{bmatrix} \begin{bmatrix} M_{ap} \\ M_{bp} \\ M_{cp} \\ M_{dp} \\ M_{ep} \\ M_{fp} \\ M_{gp} \\ M_{hp} \\ M_{ip} \end{bmatrix} \quad (5.9)$$

$\alpha = \frac{2\pi}{9}$, $S = \sin$, $C = \cos$, $\theta = \text{rotor angle}$

5.2.2 Controller Design

In this section, relationship between the reference currents of the q and d axis is generated. The q axis current reference can be generated from the speed controller loop and the resulting current can be used to generate the d axis current. The desired d axis reference current is generated based on the minimum copper loss strategy that is derived using Lagrange optimization method. The proper relationship between q and d axis current can be derived based on the machine equations in the rotor reference frame. From chapter 3 the machine equations for the salient pole (IPM) in the steady state conditions are:

$$\begin{aligned} V_{q1r} &= r_s i_{q1r} + \omega_r (\lambda_{d1r}) \\ V_{d1r} &= r_s i_{d1r} - \omega_r (\lambda_{q1r}) \end{aligned} \quad (5.10)$$

To obtain the simpler form of the machine equations, the d axis of the rotor reference frame can be aligned to the flux linkage of the rotor permanent magnets. After alignment, the flux linkages of the machine in the rotor reference frame could be presented as:

$$\begin{aligned} \lambda_{d1r} &= L_{d1d1} i_{d1r} + \lambda_{pmd1r} \\ \lambda_{q1r} &= L_{q1q1} i_{q1r} \end{aligned} \quad (5.11)$$

Where ‘ L_{d1d1} ’ and ‘ L_{q1q1} ’ are the stator inductances of the q and d axis in the rotor reference frame respectively. And ‘ λ_{pmd1r} ’ is the magnetic flux linkage of the permanent magnet bars of the rotor in the d axis of the rotor reference frame. The electromagnetic torque also is presented in equation (5.12).

$$T_e = \frac{9P}{4} [(L_{q1q1} - L_{d1d1}) i_{q1r} i_{d1r} + i_{q1r} \lambda_{pmd1r}] \quad (5.12)$$

The stator copper loss can be defined as:

$$P_{loss} = \frac{9}{4} r_s (i_{d1r}^2 + i_{q1r}^2) \quad (5.13)$$

To obtain the minimum loss, the minimum point of the equation (5.13) should be found while the electromagnetic torque is equal to the load torque according to equation (5.14).

$$T_L - \frac{9P}{4} [(L_{q1q1} - L_{d1d1})i_{q1r}i_{d1r} + i_{q1r}\lambda_{pmd1r}] = 0 \quad (5.14)$$

Therefor the Lagrange function can be defined as equation (5.15). In this equation ‘ λ ’ is the Lagrange multiplier [158]:

$$L = \frac{9}{4} r_s (i_{d1r}^2 + i_{q1r}^2) + \lambda \left(T_L - \frac{9P}{4} [(L_{q1q1} - L_{d1d1})i_{q1r}i_{d1r} + i_{q1r}\lambda_{pmd1r}] \right) \quad (5.15)$$

Now the essential conditions for the controller can be obtained from the equations (5.16) to (5.17). Note that: the common solutions for the Lagrange derivations show the minimum point of the copper loss.

$$\frac{dL}{di_{d1r}} = \frac{9}{2} r_s (i_{d1r}) + \lambda \left(-\frac{9P}{4} (L_{q1q1} - L_{d1d1})i_{q1r} \right) = 0 \quad (5.16)$$

$$\frac{dL}{di_{q1r}} = \frac{9}{2} r_s (i_{q1r}) + \lambda \left(-\frac{9P}{4} [(L_{q1q1} - L_{d1d1})i_{d1r} + \lambda_{pmd1r}] \right) = 0 \quad (5.17)$$

$$\frac{dL}{d\lambda} = T_L - \frac{9P}{4} [(L_{q1q1} - L_{d1d1})i_{q1r}i_{d1r} + i_{q1r}\lambda_{pmd1r}] = 0 \quad (5.18)$$

From the equations (5.16) and (5.17) the relationship for the q and d axis currents can be derived as:

$$\lambda = \frac{i_{d1r}}{(L_{q1q1} - L_{d1d1})i_{q1r}} = \frac{i_{q1r}}{[(L_{q1q1} - L_{d1d1})i_{d1r} + \lambda_{pmd1r}]} \quad (5.19)$$

Equation (5.19) results in:

$$(L_{q1q1} - L_{d1d1})i_{d1r}^2 + \lambda_{pmd1r}i_{d1r} - (L_{q1q1} - L_{d1d1})i_{q1r}^2 = 0 \quad (5.20)$$

The equation (5.20) is representing an ellipse. Using MATLAB/EZPLOT the ellipse could be plotted as Figure 5.2.

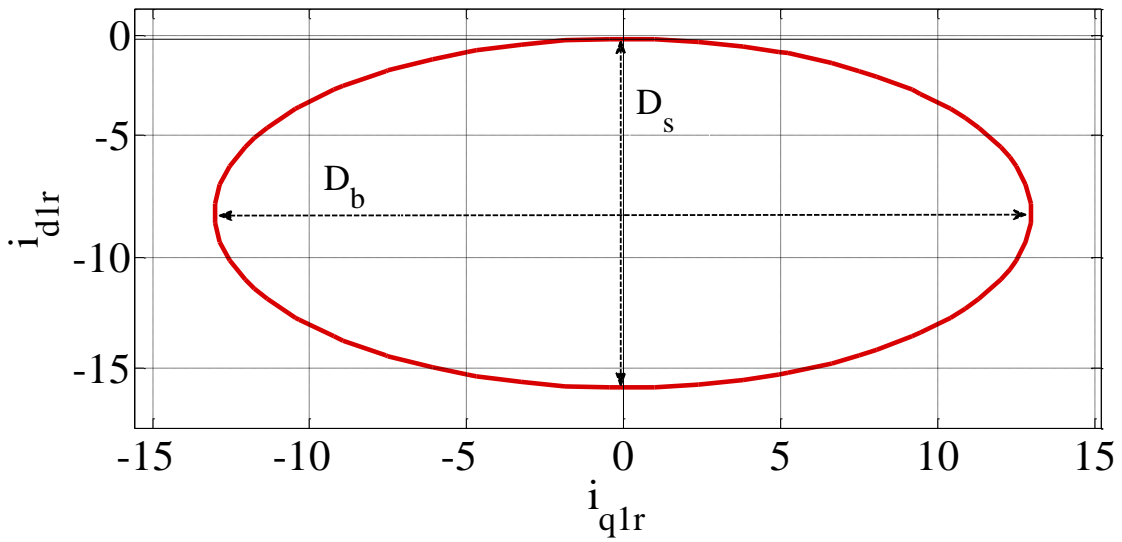


Figure 5.2: The plot of the ellipse representing the q and d axis current relationship.

The smaller and bigger diameters and also the central point of the ellipse are represented in the equations (5.21), (5.22) and (5.23) respectively.

$$D_s = \frac{\lambda_{pmd1r}}{(L_{q1q1} - L_{d1d1})} \quad (5.21)$$

$$D_b = \frac{2\sqrt{2}\lambda_{pmd1r}}{(L_{q1q1} - L_{d1d1})} \quad (5.22)$$

$$(i_{d1r}, i_{q1r})_{center} = \left(\frac{\lambda_{pmd1r}}{2(L_{q1q1} - L_{d1d1})}, 0 \right) \quad (5.23)$$

The equation (5.20) could be considered as a quadratic equation in terms of ‘ i_{d1r} ’. From this equation the d axis current can be calculated from q axis current. This equation shows the condition between the q and d axis currents in which the copper loss is minimized.

$$i_{d1r} = \frac{-\frac{\lambda_{pmd1r}}{(L_{d1d1} - L_{q1q1})} \pm \sqrt{\frac{\lambda_{pmd1r}^2}{(L_{d1d1} - L_{q1q1})^2} + 4i_{q1r}^2}}{2} \quad (5.24)$$

5.2.3 Speed Controller Design

The speed controller loop can be designed using the mechanical dynamic equation which relates the rotor speed to the electromagnetic and load torque. The mechanical dynamic equation is shown in the equation (5.25).

$$T_e = J \left(\frac{2}{P} \right) p \omega_r + T_L \quad (5.25)$$

From this equation, the derivation of the rotor speed is:

$$J \left(\frac{2}{P} \right) p \omega_r = T_e - T_L = \delta_{\omega_r} = K_{\omega_r}(S) (\omega_r^* - \omega_r) \quad (5.26)$$

The speed controller loop is also shown in the Figure 5.3. It can be seen that the PI controller ($K_{\omega_r}(S)$) is operating on the error between the reference (ω_r^*) and the rotor (ω_r) speeds.

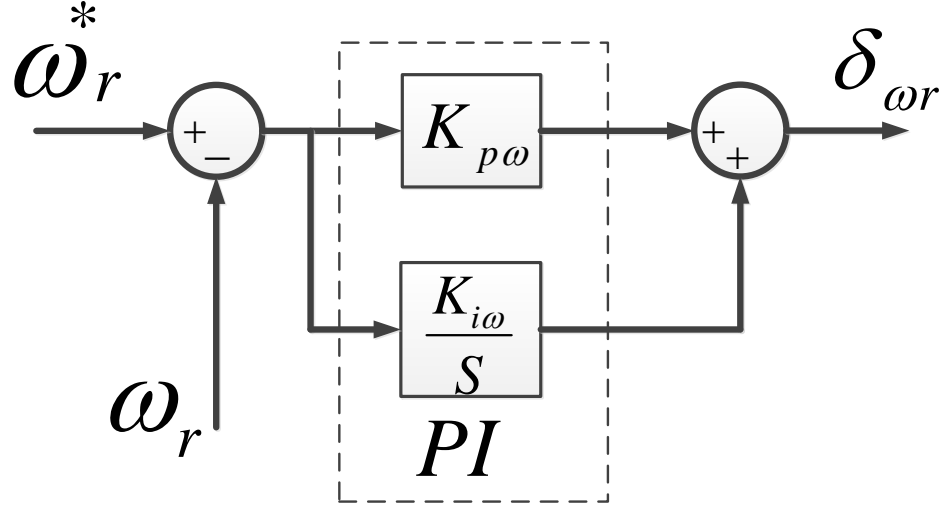


Figure 5.3: The speed controller loop.

Substituting the electromagnetic torque to the equation (5.26) results in:

$$T_e = \delta_{\omega r} + T_L \rightarrow \frac{9P}{4} [(L_{q1q1} - L_{d1d1})i_{q1r}i_{d1r} + i_{q1r}\lambda_{pmd1r}] = \delta_{\omega r} + T_L \quad (5.27)$$

The last equation can be solved with the equation (5.24) to obtain the reference value for the q axis current according to equation (5.28). By solving the equation (5.28), the equation (5.29) can be derived which can be used for generating the reference value for the q axis current. By substituting the reference of the q axis current in to the equation (5.24) the reference value for the d axis current also can be calculated.

$$\left\{ \begin{array}{l} \frac{9P}{4} [(L_{q1q1} - L_{d1d1})i_{q1r}i_{d1r} + i_{q1r}\lambda_{pmd1r}] = \delta_{\omega r} + T_L \\ i_{d1r} = \frac{-\frac{\lambda_{pmd1r}}{(L_{d1d1} - L_{q1q1})} \pm \sqrt{\frac{\lambda_{pmd1r}^2}{(L_{d1d1} - L_{q1q1})^2} + 4i_{q1r}^2}}{2} \end{array} \right. \quad (5.28)$$

$$(L_{q1q1} - L_{d1d1})^2 i_{q1r}^4 + \frac{4}{9P} (\delta_\omega + T_L) \lambda_{pmd1r} I_{q1r} - \left(\frac{4}{9P} (\delta_\omega + T_L) \right)^2 = 0 \quad (5.29)$$

The PI controller for the speed controller loop can be designed using the mechanical dynamic equation as:

$$p\omega_r = \left(K_{p\omega} + \frac{K_{i\omega}}{S} \right) (\omega_r^* - \omega_r) \quad (5.30)$$

The above equation results in:

$$\frac{\omega_r}{\omega_r^*} = \frac{SK_{p\omega} + K_{i\omega}}{S^2 + K_{p\omega}S + K_{i\omega}} \quad (5.31)$$

By setting the denominator of the transfer function to be equal to the second order Butterworth polynomial the controller coefficients can be designed [161].

$$S^2 + K_{p\omega}S + K_{i\omega} = p^2 + \sqrt{2}p\omega_o + \omega_o \quad (5.32)$$

The speed controller loop has to be at least 10 times faster than the desired rotor speed profile [157]. The final desired speed profile is a trapezoidal waveform that has the frequency of up to 0.05 (Hz). Therefore, the frequency of the speed controller loop has to be selected bigger than 0.5 (Hz). Setting $\omega_o = 7$ the correspondent relationship between the denominator of the transfer function and the Butterworth polynomial yields:

$$K_{p\omega} = \sqrt{2}\omega_o = 7\sqrt{2} \quad (5.33)$$

$$K_{i\omega} = \omega_o^2 = 98 \quad (5.34)$$

5.2.4 Current Regulator Design

Using the dynamic equations of the q and d axis voltages in the rotor reference frame, the current regulators for controlling the ‘ i_{q1r} ’ and ‘ i_{d1r} ’ can be designed. The equations are repeated here from chapter 3.

$$V_{q1r} = r_s i_{q1r} + pL_{q1q1} i_{q1r} - \omega_r L_{d1d1} i_{d1r} - \omega_r \lambda_{pmd1r} \quad (5.35)$$

$$V_{d1r} = r_s i_{d1r} + pL_{d1d1} i_{d1r} + \omega_r L_{q1q1} i_{q1r} \quad (5.36)$$

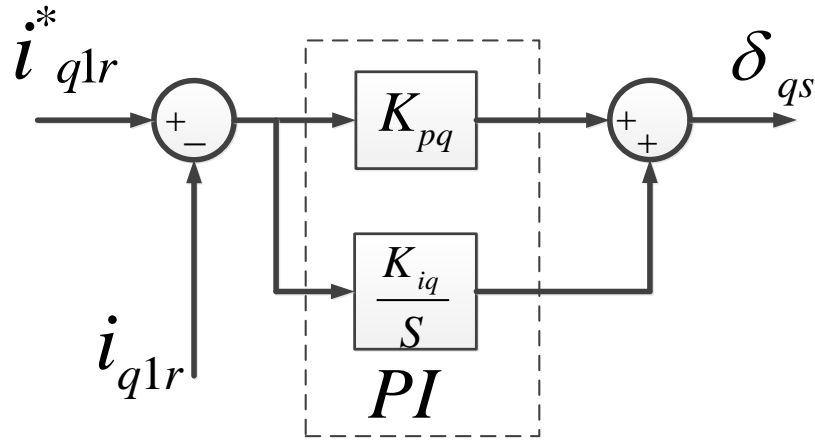


Figure 5.4: The q axis current regulator.

The q axis current controller is designed as:

$$r_s i_{q1r} + pL_{q1q1} i_{q1r} = \delta_{qs} = K_{qs} (i_{q1r}^* - i_{q1r}) \quad (5.37)$$

According the Figure 5.4 ‘ K_{qs} ’ is a PI controller therefore it can be expressed as:

$$K_{qs} = \left(K_{pq} + \frac{k_{iq}}{S} \right) \quad (5.38)$$

Substituting the controller equation in the voltage equation results in:

$$r_s i_{q1r} + pL_{q1q1} i_{q1r} = \left(K_{pq} + \frac{k_{iq}}{S} \right) (i_{q1r}^* - i_{q1r}) \quad (5.39)$$

$$r_s i_{q1r} + pL_{q1q1} i_{q1r} + K_{pq} i_{q1r} + \frac{k_{iq}}{S} i_{q1r} = \left(K_{pq} + \frac{k_{iq}}{S} \right) (i_{q1r}^*) \quad (5.40)$$

$$\frac{i_{q1r}}{i_{q1r}^*} = \frac{\left(K_{pq} + \frac{K_{iq}}{S} \right)}{r_s + pL_{q1q1} + K_{pq} + \frac{K_{iq}}{S}} = \frac{\left(\frac{SK_{pq} + K_{iq}}{L_{q1}} \right)}{S^2 + S \frac{(r_s + K_{pq})}{L_{q1}} + \frac{K_{iq}}{L_{q1}}} \quad (5.41)$$

The denominator of the equation (5.41) can be set equal to the second order Butterworth polynomial to obtain the ‘ K_{pq} ’ and ‘ K_{iq} ’. Using the machine parameters from chapter 3 the controller coefficients are calculated using equation (5.42).

$$p^2 + p \frac{(r_s + K_{pq})}{L_{q1q1}} + \frac{K_{iq}}{L_{q1q1}} = p^2 + \sqrt{2} p \omega_o + \omega_o^2 \quad (5.42)$$

The internal loops of a current controller have to be at least 10 times faster than the rotor speed controller loop [155]. Since the frequency of the speed controller loop is selected as 7 (Hz) the frequency of the current regulator has to be at least 70 (Hz). Selecting $\omega_o = 200$ (rad/sec) results in:

$$\sqrt{2} \omega_o = \frac{(r_s + K_{pq})}{L_{q1q1}} \quad (5.43)$$

Where: $L_{q1q1} = 0.0026$ (H).

$$K_{pq} = \sqrt{2} \omega_o L_{q1q1} - r_s = 0.73539 - 0.01 = 0.725397 \quad (5.44)$$

$$\frac{K_{iq}}{L_{q1q1}} = \omega_o^2 \rightarrow K_{iq} = 104 \quad (5.45)$$

The d axis current controller also can be designed as:

$$r_s i_{d1r} + pL_{d1d1} i_{d1r} = \delta_{ds} = K_{ds} (i_{d1r}^* - i_{d1r}) \quad (5.46)$$

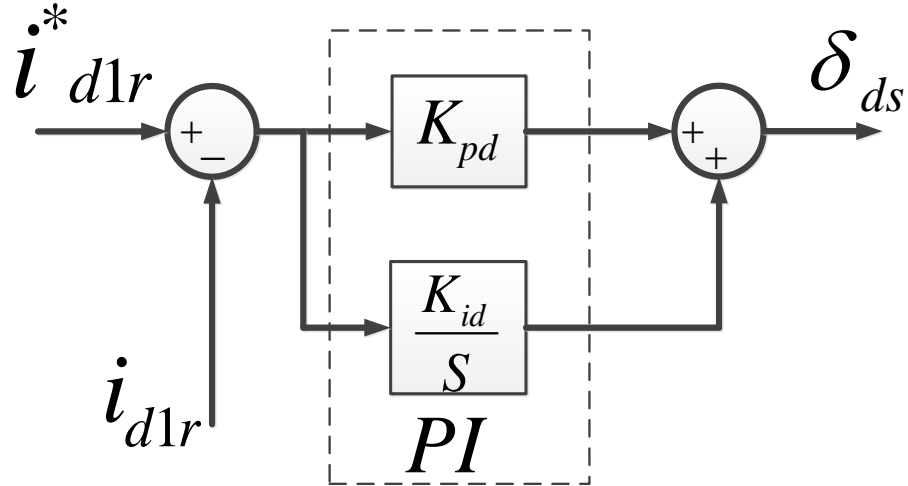


Figure 5.5: The d axis current regulator.

According to the Figure 5.5 the K_{ds} can be considered as a PI controller according to equation (5.47).

$$K_{ds} = \left(K_{pd} + \frac{K_{id}}{S} \right) \quad (5.47)$$

$$r_s i_{d1r} + pL_{d1d1} i_{d1r} = \delta_{ds} = \left(K_{pd} + \frac{K_{id}}{S} \right) (i_{d1r}^* - i_{d1r}) \quad (5.48)$$

$$r_s i_{d1r} + pL_{d1d1} i_{d1r} + K_{pd} i_{d1r} + \frac{K_{id}}{S} i_{d1r} = \left(K_{pd} + \frac{K_{id}}{S} \right) (i_{d1r}^*) \quad (5.49)$$

$$\frac{i_{d1r}}{i_{d1r}^*} = \frac{\left(K_{pd} + \frac{K_{id}}{S} \right)}{r_s + pL_{d1d1} + K_{pd} + \frac{K_{id}}{S}} = \frac{\left(\frac{pK_{pd} + K_{id}}{L_{d1d1}} \right)}{p^2 + p \frac{(r_s + K_{pd})}{L_{d1d1}} + \frac{K_{id}}{L_{d1d1}}} \quad (5.50)$$

The denominator of the equation (5.50) can be set equal to the second order Butterworth polynomial to obtain the ‘ K_{pd} ’ and ‘ K_{id} ’.

$$\sqrt{2}\omega_o = \frac{(r_s + K_{pd})}{L_{d1d1}} \quad (5.51)$$

By substituting the $L_{d1d1}=0.0012$ (H), the controller coefficients can be calculated as:

$$K_{pd} = \sqrt{2}\omega_o L_{d1d1} - r_s = \sqrt{2} \times 200 \times 0.0012 - 0.01 = 0.3294 \quad (5.52)$$

$$\frac{K_{id}}{L_{d1d1}} = \omega_o^2 \rightarrow K_{id} = 48 \quad (5.53)$$

By substituting the δ_{ds} and δ_{qs} back in to the dynamic equation of the q and d axis voltages, they can be rewritten as:

$$r_s i_{d1r} + pL_{d1d1} i_{d1r} = \delta_{ds} = V_{d1r} - p\lambda_{pmd1r} - \omega_r L_{q1q1} i_{q1r} \quad (5.54)$$

Since the flux linkage due to the permanent magnet is constant the derivation of that would remain zero. Therefore, the above equation will change to the equation (5.55).

$$r_s i_{d1r} + pL_{d1d1} i_{d1r} = \delta_{ds} = V_{d1r} - \omega_r L_{q1q1} i_{q1r} \quad (5.55)$$

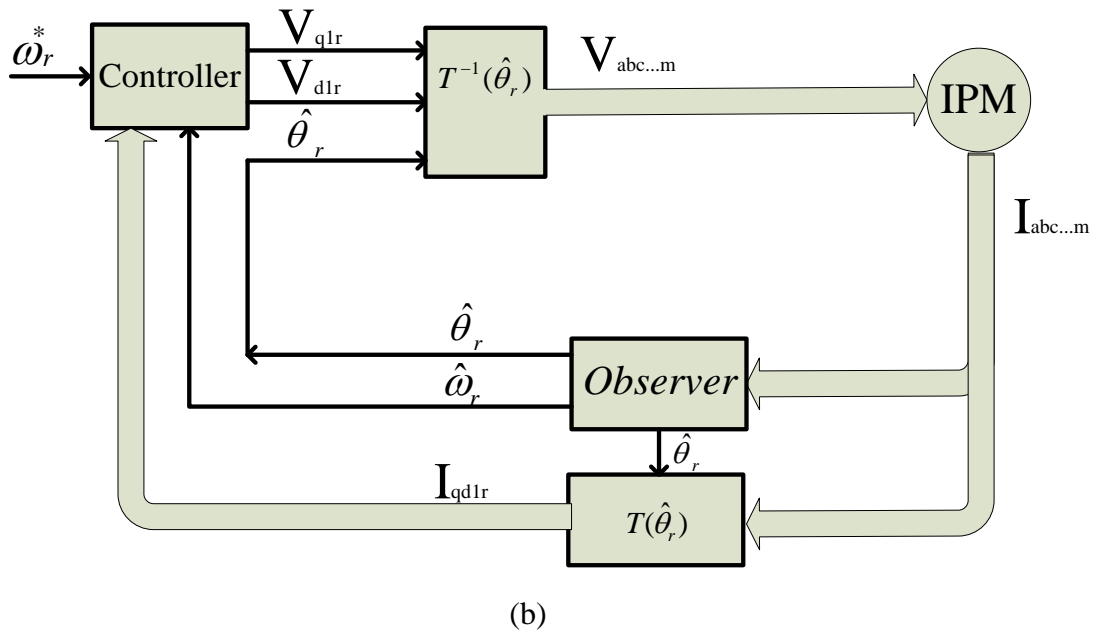
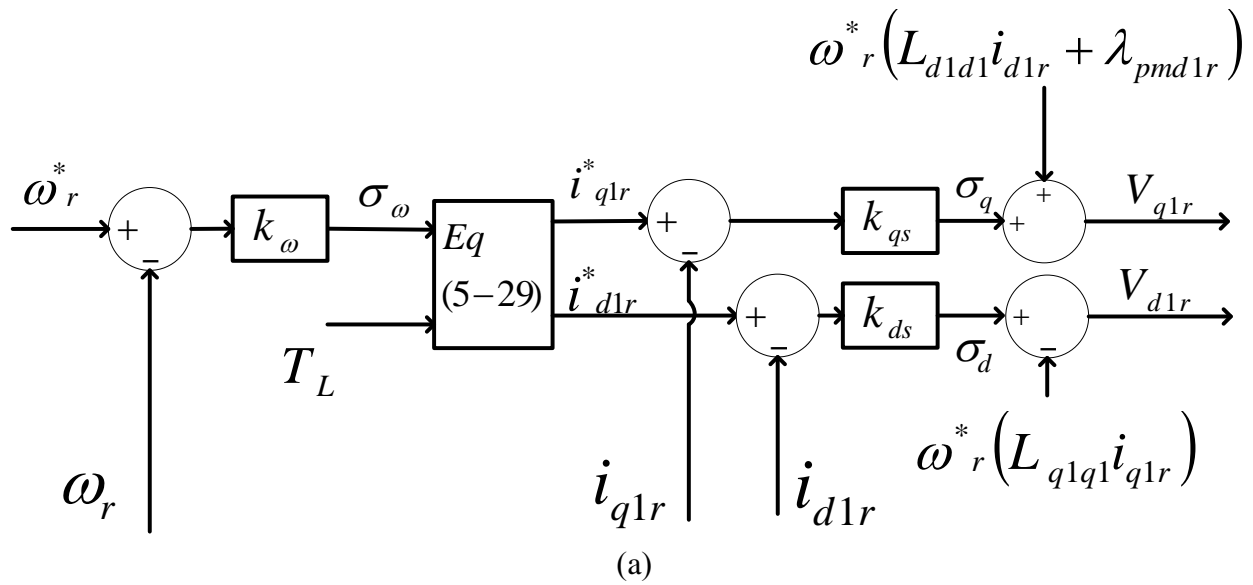


Figure 5.6: (a) Controller diagram of the machine, (b) The drive diagram.

Also the voltage equation for q axis can be expressed as:

$$r_s i_{q1r} + pL_{q1q1} i_{q1r} = \delta_{qs} = V_{q1r} + \omega_r L_{d1d1} i_{d1r} + \omega_r \lambda_{pmd1r} \quad (5.56)$$

The block diagram of the designed controller is shown in the Figure 5.6. In this controller after obtaining the voltage references for q and d axis they can be transformed to the natural quantities to be fed to the stator phases. The feedback signals (i_{q1r} , i_{d1r}) are coming from the

measurement and the flux linkages (λ_{q1r} and λ_{d1r}) are calculated using the stator inductances and feedback currents. Since the load torque is not known the T_L is set equal to zero which means the load torque will be the system disturbance. In this procedure the exact position of the rotor flux linkage ($\hat{\theta}_r$) is needed. The goal of the next sections of this chapter is to design an estimator to estimate the rotor angle and rotor speed.

5.3 High Frequency Injection

To implement the position estimation using the high frequency injection, the form of the currents due to the high frequency voltage injected to the machine needs to be known. The motivation of this section is to design a proper signal processing method to extract the position information from the high frequency currents of the machine stator. The high frequency voltages that are used in this study will be injected in the third sequence of stationary reference frame of the machine which means that the equivalent circuit of this sequence is needed to be derived and used in high frequency investigates.

To obtain the inductances of the third sequence, the different sequences of the airgap function and the winding function need to be obtained. The winding function of the machine is generated in the section 3.2. Figures 3.8 to 3.16 show the different components of the winding function. The Fourier series of the winding function is repeated here in equation (5.57).

$$n_x = N_1 \sin(\varphi - k\alpha) + N_3 \sin 3(\varphi - k\alpha) + N_5 \sin 5(\varphi - k\alpha) + N_7 \sin 7(\varphi - k\alpha) \quad (5.57)$$

$$x = a, b, c, \dots, i, \quad k = 0, 1, 2, 3, \dots, 8, \quad \alpha = \frac{2\pi}{9}$$

Also the Fourier series of the air gap function can be generated from the air gap function of the Figure 3.6. Equation (5.58) represents the Fourier series of the air gap function.

$$g^{-1}(\varphi, \theta_r) = a_0 + a_1 \cos 2(\varphi - \theta_r) + a_2 \cos 6(\varphi - \theta_r) + a_3 \cos 10(\varphi - \theta_r) + a_4 \cos 14(\varphi - \theta_r) \quad (5.58)$$

$$a_0 = a, a_1 = -b, a_2 = -\frac{b}{3}, a_3 = -\frac{b}{5}, a_4 = -\frac{b}{7}$$

$$a = \frac{1}{2} \left(\frac{1}{g_b} + \frac{1}{g_a} \right), b = \frac{1}{2} \left(\frac{1}{g_b} - \frac{1}{g_a} \right)$$

Using the Fourier series of the winding function, the air gap function and also the equation (3.4) the self and mutual inductances can be expressed as equation (5.59) [87].

$$L_{jk} = 2\mu_o r l [a_o (N_1^2 \cos(k-j)\alpha + \frac{N_7^2}{49} \cos 7(k-j)\alpha + \frac{N_5^2}{25} \cos 5(k-j)\alpha + \frac{N_3^2}{9} \cos 3(k-j)\alpha) + \frac{1}{2} (a_1 N_1^2) \cos(-2(k-j)\alpha + 2\theta_r) + \frac{1}{2} (\frac{a_2 N_3^2}{9}) \cos(-6k(k-j)\alpha + 6\theta_r) + \frac{1}{2} (\frac{a_3 N_5^2}{25}) \cos(-10k(k-j)\alpha + 10\theta_r) + (\frac{a_4 N_7^2}{98}) \cos(-14k(k-j)\alpha + 14\theta_r)], \alpha = \frac{2\pi}{9} \quad (5.59)$$

Where “k” and ‘j’ represent the machine phase number according to Table 5.1, “ a_i ” are the coefficients of the Fourier series of the air gap function, presented in equation (5.58) and “ N_i ” represents the coefficients of the Fourier series of the winding functions. For example, the self-inductances of the phase ‘a’ can be expressed as equation (5.60).

Table 5.1 The corresponding numbers for k and j.

Name of The Phase	K and j
a	0
b	1
c	2
d	3
e	4
f	5
g	6
h	7
i	8

$$L_{aa} = 2\pi r l \mu_o \left[\begin{aligned} & a_o \left(N_1^2 + \frac{N_7^2}{49} + \frac{N_5^2}{25} + \frac{N_3^2}{9} \right) + \frac{a_1}{2} \left(N_1^2 + \frac{N_3 N_1}{3} + \frac{N_7 N_5}{35} + \frac{N_1 N_7}{35} \right) \text{Cos}(2\theta_r) \\ & + \frac{a_2}{2} \left(\frac{N_5 N_1}{5} + \frac{N_3^2}{9} + \frac{N_1 N_5}{5} + \frac{N_1 N_7}{7} \right) \text{Cos}(6\theta_r) \\ & + \frac{a_3}{2} \left(\frac{N_7 N_3}{21} + \frac{N_5^2}{25} + \frac{N_3 N_7}{21} \right) \text{Cos}(10\theta_r) + \frac{a_4 N_7^2}{98} \text{Cos}(14\theta_r) \end{aligned} \right] \quad (5.60)$$

Neglecting the coupling terms between the different harmonics of the turn function results

in:

$$L_{abc\dots l} = 2\pi r l \mu_o \left[\begin{aligned} & a_o \left(N_1^2 + \frac{N_7^2}{49} + \frac{N_5^2}{25} + \frac{N_3^2}{9} \right) \\ & + \frac{a_1}{2} (N_1^2) \text{Cos}(-2K\alpha + 2\theta_r) \\ & + \frac{a_2}{2} \left(\frac{N_3^2}{9} \right) \text{Cos}(-6K\alpha + 6\theta_r) \\ & + \frac{a_3}{2} \left(\frac{N_5^2}{25} \right) \text{Cos}(-10K\alpha + 10\theta_r) \\ & + \frac{a_4 N_7^2}{98} \text{Cos}(-14K\alpha + 14\theta_r) \end{aligned} \right] \quad (5.61)$$

Finally, the inductances can be arranged in the matrix of equation (5.62).

$$L_{ss} = \begin{bmatrix} L_{ls} + L_{aa} & L_{ab} & L_{ac} & L_{ad} & L_{ae} & L_{af} & L_{ag} & L_{ah} & L_{ai} \\ L_{ba} & L_{ls} + L_{bb} & L_{bc} & L_{bd} & L_{be} & L_{bf} & L_{bg} & L_{bh} & L_{bi} \\ L_{ca} & L_{cb} & L_{ls} + L_{cc} & L_{cd} & L_{ce} & L_{cf} & L_{cg} & L_{ch} & L_{ci} \\ L_{da} & L_{db} & L_{dc} & L_{ls} + L_{dd} & L_{de} & L_{df} & L_{dg} & L_{dh} & L_{di} \\ L_{ea} & L_{eb} & L_{ec} & L_{ed} & L_{ls} + L_{ee} & L_{ef} & L_{eg} & L_{eh} & L_{ei} \\ L_{fa} & L_{fb} & L_{fc} & L_{fd} & L_{fe} & L_{ls} + L_{ff} & L_{fg} & L_{fh} & L_{fi} \\ L_{ga} & L_{gb} & L_{gc} & L_{gd} & L_{ge} & L_{gf} & L_{ls} + L_{gg} & L_{gh} & L_{gi} \\ L_{ha} & L_{hb} & L_{hc} & L_{hd} & L_{he} & L_{hf} & L_{hg} & L_{ls} + L_{hh} & L_{hi} \\ L_{ia} & L_{ib} & L_{ic} & L_{id} & L_{ie} & L_{if} & L_{ig} & L_{ih} & L_{ls} + L_{ii} \end{bmatrix} \quad (5.62)$$

Then using the transformation matrix of the equation (5.63) the various components of the inductances in stationary reference frame can be obtain.

$$T(0) =$$

$$\frac{2}{9} \begin{bmatrix} c(\theta) & c(\theta - \alpha) & c(\theta - 2\alpha) & c(\theta - 3\alpha) & c(\theta - 4\alpha) & c(\theta - 5\alpha) & c(\theta - 6\alpha) & c(\theta - 7\alpha) & c(\theta - 8\alpha) \\ s(\theta) & s(\theta - \alpha) & s(\theta - 2\alpha) & s(\theta - 3\alpha) & s(\theta - 4\alpha) & s(\theta - 5\alpha) & s(\theta - 6\alpha) & s(\theta - 7\alpha) & s(\theta - 8\alpha) \\ c(3\theta) & c3(\theta - \alpha) & c3(\theta - 2\alpha) & c3(\theta - 3\alpha) & c3(\theta - 4\alpha) & c3(\theta - 5\alpha) & c3(\theta - 6\alpha) & c3(\theta - 7\alpha) & c3(\theta - 8\alpha) \\ s(3\theta) & s3(\theta - \alpha) & s3(\theta - 2\alpha) & s3(\theta - 3\alpha) & s3(\theta - 4\alpha) & s3(\theta - 5\alpha) & s3(\theta - 6\alpha) & s3(\theta - 7\alpha) & s3(\theta - 8\alpha) \\ c(5\theta) & c5(\theta - \alpha) & c5(\theta - 2\alpha) & c5(\theta - 3\alpha) & c5(\theta - 4\alpha) & c5(\theta - 5\alpha) & c5(\theta - 6\alpha) & c5(\theta - 7\alpha) & c5(\theta - 8\alpha) \\ s(5\theta) & s5(\theta - \alpha) & s5(\theta - 2\alpha) & s5(\theta - 3\alpha) & s5(\theta - 4\alpha) & s5(\theta - 5\alpha) & s5(\theta - 6\alpha) & s5(\theta - 7\alpha) & s5(\theta - 8\alpha) \\ c(7\theta) & c7(\theta - \alpha) & c7(\theta - 2\alpha) & c7(\theta - 3\alpha) & c7(\theta - 4\alpha) & c7(\theta - 5\alpha) & c7(\theta - 6\alpha) & c7(\theta - 7\alpha) & c7(\theta - 8\alpha) \\ s(7\theta) & s7(\theta - \alpha) & s7(\theta - 2\alpha) & s7(\theta - 3\alpha) & s7(\theta - 4\alpha) & s7(\theta - 5\alpha) & s7(\theta - 6\alpha) & s7(\theta - 7\alpha) & s7(\theta - 8\alpha) \\ 1/2 & 1/2 & 1/2 & 1/2 & 1/2 & 1/2 & 1/2 & 1/2 & 1/2 \end{bmatrix} \quad (5.63)$$

$$\alpha = \frac{2\pi}{9}, \theta = 0$$

$$L_{qdo} = T(0)L_{ss}T^{-1}(0) \quad (5.64)$$

The qdo model of the machine can be obtained by transforming the natural variable equations to the stationary reference frame. The third qd sequence equivalent circuit to be used for the rotor angle estimation, has the q and d inductances expressed in equations (5.65) and (5.66), which are clearly dependent on the rotor angle. Hence the third sequence equivalent circuit, which is non-

torque producing, will be used to modulate the high frequency voltage to estimate the position of the rotor.

$$L_{q3} = 1.06(a_2 \frac{N_3^2}{9}) \text{Cos}(6\theta_r) \quad (5.65)$$

$$L_{d3} = 1.06(a_2 \frac{N_3^2}{9}) \text{Cos}(6\theta_r + \frac{\pi}{2}) \quad (5.66)$$

A high frequency voltage set according the equation (5.67) is injected into the third sequence of the nine-phase IPM in the stationary reference frame to generate the rotor angle dependent component of the stator currents.

$$\begin{bmatrix} V_{q3} \\ V_{d3} \end{bmatrix} = A \begin{bmatrix} \text{Cos}(\omega_s t) \\ \text{Cos}(\omega_s t - \frac{\pi}{2}) \end{bmatrix} \quad (5.67)$$

The voltages of the equations (5.67) can be transformed back to the stationary reference frame to give equation (5.68). It should be noted that in the injected vector of the equation (5.68) all the components excluding the third ones (First, Fifth, Seventh) are zero:

$$\begin{bmatrix} V_a \\ V_b \\ V_c \\ V_d \\ V_e \\ V_f \\ V_g \\ V_h \\ V_m \end{bmatrix} = T^{-1}(0) \begin{bmatrix} 0 \\ 0 \\ V_{q3} \\ V_{d3} \\ 0 \\ 0 \\ 0 \\ 0 \\ 0 \end{bmatrix} = V \begin{bmatrix} \cos(\omega_s t) \\ \cos(-3\alpha + \omega_s t) \\ \cos(-6\alpha + \omega_s t) \\ \cos(-9\alpha + \omega_s t) \\ \cos(-12\alpha + \omega_s t) \\ \cos(-15\alpha + \omega_s t) \\ \cos(-18\alpha + \omega_s t) \\ \cos(-21\alpha + \omega_s t) \\ \cos(-24\alpha + \omega_s t) \end{bmatrix}, \alpha = 2 \frac{\pi}{9} \quad (5.68)$$

Using the qd inductances in equations (5.65) and (5.66), the voltage equation for third sequence of the machine in stationary reference frame can be expressed as equation (5.69).

$$\begin{bmatrix} V_{q3} \\ V_{d3} \end{bmatrix} = A \begin{bmatrix} \cos(\omega_s t) \\ \cos(\omega_s t - \frac{\pi}{2}) \end{bmatrix} = r_s \begin{bmatrix} i_{q3} \\ i_{d3} \end{bmatrix} + p \begin{bmatrix} \lambda_{q3} \\ \lambda_{d3} \end{bmatrix} \quad (5.69)$$

The q_3d_3 flux linkage equations are:

$$\begin{bmatrix} \lambda_{q3} \\ \lambda_{d3} \end{bmatrix} = \begin{bmatrix} L_{q3} & 0 \\ 0 & L_{d3} \end{bmatrix} \begin{bmatrix} i_{q3} \\ i_{d3} \end{bmatrix} \quad (5.70)$$

The equations (5.69) and (5.70) result in:

$$A \begin{bmatrix} \cos(\omega_s t) \\ \cos(\omega_s t + \frac{\pi}{2}) \end{bmatrix} = r_s \begin{bmatrix} i_{q3} \\ i_{d3} \end{bmatrix} + p \begin{bmatrix} \frac{a_2 N_3^2}{9} \cos(6\theta_r) & 0 \\ 0 & \frac{a_2 N_3^2}{9} \sin(6\theta_r) \end{bmatrix} \begin{bmatrix} i_{q3} \\ i_{d3} \end{bmatrix} \quad (5.71)$$

Applying the derivations result in:

$$A \cos(\omega_s t) = r_s i_{q3} - \frac{6\omega_r a_2 N_3^2}{9} \sin(6\theta_r) i_{q3} + \frac{a_2 N_3^2}{9} \cos(6\theta_r) p i_{q3} \quad (5.72)$$

$$A \sin(\omega_s t) = r_s i_{d3} + \frac{6\omega_r a_2 N_3^2}{9} \cos(6\theta_r) i_{d3} + \frac{a_2 N_3^2}{9} \sin(6\theta_r) p i_{d3} \quad (5.73)$$

The general form of high frequency current i_{qd3} can be obtained using the harmonic balance technique [167]. The general form of the high frequency current is assumed to have the form of equation (5.74).

$$i_{qd3} = I e^{j(\theta_i)} \quad (5.74)$$

By separating the q and d axis components of the high frequency current they could be expressed as:

$$i_{q3} = I \cos(\theta_i) \quad (5.75)$$

$$i_{d3} = I \sin(\theta_i) \quad (5.76)$$

Substituting the currents in to equations (5.72) and (5.73) result in:

$$A \sin(\omega_s t) = r_s i_{d3} + \frac{6\omega_r a_2 N_3^2}{9} \cos(6\theta_r) I \sin(\theta_i) + \frac{\omega_i a_2 N_3^2}{9} \cos(6\theta_r) I \cos(\theta_i) \quad (5.77)$$

$$A \cos(\omega_s t) = r_s i_{q3} - \frac{6\omega_r a_2 N_3^2}{9} \sin(6\theta_r) I \cos(\theta_i) - \frac{\omega_i a_2 N_3^2}{9} \cos(6\theta_r) I \sin(\theta_i) \quad (5.78)$$

Where $\omega_r = \frac{d\theta_r}{dt}$ and $\omega_i = \frac{d\theta_i}{dt}$. The last equations can be expanded to equations (5.79) and (5.80).

$$A \cos(\omega_s t) = r_s i_{q3} - \frac{3\omega_r a_2 N_3^2 I}{9} [\sin(6\theta_r + \theta_i) + \sin(6\theta_r - \theta_i)] \quad (5.79)$$

$$- \frac{\omega_i a_2 N_3^2 I}{18} [\sin(6\theta_r + \theta_i) + \sin(\theta_i - 6\theta_r)]$$

$$A \sin(\omega_s t) = r_s i_{d3} + \frac{3\omega_r a_2 N_3^2 I}{9} [\sin(6\theta_r + \theta_i) + \sin(\theta_i - 6\theta_r)] \quad (5.80)$$

$$+ \frac{\omega_i a_2 N_3^2 I}{18} [\cos(6\theta_r + \theta_i) + \cos(6\theta_r - \theta_i)]$$

Neglecting the first and the second term because of their low magnitudes compared to the third one results in:

$$A [\cos(\omega_s t) + j \sin(\omega_s t)] = \quad (5.81)$$

$$\frac{\omega_i a_2 N_3^2 I}{18} [-\sin(6\theta_r + \theta_i) + \sin(6\theta_r - \theta_i) + j \cos(6\theta_r + \theta_i) + j \cos(6\theta_r - \theta_i)]$$

The currents can be expressed in the polar form as:

$$Ae^{j(\omega_s t)} = \frac{\omega_i a_2 N_3^2 I}{18} \left[e^{-j(6\theta_r + \theta_i + \frac{\pi}{2})} + e^{j(6\theta_r - \theta_i - \frac{\pi}{2})} \right] \quad (5.82)$$

From equation (5.82) the harmonic balance technique results in:

$$\begin{aligned} (6\theta_r + \theta_i + \frac{\pi}{2}) = \omega_s t &\rightarrow \theta_i = \omega_s t - 6\theta_r - \frac{\pi}{2} \\ -(6\theta_r - \theta_i - \frac{\pi}{2}) = \omega_s t &\rightarrow \theta_i = \omega_s t + 6\theta_r - \frac{\pi}{2} \end{aligned} \quad (5.83)$$

The $q_3 d_3$ currents due to the high frequency voltage set expressed in complex form are given as:

$$I = I_1 e^{j(-6\theta_r + \omega_s t - \frac{\pi}{2})} + I_2 e^{j(6\theta_r + \omega_s t - \frac{\pi}{2})} \quad (5.84)$$

Where:

$$I_1 = I_2 = \frac{18A}{\omega_i a_2 N_3^2} \quad (5.85)$$

It should be noted that the mentioned currents here are the components due to the interaction between the machine saliency and the high frequency currents of the stator. The high frequency currents arguments have two angles, one angle is related to the frequency of the injected high frequency voltage ($\omega_s t$) and the Second angle related to the rotor angle (θ_r). To extract the rotor position information, the signal of equation (5.84), is multiplied by $e^{-j(\omega_s t)}$ which results in:

$$i_{qd3} = \frac{18Ae^{j(6\theta_r - \frac{\pi}{2})}}{(\omega_i) a_2 N_3^2} + \frac{18Ae^{j(-6\theta_r - \frac{\pi}{2})}}{(\omega_i) a_2 N_3^2} \quad (5.86)$$

A low pass filter can remove any remaining high frequency noise that may still lingers in the equation (5.86). The output of the filter has a variable magnitude which varies with the rotor speed. Normalizing that can be done by using the equation (5.87).

$$i_{nq3} = \frac{i_{q3}}{\sqrt{i_{q3}^2 + i_{d3}^2}}, \quad i_{nd3} = \frac{i_{d3}}{\sqrt{i_{q3}^2 + i_{d3}^2}} \quad (5.87)$$

Equation (5.88) presents the signal after normalizing. This signal can be used as the input of the observer.

$$i_{nqd3} = e^{j(6\theta_r - \frac{\pi}{2})} + e^{j(-6\theta_r - \frac{\pi}{2})} \quad (5.88)$$

5.4 Design of the Position Observer

5.4.1 Design of the Luenberger Observer

The high frequency voltages injected to the stator windings of the machine can generate the position dependent signal which is used for the estimation. To extract the information carried by the high frequency current a proper estimator needs to be designed. The mechanical dynamic equations of the rotor can be used for designing the position estimator.

Based on Figure 5.7, the mechanical dynamic model of a rotor is:

$$\frac{2J}{P} p\omega_r + B\omega_r = T_e - T_L \quad (5.89)$$

$$p\theta_r = \omega_r \quad (5.90)$$

In the above equations the ‘ P ’ is the number of the poles of the machine, ‘ B ’ is the friction coefficient, ‘ J ’ is the momentum of inertia of the rotor, ‘ θ_r ’ is the rotor position, ‘ T_e ’ is the electromagnetic torque produced by the machine and ‘ T_L ’ is the load torque.

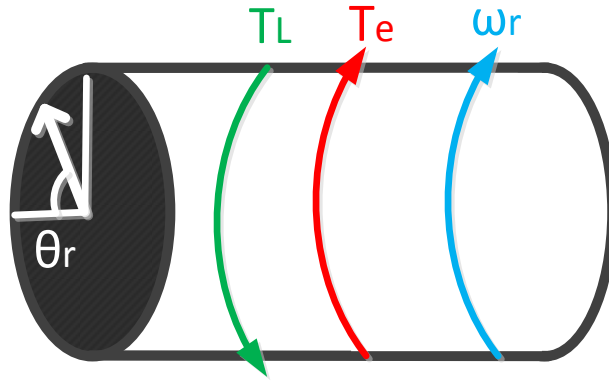


Figure 5.7: The rotor of the machine.

The dynamic equations of the rotor are presented in equation (5.91). Using that, the observer can be designed as equation (5.92) which is the standard form of a close loop observer [160]. In this equation ‘A’ represents the system matrix, ‘B’ is the input matrix, ‘U’ is the input of the system, ‘C’ is the output matrix and ‘X’ represents the state vector of the system.

$$\dot{X} = AX + BU \quad (5.91)$$

$$Y = CX$$

$$\dot{\hat{X}} = A\hat{X} + BU + K(Y - C\hat{X}) \quad (5.92)$$

In the equation (5.92) the term \hat{X} is the estimated state variables. The error between the estimated and real state and also the derivation of the error are:

$$e = X - \hat{X} \quad (5.93)$$

$$\dot{e} = \dot{X} - \dot{\hat{X}} \quad (5.94)$$

Substituting the \dot{X} and $\dot{\hat{X}}$ from equations (5.93) and (5.94) in to the (5.92) results in:

$$\dot{e} = AX + BU - A\hat{X} - BU + K(CX - C\hat{X}) \quad (5.95)$$

Rearranging the equation results in:

$$\dot{e} = A(X - \hat{X}) + K(CX - C\hat{X}) = Ae + KCe \quad (5.96)$$

The standard form of mechanical dynamic equations can be written as:

$$p \begin{bmatrix} \omega_r \\ \theta_r \end{bmatrix} = \begin{bmatrix} -\frac{PB}{2J} & 0 \\ 1 & 0 \end{bmatrix} \begin{bmatrix} \omega_r \\ \theta_r \end{bmatrix} + \begin{bmatrix} \frac{P}{2J} \\ 0 \end{bmatrix} T_e - \begin{bmatrix} \frac{P}{2J} \\ 0 \end{bmatrix} T_L \quad (5.97)$$

The observer is a closed loop one. According to the equation (5.88) the input signals carry the information of the position, therefore to be able to compare the output and the input, the output of the system has to be the position. Based on that the output is defined as:

$$Y = [0 \quad 1] \begin{bmatrix} \omega_r \\ \theta_r \end{bmatrix} \quad (5.98)$$

Substituting the mechanical dynamic equations to the observer equations results in:

$$p \hat{\omega}_r = -\frac{PB}{2J} \hat{\omega}_r + K_1 (\theta_r - \hat{\theta}_r) + \frac{P}{2J} (T_e - T_L) \quad (5.99)$$

$$p \hat{\theta}_r = \hat{\omega}_r + K_2 (\theta_r - \hat{\theta}_r) \quad (5.100)$$

Using the equations (5.99) and (5.100), the position estimator can be built according to Figure 5.8.

To design the observer gains (K_1, K_2) the characteristic polynomial of the observer is needed. The characteristic polynomial of the observer can be derived using the procedure outlined below.

The errors can be defined as:

$$e_1 = \omega_r - \hat{\omega}_r \quad (5.101)$$

$$e_2 = \theta_r - \hat{\theta}_r \quad (5.102)$$

Therefore, the derivative of the rotor speed error can be shown as:

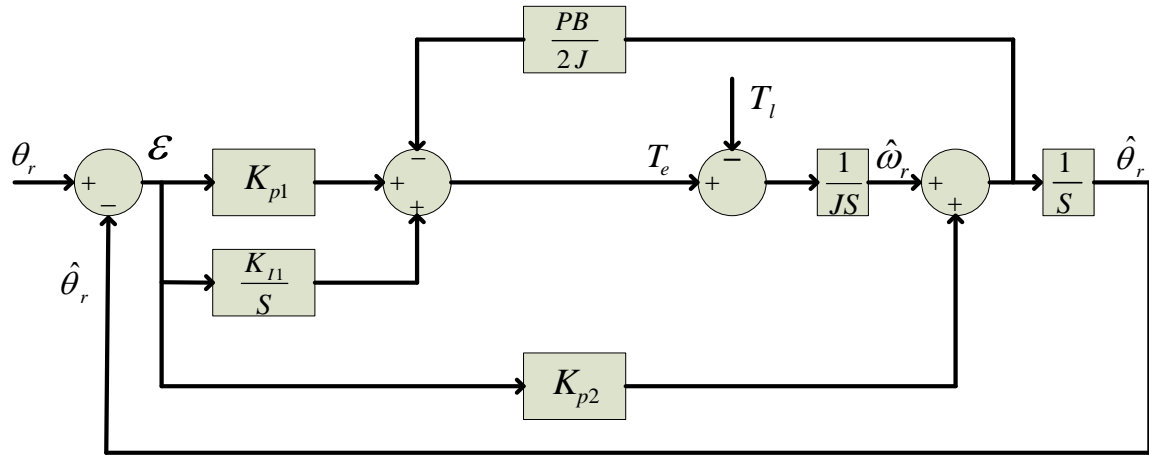


Figure 5.8: The position observer.

$$pe_1 = p\omega_r - p\hat{\omega}_r \quad (5.103)$$

Substituting the actual and estimated rotor speed from the mechanical dynamic equation and the equation (5.99) into the equation (5.103) results in:

$$pe_1 = \frac{P}{2J}(T_e - T_L) - \frac{PB}{2J}\omega_r - \frac{P}{2J}(T_e - T_L) + \frac{PB}{2J}\hat{\omega}_r - K_1(\theta_r - \hat{\theta}_r) \quad (5.104)$$

This equation can be rearranged as:

$$pe_1 = \frac{PB}{2J}(\hat{\omega}_r - \omega_r) - K_1(\theta_r - \hat{\theta}_r) = -\frac{PB}{2J}e_1 - K_1e_2 \quad (5.105)$$

To have zero position error, K_1 needs to be replaced with a PI which can be represented as:

$$pe_1 = -\frac{PB}{2J}e_1 - \left(K_{p1} + \frac{K_{i1}}{p}\right)e_2 \quad (5.106)$$

Also the derivative of the e_2 can be defined as:

$$pe_2 = p(\theta_r - \hat{\theta}_r) = p\theta_r - p\hat{\theta}_r \quad (5.107)$$

Substituting the derivations of the actual and estimated positions from equations (5.99) and (5.100) results:

$$pe_2 = p\omega_r - p\hat{\omega}_r - K_2(\theta_r - \hat{\theta}_r) = e_1 - K_2e_2 \quad (5.108)$$

By defining a new state variable as equation (5.109) the state space equations of the observer can be represented as equation (5.110).

$$pe_3 = e_2 \quad (5.109)$$

$$p \begin{bmatrix} e_1 \\ e_2 \\ e_3 \end{bmatrix} = \begin{bmatrix} -\frac{PB}{2J} & -K_{p1} & -K_{I1} \\ 1 & -K_{p2} & 0 \\ 0 & 1 & 0 \end{bmatrix} \begin{bmatrix} e_1 \\ e_2 \\ e_3 \end{bmatrix} \quad (5.110)$$

The characteristic polynomial of the estimator can be derived as:

$$|\lambda I - A| = \begin{vmatrix} \lambda + \frac{PB}{2J} & K_{p1} & K_{I1} \\ -1 & \lambda + K_{p2} & 0 \\ 0 & -1 & \lambda \end{vmatrix} \quad (5.111)$$

$$\left(\lambda + \frac{PB}{2J}\right)(\lambda^2 + \lambda K_{p2}) + (\lambda K_{p1} + K_{I1}) = \lambda^3 + \lambda^2 \left(K_{p2} + \frac{PB}{2J}\right) + \lambda \left(\frac{PBK_{p2}}{2J} + K_{p1}\right) + K_{I1} \quad (5.112)$$

Setting the above equation equal to the third order Butterworth polynomial [161] results in:

$$\lambda^3 + \lambda^2 \left(K_{p2} + \frac{PB}{2J}\right) + \lambda \left(\frac{PBK_{p2}}{2J} + K_{p1}\right) + K_{I1} = \lambda^3 + 2\omega_n \lambda^2 + 2\omega_n^2 \lambda + \omega_n^3 \quad (5.113)$$

The mechanical parameters of the machine can be found in the Table 5.2 [153].

Table 5.2 The mechanical parameters of the machine.

B	0.01 N.m.sec/rad
J	0.1 N.m.sec ² /rad
Rotor Rated Speed	377 rad/sec

To be able to operate in all operating range the frequency of the polynomial should be selected to be bigger than the maximum rotor frequency and the frequency of the speed controller loop in equation (5.34).

$$\omega_n > \omega_{r-Rated} \gg \omega_o \quad (5.114)$$

Using the equation (5.114) the ‘ ω_n ’ is selected to be 500 (rad/sec). Therefore, using the equation (5.113) the coefficients of the observer can be designed as:

$$\lambda^3 + \lambda^2 \left(K_{p2} + \frac{PB}{2J} \right) + \lambda \left(\frac{PBK_{p2}}{2J} + K_{p1} \right) + K_{I1} \quad (5.115)$$

$$= \lambda^3 + 1000\lambda^2 + 500000\lambda + 125000000$$

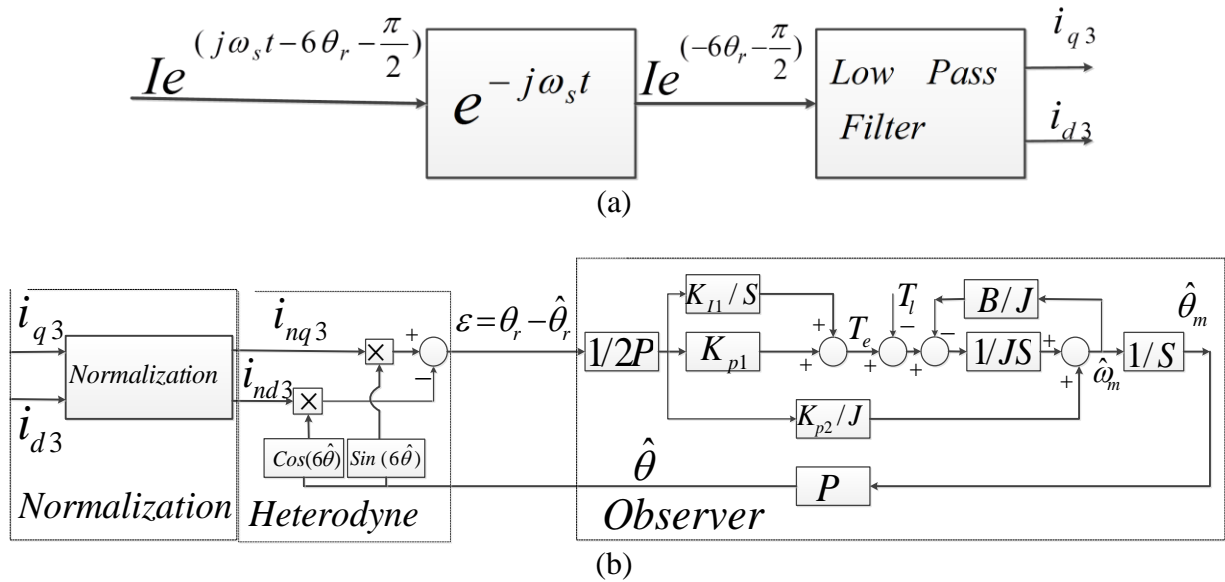


Figure 5.9: (a) The block diagram used to extract signal for observer, (b) The Luenberger observer.

Substituting machine parameters from Table 5.2 in to the equation (5.115), the different coefficients of the observer can be calculated as:

$$\left(K_{p2} + \frac{PB}{2J} \right) = 1000 \rightarrow K_{p2} = 999.9 \quad (5.116)$$

$$\left(\frac{PBK_{p2}}{2J} + K_{p1} \right) = 500000 \rightarrow K_{p1} = 499900.1 \quad (5.117)$$

$$K_{r1} = 125000000 \quad (5.118)$$

The input of the Figure 5.8 is ' θ_r ' while the observer is fed with the currents generated from high frequency signal injection. The input signals which are derived in the section 5.2 have the form of the equation (5.88) by separating the real and imaginary parts of the signal they can be shown as equations (5.119) and (5.120) respectively.

$$i_{nq3} = \text{Sin}(6\theta_r) \quad (5.119)$$

$$i_{nd3} = \text{Cos}(6\theta_r) \quad (5.120)$$

To extract the rotor position from the above signals a function is needed to extract the ' θ_r ' and subtract the output value from it and to obtain the error. The first solution for this case is proposed according equation (5.121).

$$\varepsilon = i_{nq3} \text{Cos}(6\hat{\theta}_r) - i_{nd3} \text{Sin}(6\hat{\theta}_r) \quad (5.121)$$

Substituting the currents from equations (5.119) and (5.120) in to the (5.121) results in:

$$\varepsilon = \text{Sin}(6\theta_r) \text{Cos}(6\hat{\theta}_r) - \text{Cos}(6\theta_r) \text{Sin}(6\hat{\theta}_r) = \text{Sin}(6\theta_r - 6\hat{\theta}_r) \quad (5.122)$$

At the steady state when the observer is tracking the real position the equation (5.122) can be approximated as:

$$\varepsilon = \text{Sin}(6\theta_r - 6\hat{\theta}_r) \cong (6\theta_r - 6\hat{\theta}_r) \quad (5.123)$$

Therefore, by substituting the block that generates the estimation error (ε) in the Figure 5.8 by the equation (5.122) and also adding the normalizing block and low pass filter, the observer can be changed to the one shown in Figure 5.9. The observer has four parts as shown in the Figure 5.5. The first part is normalizing part that normalizes the input signals which have a variable

magnitude to bring the magnitude to unity. The second part is heterodyning to compare the input position with the estimated one and calculate the error between the input angle and the estimated angle. The third part is the PI controller of the observer to force the observer to operate at zero error in steady state. And the last part is the mechanical model of the rotor to calculate the rotor speed and the rotor position.

5.4.2 Design of the Low Pass Filters

According to the Figure 5.9 the observer also has a low pass filter which removes the extra high frequency components of the signals after the heterodyning process. The low pass filter general form is presented in equation (5.124).

$$f = \frac{\omega_n^2}{S^2 + 2\xi\omega_n S + \omega_n^2} \quad (5.124)$$

Where ‘ ξ ’ is the damping factor of the filter and ‘ ω_n ’ is the cut frequency. The frequency of the high frequency signal that is injected for position estimation is more than 6000 (rad/sec) therefore, the cut frequency of the filter needs to be below this value to be able to remove the remaining of the harmonic distortions after heterodyning. By selecting the cut frequency equal to 1000 (rad/sec) and ‘ ξ ’ equal to $\sqrt{2}$, the transfer function of the filter can be presented as equation (5.125).

$$f = \frac{10^6}{S^2 + 2\sqrt{2}10^3 S + 10^6} \quad (5.125)$$

5.4.3 Robustness of the Observer

The stability of the observer that is designed in this section can be affected by changings of some variable parameters, such as the changings of the third sequence inductances of the machine by increasing the stator current. In this section the poles of the third sequence circuit are plotted for different stator current levels. It should be noted that the Lunberger observer is using the mechanical dynamic equation which is independent of the machine inductances, therefore, the stability of the observer just depends on its gains which are designed to be stable. The filters are also independent of the machine parameters, therefore, their stability cannot be affected by the changes of parameters. The dynamic equation for the third sequence circuit is presented in the equation (5.71). To investigate the stability of this circuit, the third sequence inductances are needed for the all ranges of the stator current. The equation (5.71) can be expanded as equation (5.126).

$$\begin{bmatrix} V_{q3} \\ V_{d3} \end{bmatrix} = r_s \begin{bmatrix} i_{q3} \\ i_{d3} \end{bmatrix} + \begin{bmatrix} -6\omega_r L_{q3} \sin(6\theta_r) & 0 \\ 0 & 6\omega_r L_{d3} \cos(6\theta_r) \end{bmatrix} \begin{bmatrix} i_{q3} \\ i_{d3} \end{bmatrix} + \quad (5.126)$$

$$\begin{bmatrix} L_{q3} \cos(6\theta_r) & 0 \\ 0 & L_{d3} \sin(6\theta_r) \end{bmatrix} p \begin{bmatrix} i_{q3} \\ i_{d3} \end{bmatrix}$$

Equation (5.126) can be rewritten in standard form as equation (5.127).

$$\begin{aligned} pX &= AX + Bu \\ Y &= CX + Du \end{aligned} \quad (5.127)$$

$$P \begin{bmatrix} i_{q3} \\ i_{d3} \end{bmatrix} = - \begin{bmatrix} \frac{L_{d3} \sin(6\theta_r)(6\omega_r L_{q3} \sin(6\theta_r) - r_s)}{0.5L_{q3}L_{d3} \sin(3\theta_r)} & 0 \\ 0 & \frac{L_{q3} \cos(6\theta_r)(6\omega_r L_{d3} \cos(6\theta_r) - r_s)}{0.5L_{q3}L_{d3} \sin(3\theta_r)} \end{bmatrix} \begin{bmatrix} i_{q3} \\ i_{d3} \end{bmatrix} \quad (5.128)$$

$$- \frac{1}{0.5L_{q3}L_{d3} \sin(3\theta_r)} \begin{bmatrix} L_{d3} \sin(6\theta_r) & 0 \\ 0 & L_{q3} \cos(6\theta_r) \end{bmatrix} \begin{bmatrix} V_{q3} \\ V_{d3} \end{bmatrix}$$

$$Y = \begin{bmatrix} 1 & 0 \\ 0 & 1 \end{bmatrix} \begin{bmatrix} i_{q3} \\ i_{d3} \end{bmatrix} \quad (5.129)$$

For $\theta_r = K \frac{\pi}{3}$, $K = 1, 2, 3, \dots$ the 'A' matrix is not defined. Therefore, the stability of such points need to be checked separately. For $\theta_r = K \frac{\pi}{3}$, $K = 1, 2, 3, \dots$ the third sequence circuit model can be presented as equation (5.130).

$$\begin{bmatrix} V_{q3} \\ V_{d3} \end{bmatrix} = r_s \begin{bmatrix} i_{q3} \\ i_{d3} \end{bmatrix} + \begin{bmatrix} 0 & 0 \\ 0 & 6\omega_r L_{d3} \end{bmatrix} \begin{bmatrix} i_{q3} \\ i_{d3} \end{bmatrix} + \begin{bmatrix} L_{q3} & 0 \\ 0 & 0 \end{bmatrix} P \begin{bmatrix} i_{q3} \\ i_{d3} \end{bmatrix} \quad (5.130)$$

First and second rows of the Equation (5.130) can be separated as shown in equations (5.131) and (5.132).

$$V_{q3} = r_s i_{q3} + p L_{q3} i_{q3} \quad (5.131)$$

$$V_{d3} = r_s i_{d3} + 6\omega_r L_{d3} i_{d3} \quad (5.132)$$

The equation (5.131) has a pole in ($S = -r_s/L_{q3}$) therefore, it is stable. The equation (5.132) is algebraic and it is stable. For the rest of the points the characteristic equation of the system is needed. The characteristic equation of the matrix A can be presented as equation (5.133).

$$|SI - A| = \left(S + \frac{L_{d3} \sin(6\theta_r)(6\omega_r L_{q3} \sin(6\theta_r) - r_s)}{0.5L_{q3}L_{d3} \sin(3\theta_r)} \right) \left(S + \frac{L_{q3} \cos(6\theta_r)(6\omega_r L_{d3} \cos(6\theta_r) - r_s)}{0.5L_{q3}L_{d3} \sin(3\theta_r)} \right) = \quad (5.133)$$

$$S^2 + S \left(\frac{L_{d3} \sin(6\theta_r)(6\omega_r L_{q3} \sin(6\theta_r) - r_s) + L_{q3} \cos(6\theta_r)(6\omega_r L_{d3} \cos(6\theta_r) - r_s)}{0.5L_{q3}L_{d3} \sin(3\theta_r)} \right) + \frac{(L_{d3} \sin(6\theta_r)(6\omega_r L_{q3} \sin(6\theta_r) - r_s))(L_{q3} \cos(6\theta_r)(6\omega_r L_{d3} \cos(6\theta_r) - r_s))}{(0.5L_{q3}L_{d3} \sin(3\theta_r))^2}$$

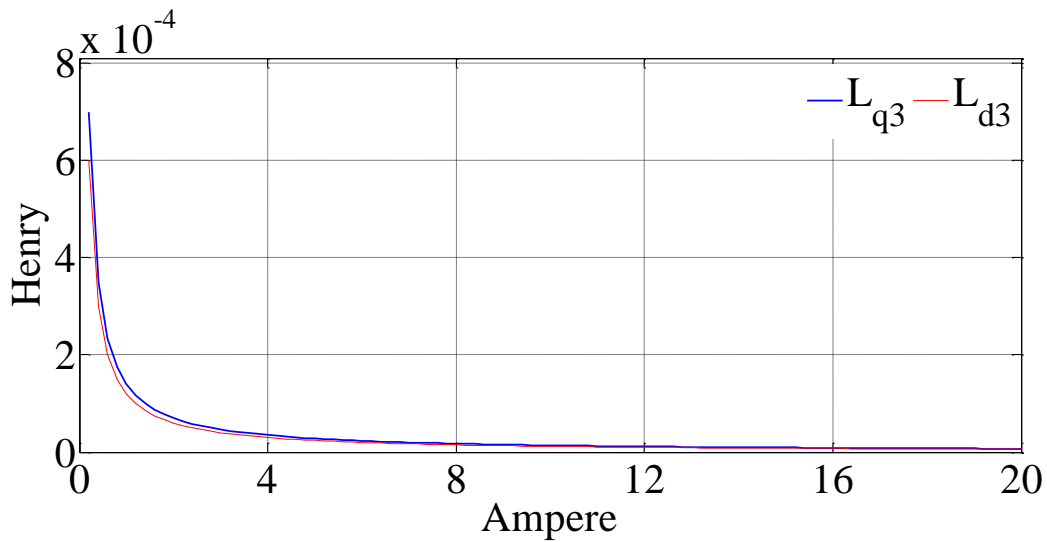


Figure 5.10: The magnitude of third sequence inductance of the stationary reference frame versus stator current.

Using FEMM the magnitude of q and d inductances of the third sequence versus the RMS value of the stator current are generated as Figure 5.10. Using the inductances of the Figure 5.10 the poles of the equation (5.130) can be plotted as Figure 5.11. It can be seen that for all the ranges of the stator current the poles are stable.

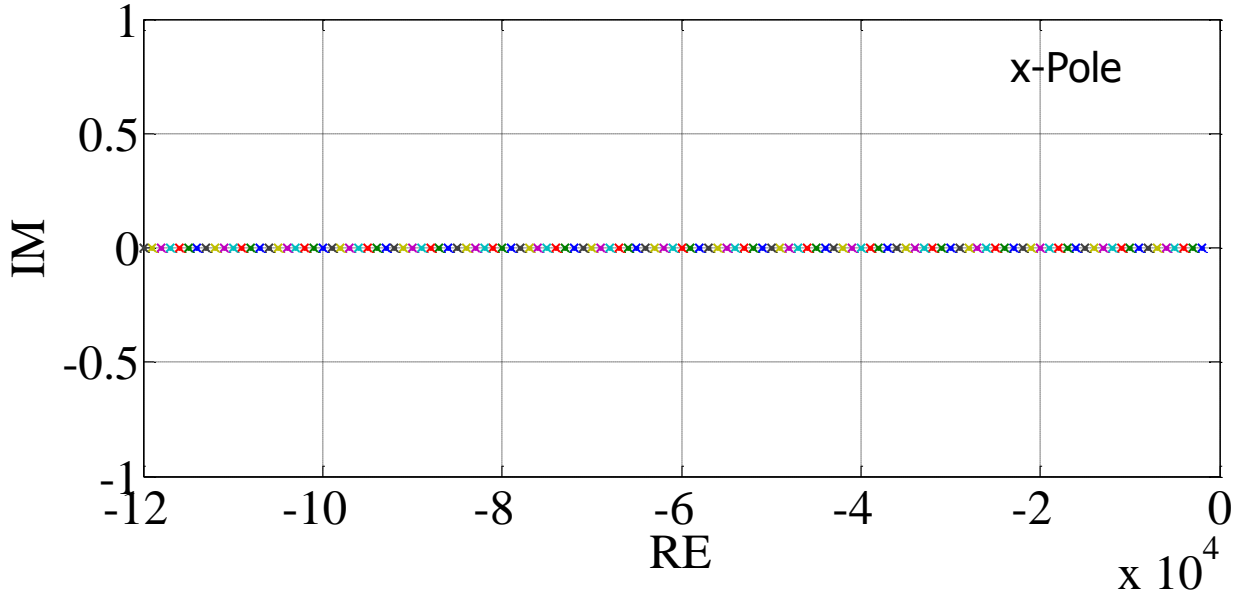


Figure 5.11: The poles of the third sequence circuit for different stator current levels.

5.5 Implementation of the Sensorless Nine-Phase IPM Drive

5.5.1 Discretizing the Controller

The controllers that were designed in the previous sections of this chapter are discretized and translated to C++ language and implemented in the DSP. The discretizing process can be done using the dynamic equations of the controller. From the equation (5.25) the equation of the speed control loop can be discretized. The equation (5.25) is repeated in equation (5.134).

$$p\omega_r = \left(K_{p\omega} + \frac{K_{I\omega}}{S} \right) (\omega_r^* - \omega_r) = \delta_{\omega_r} \quad (5.134)$$

As it can be seen this equation is in the 'S' domain. To convert it to the 'Z' domain the 'S' can be replaced by Tustin approximation which is one of the simplest 'Z' domain approximations

and therefore, it is easy to implement in DSP [159]. The Tustin approximation of the term ‘S’ is represented in equation (5.135).

$$S = \frac{2}{T} \frac{1 - z^{-1}}{1 + z^{-1}} \quad (5.135)$$

Where: T is the sampling period of the controller. By substituting the equation (5.135) in to the equation (5.134) the controller loop can be rewritten as:

$$2\delta_{\omega_r}(1 - z^{-1}) = (2K_{P\omega}(1 - z^{-1}) + T(1 + z^{-1})K_{I\omega})(\omega_r^* - \omega_r) \quad (5.136)$$

The equation (5.136) can be rewritten as:

$$2\delta_{\omega_r} - 2\delta_{\omega_r}z^{-1} = 2K_{P\omega}e_{\omega_r} - 2K_{P\omega}z^{-1}e_{\omega_r} + TK_{I\omega}e_{\omega_r} + TK_{I\omega}z^{-1}e_{\omega_r} \quad (5.137)$$

Where:

$$e_{\omega_r} = \omega_r^* - \omega_r \quad (5.138)$$

In the above equations the term ‘ z^{-1} ’, represents one delay. Therefore, it can be replaced by a delay in the sampling process. The resulting equation can be presented as:

$$\begin{aligned} \delta_{\omega_r}(K) &= K_{P\omega}e_{\omega_r}(K) - K_{P\omega}e_{\omega_r}(K-1) + \\ &\frac{T}{2}K_{I\omega}e_{\omega_r}(K) + \frac{T}{2}K_{I\omega}e_{\omega_r}(K-1) + \delta_{\omega_r}(K-1) \end{aligned} \quad (5.139)$$

Where K is the sample number. The output of this control loop can be used to generate the reference of the q axis current according to the equation (5.140).

$$\begin{aligned} &(L_{q1q1} - L_{d1d1})^2 i_{q1r}^*(K) + \frac{4}{9P}(\delta_{\omega}(K) + T_L(K))\lambda_{pmd1r} i_{q1r}^*(K) \\ &- \left(\frac{4}{9P}(\delta_{\omega}(K) + T_L(K)) \right)^2 = 0 \end{aligned} \quad (5.140)$$

The reference of the q axis current that is generated by the equation (5.140) can be used in equation (5.141) to generate the reference current of the d axis current. The equation (5.141) is the same as equation (5.24) that is derived from the minimum loss strategy.

$$i_{d1r}^*(K) = \frac{-\frac{\lambda_{pmd1r}}{(L_{d1d1} - L_{q1q1})} \pm \sqrt{\frac{\lambda_{pmd1r}^2}{(L_{d1d1} - L_{q1q1})^2} + 4i_{q1r}^*(K)^2}}{2} \quad (5.141)$$

Now the q and d axis currents reference can be used in the current regulators dynamic equations to generate the output voltages. The equation (5.142) shows the dynamic equation for the q axis current.

$$\delta_{qs}(K) = \left(K_{pq} + \frac{k_{iq}}{S} \right) e_{iq}(K) \quad (5.142)$$

Where:

$$e_{iq}(K) = (i_{q1r}^*(K) - i_{q1r}(K)) \quad (5.143)$$

Substituting the 'S' from the equation (5.135) into the equation (5.143) results in:

$$2(1 - z^{-1})\delta_{qs}(K) = 2K_{pq}(1 - z^{-1})e_{iq}(K) + Tk_{iq}(1 + z^{-1})e_{iq}(K) \quad (5.144)$$

In the above equation the term ' z^{-1} ', is one step delay therefore the equation (5.144) can be rewritten as:

$$\begin{aligned} \delta_{qs}(K) &= K_{pq}e_{iq}(K) - \frac{e_{iq}(K-1)}{2} + 2K_{pq}Tk_{iq}e_{iq}(K) \\ &+ 2K_{pq}Tk_{iq}e_{iq}(K-1) + \delta_{qs}(K-1) \end{aligned} \quad (5.145)$$

The current regulator for the d axis current also can be discretized using the dynamic equation of the d axis controller.

$$\delta_{ds}(K) = \left(K_{pd} + \frac{K_{id}}{S} \right) e_{id}(K) \quad (5.146)$$

Where:

$$V_{d1r}(K) = \delta_{ds}(K) + \omega_r(K)L_{q1q1}i_{q1r}(K) \quad (5.150)$$

Also the voltage equation for q axis can be expressed as:

$$V_{q1r}(K) = \delta_{qs}(K) - \omega_r(K)L_{d1d1}i_{d1r}(K) - \omega_r(K)\lambda_{pmd1r} \quad (5.151)$$

Using the generated discrete equations, the flow chart of the machine controller is generated according to Figure 5.12.

5.5.2 Discretizing the Position Estimator

The position observer (designed in section 5.4) is composed of low pass filters, heterodyning and Luenberger observer. All the components should be discretized to be implemented in the DSP. The first step is to discretize the filter. The filter transfer function is presented in equation (5.152).

$$f = \frac{10^6}{S^2 + 1414S + 10^6} \quad (5.152)$$

Now, to derive the discretized function the term ‘S’ can be substituted with the equation (5.153).

$$f = \frac{i_o}{i_{in}} = \frac{10^6}{\left(\frac{2}{T} \frac{1-z^{-1}}{1+z^{-1}}\right)^2 + 1414\left(\frac{2}{T} \frac{1-z^{-1}}{1+z^{-1}}\right) + 10^6} \quad (5.153)$$

Then finally to implement the equation in the DSP is written in the below form.

$$f = \frac{i_o}{i_{in}} = \frac{(T(1+z^{-1}))^2 10^6}{4(1-z^{-1})^2 + 2828(T(1+z^{-1}))(1-z^{-1}) + 10^6(T(1+z^{-1}))^2} \quad (5.154)$$

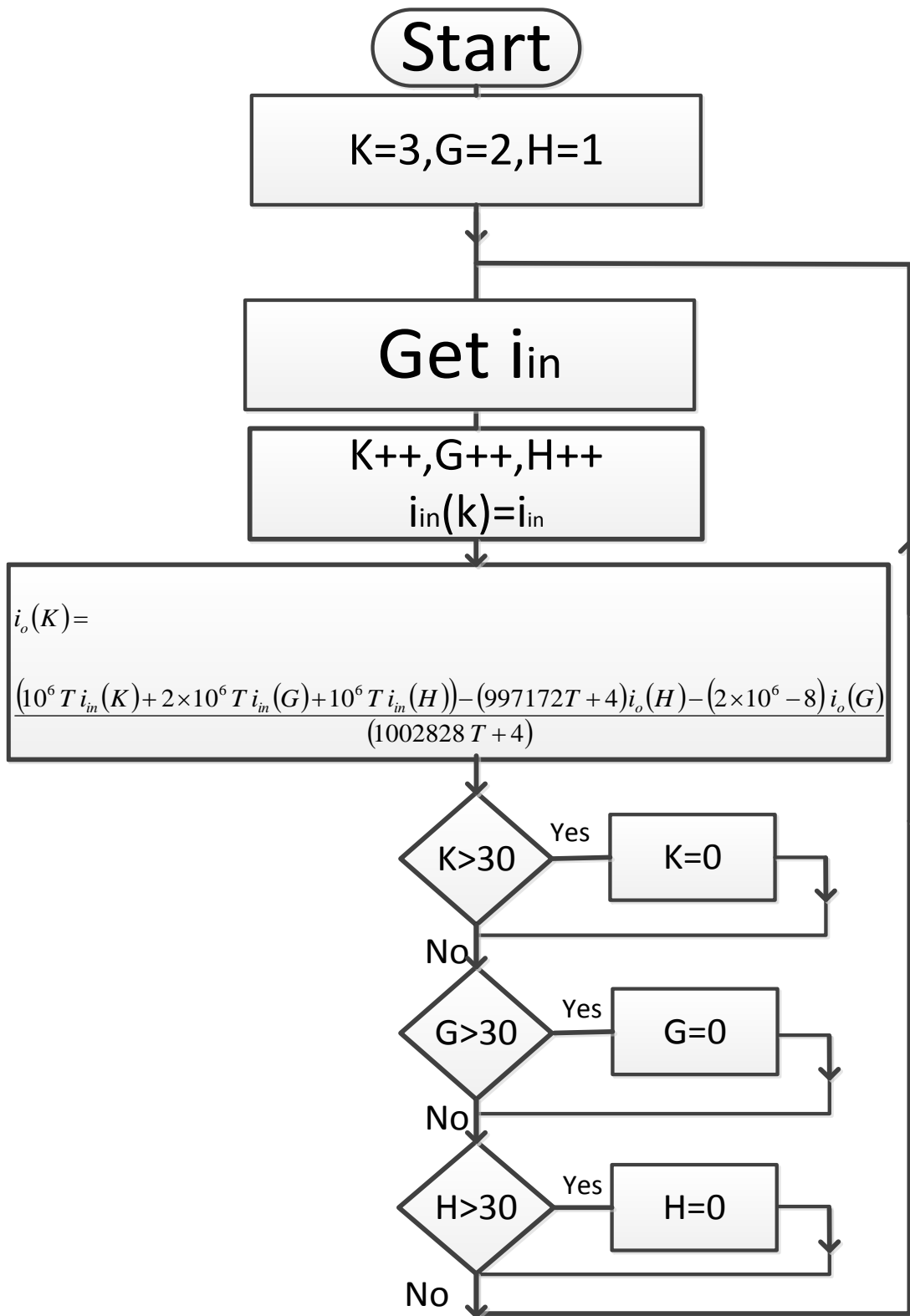


Figure 5.13: The flow chart for the filter.

$$i_o(K) = \frac{\left(\begin{array}{l} (10^6 T i_{in}(K) + 2 \times 10^6 T i_{in}(K-1) + 10^6 T i_{in}(K-2)) \\ -(997172T + 4)i_o(K-2) - (2 \times 10^6 - 8)i_o(K-1) \end{array} \right)}{(1002828 T + 4)} \quad (5.155)$$

Now the filter can be shown in the flow chart of Figure 5.13. For the observer (shown in Figure 5.14) itself (with B=0) transfer functions can be generated.

$$\frac{\hat{\omega}_r}{\varepsilon} = \frac{K_{I1} + K_{p1}}{JS} + K_{p2} \quad (5.156)$$

$$\hat{\theta}_r = \frac{\hat{\omega}_r}{S} \quad (5.157)$$

By combining the equations (5.156) and (5.157) the transfer function between the input error and the output can be generated as:

$$\frac{\hat{\theta}_r}{\varepsilon} = \frac{K_{I1} + SK_{p1} + JK_{p2}S^2}{JS^3} \quad (5.158)$$

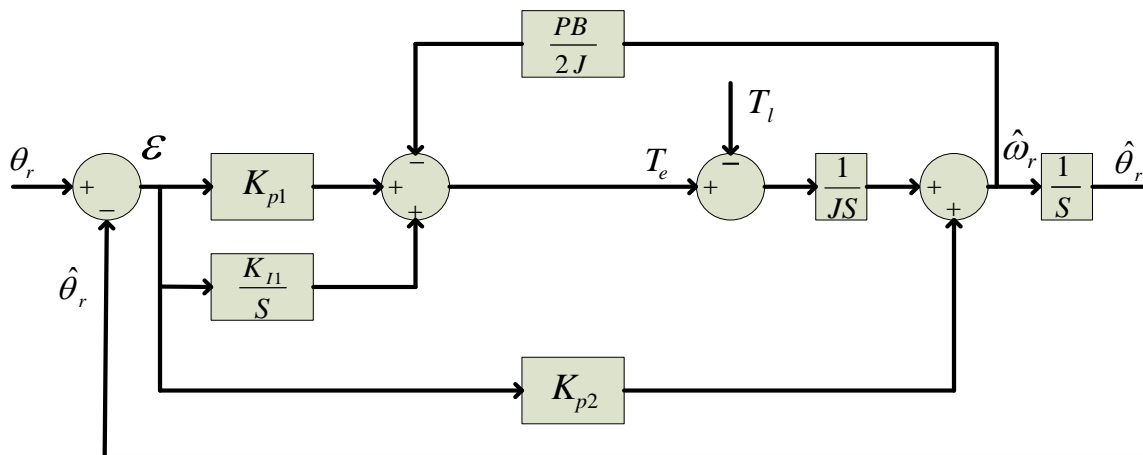


Figure 5.14: The position observer.

Finally, after transferring the equation (5.158) to the 'Z' domain the observer transfer function can be represented as:

$$\frac{\hat{\theta}_r}{\varepsilon} = \frac{K_{I1}(T(1+z^{-1}))^3 + 2K_{p1}(1-z^{-1})(T(1+z^{-1}))^2 + JK_{p2}(2(1-z^{-1}))^2(T(1+z^{-1}))}{2J(1-z^{-1})^3} \quad (5.159)$$

And from there:

$$2J\hat{\theta}_r = -2J\hat{\theta}_r(-3z^{-1} + 3z^{-2} - z^{-3}) + K_{I1}T^3(1 + 3z^{-1} + 3z^{-2} + z^{-3}) \quad (5.160)$$

$$+ 2K_{p1}T^2(1 + z^{-1} - z^{-2} - z^{-3}) + 4TJK_{p2}(1 - z^{-1} - z^{-2} + z^{-3})$$

$$2J\hat{\theta}_r(K) = 6J\hat{\theta}_r(K-1) - 6J\hat{\theta}_r(K-2) + 2J\hat{\theta}_r(K-3) + K_{I1}T^3\varepsilon(K)$$

$$+ 3K_{I1}T^3\varepsilon(K-1) + 3K_{I1}T^3\varepsilon(K-2) + K_{I1}T^3\varepsilon(K-3) + 2K_{p1}T^2\varepsilon(K)$$

$$+ 2K_{p1}T^2\varepsilon(K-1) - 2K_{p1}T^2\varepsilon(K-2) - 2K_{p1}T^2\varepsilon(K-3) + 4TJK_{p2}\varepsilon(K) \quad (5.161)$$

$$- 4TJK_{p2}\varepsilon(K-1) - 4TJK_{p2}\varepsilon(K-2) + 4TJK_{p2}\varepsilon(K-3)$$

Where:

$$\varepsilon(K) = \theta_r(K) - \hat{\theta}_r(K) \quad (5.162)$$

Using the Equation (5.162) the flow chart of the observer can be presented as Figure 5.15.

5.6 Sensorless Nine-Phase IPM Drive

In this section, the performance of the designed position observer and the controller are verified using simulation and experimental results. The simulation is done using MATLAB/Simulink and the experiment is done using DSP-FPGA controller.

5.6.1 Constant Volt/Hz Open-Loop Operation

In the first step, to check the performance of the proposed observer, the full order model of the 2hp, nine-phase IPM machine is simulated and the high frequency voltages are injected in

addition to the fundamental voltage under a constant Volt/Hz ($v/f = 1.8$) open-loop operation. The high frequency voltage (980Hz), (5V peak) set is injected in the third sequence channel of the machine. In simulation the initial speed of the machine is set at the negative rated and it increases to zero and after a short stop, the speed increases to the positive rated speed. Similarly, the proposed rotor angle estimation method has been implemented on a 2hp, nine-phase IPM using a DSP-FPGA controller which controls the machine via a nine phase voltage source inverter (switching frequency of 6 kHz).

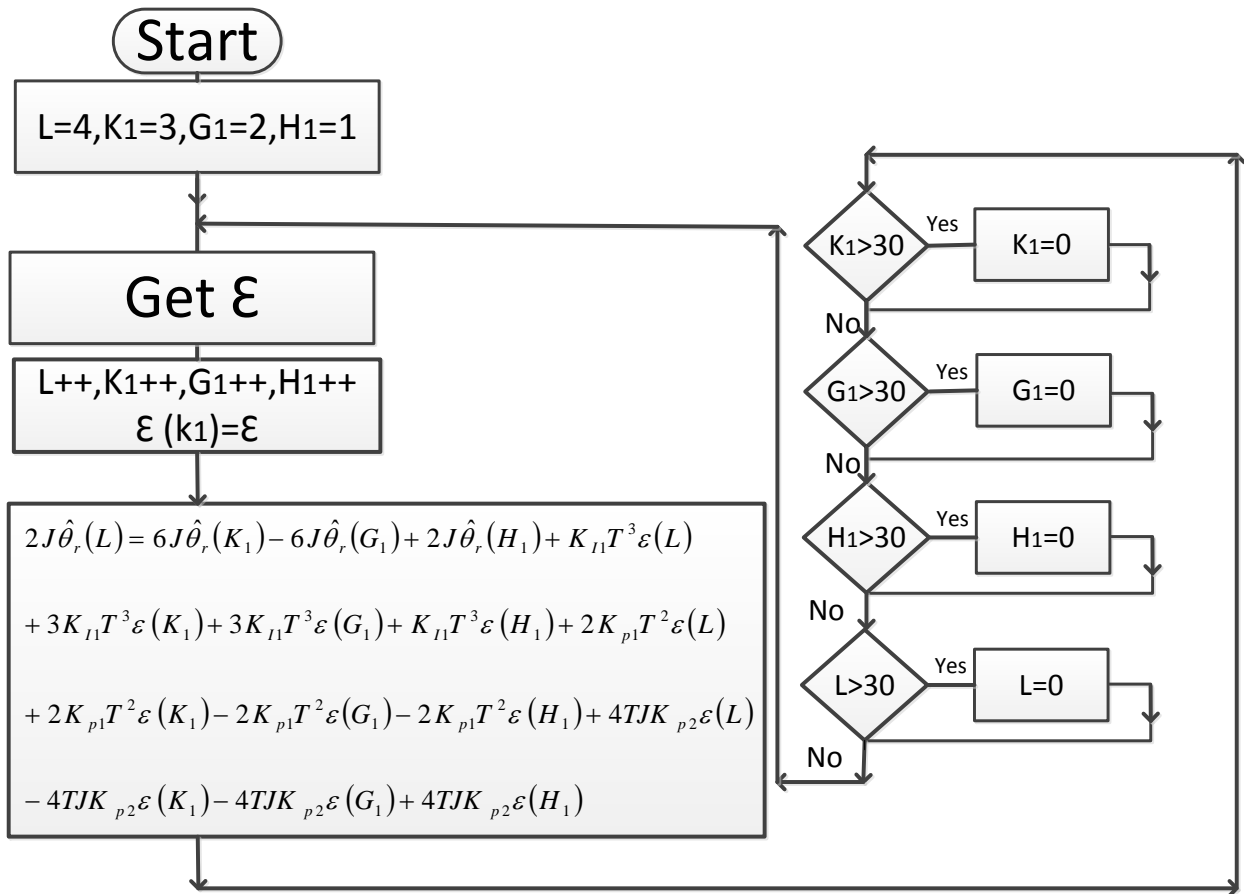


Figure 5.15: The flow chart for the observer.

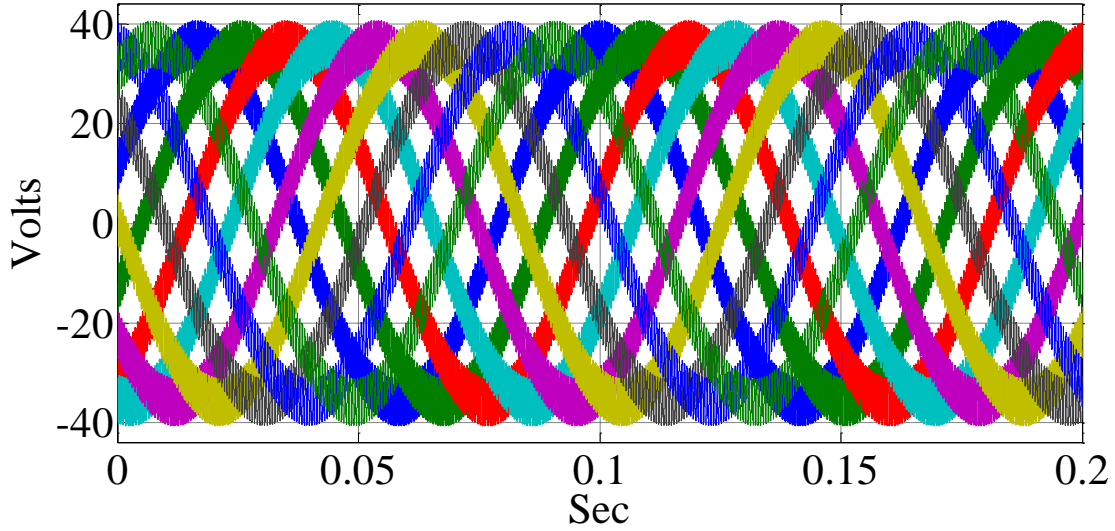
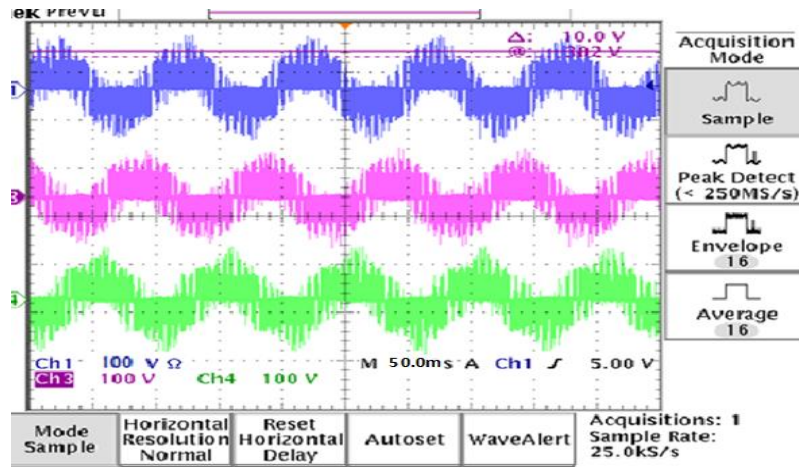


Figure 5.16: Simulation results for the nine-phase voltages applied to the stator windings.

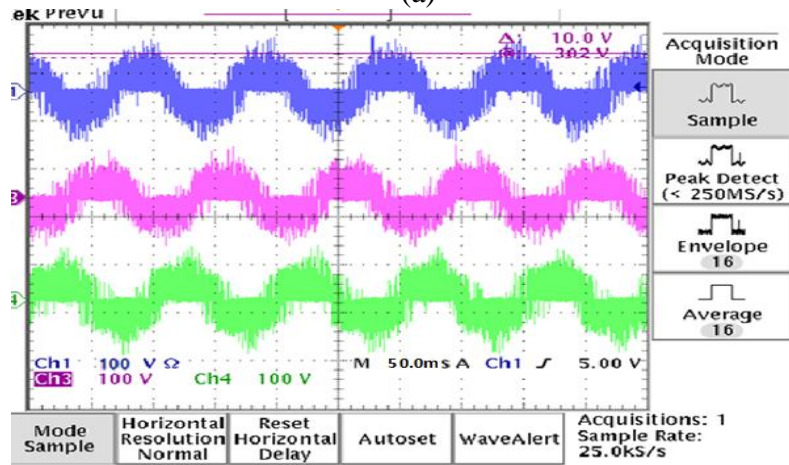
The discretized model of the observer has been implemented in the DSP (DSK TMS320C6713). The current sensors are connected to the controller with nine Analog/Digital converters with the sampling rate of 50 kHz. After generating the high frequency voltages inside the DSP they are sent to the FPGA which generates the PWM pulses for the inverter. Figure 5.16 and 5.17 show stator voltages after high frequency injection for simulation and experimental results respectively.

$$\begin{bmatrix} V_a \\ V_b \\ V_c \\ V_d \\ V_e \\ V_f \\ V_g \\ V_h \\ V_m \end{bmatrix} = \begin{bmatrix} 1.8f \cos(f \times 2\pi t) + 5 \cos(980 \times 2\pi t) \\ 1.8f \cos(f \times 2\pi t + \alpha) + 5 \cos(-3\alpha - 980 \times 2\pi t) \\ 1.8f \cos(f \times 2\pi t + 2\alpha) + 5 \cos(-6\alpha - 980 \times 2\pi t) \\ 1.8f \cos(f \times 2\pi t + 3\alpha) + 5 \cos(-9\alpha - 980 \times 2\pi t) \\ 1.8f \cos(f \times 2\pi t + 4\alpha) + 5 \cos(-12\alpha - 980 \times 2\pi t) \\ 1.8f \cos(f \times 2\pi t + 5\alpha) + 5 \cos(-15\alpha - 980 \times 2\pi t) \\ 1.8f \cos(f \times 2\pi t + 6\alpha) + 5 \cos(-18\alpha - 980 \times 2\pi t) \\ 1.8f \cos(f \times 2\pi t + 7\alpha) + 5 \cos(-21\alpha - 980 \times 2\pi t) \\ 1.8f \cos(f \times 2\pi t + 8\alpha) + 5 \cos(-24\alpha - 980 \times 2\pi t) \end{bmatrix} \quad (5.163)$$

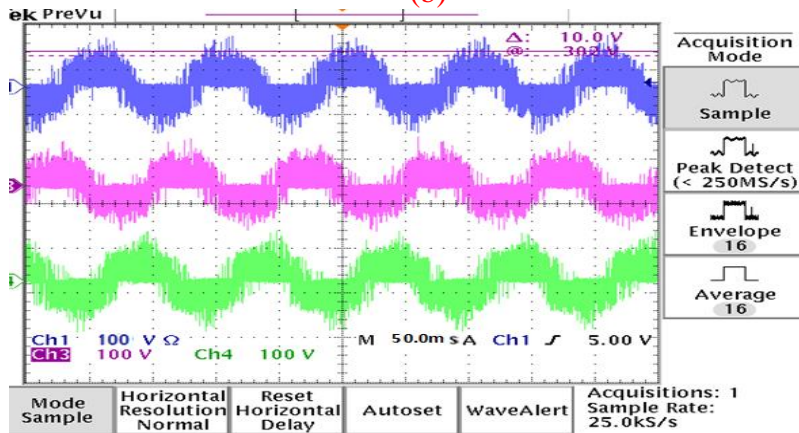
$$\alpha = 2 \frac{\pi}{9}, f = \text{Desiered Frequency}$$



(a)



(b)



(c)

Figure 5.17: Experimental results for the nine-phase voltages applied to the stator windings, (a) Phases ‘a’, ‘d’ and ‘g’, (b) Phases ‘b’, ‘e’ and ‘h’, (c) Phases ‘c’, ‘f’ and ‘i’ (40 Volt/scale).

Nine-phase currents of the machine for simulation and experimental results are shown in Figures 5.18 and 5.19 respectively. From these figures, the effect of the stator magnetic saturation

can be seen in the practical results. These currents are used for controller feedback and position estimation. Using the transformation matrix of equation (5.63) the different components of the nine phase currents are extracted which can be used for control and position estimation. The fundamental component of the stationary reference frame currents ‘ i_{d1} ’ and ‘ i_{q1} ’ for simulation and experimental results are shown in Figures 5.20 and 5.21 respectively. These currents can be used for the controller feedback. From this current it can be seen that, the practical results show more harmonics compared with the simulation result. The harmonics of the practical results are coming from some details that are not modeled in simulation such as stator magnetic saturation.

The third sequence (q,d_3) circuit currents (i_{d3}, i_{q3}) for simulation and experimental results are shown in Figures 5.22 and 5.23 respectively. These currents are used for the rotor position estimation. Currents of Figure 5.22 and 5.23 have a variable magnitude which are due to the interaction between the rotor saliency and the high frequency injected voltages. The time scales of these figures are selected such that to show the variable magnitude of the signals.

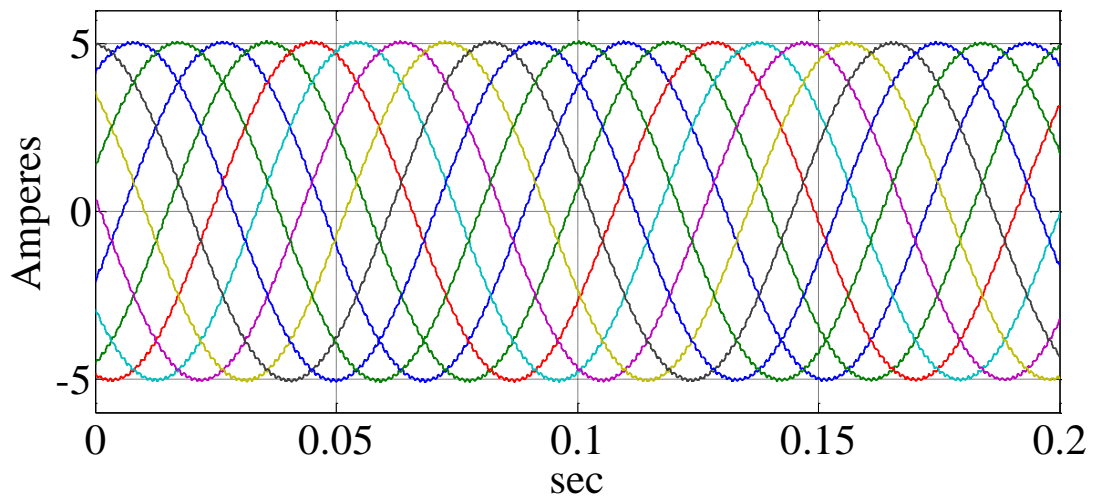
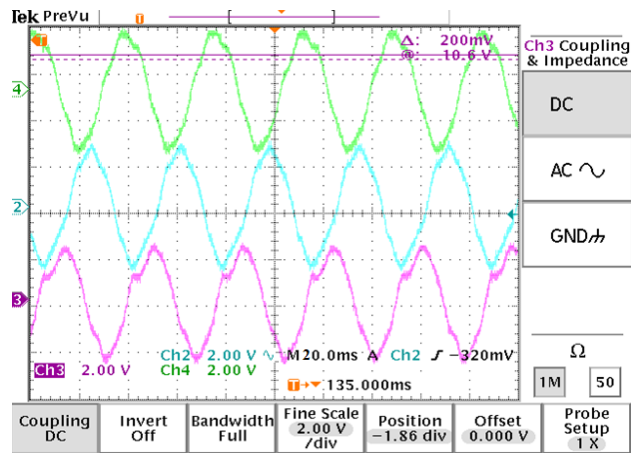
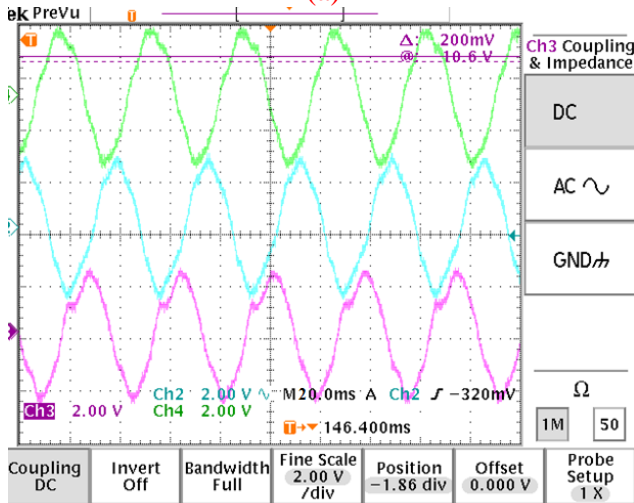


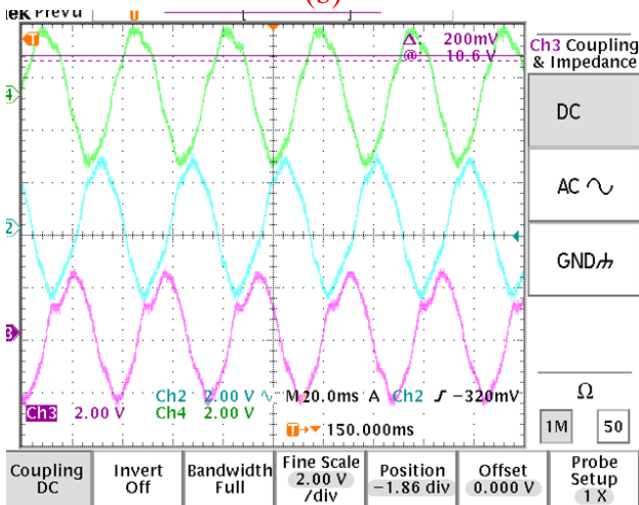
Figure 5.18: Simulation results for nine phase stator currents.



(a)



(b)



(c)

Figure 5.19: Experimental results for the nine-phase currents of the stator windings, (a) Phases ‘a’, ‘d’ and ‘g’, (b) Phases ‘b’, ‘e’ and ‘h’, (c) Phases ‘c’, ‘f’ and ‘i’ (5A/scale).

It is noted that since the high frequency currents are extracted using the sequence analysis in the stationary reference frame, there is no need for heterodyning and high pass filtering of the

phase currents to extract the high frequency signals from the nine phase currents as required in most of the existing methods.

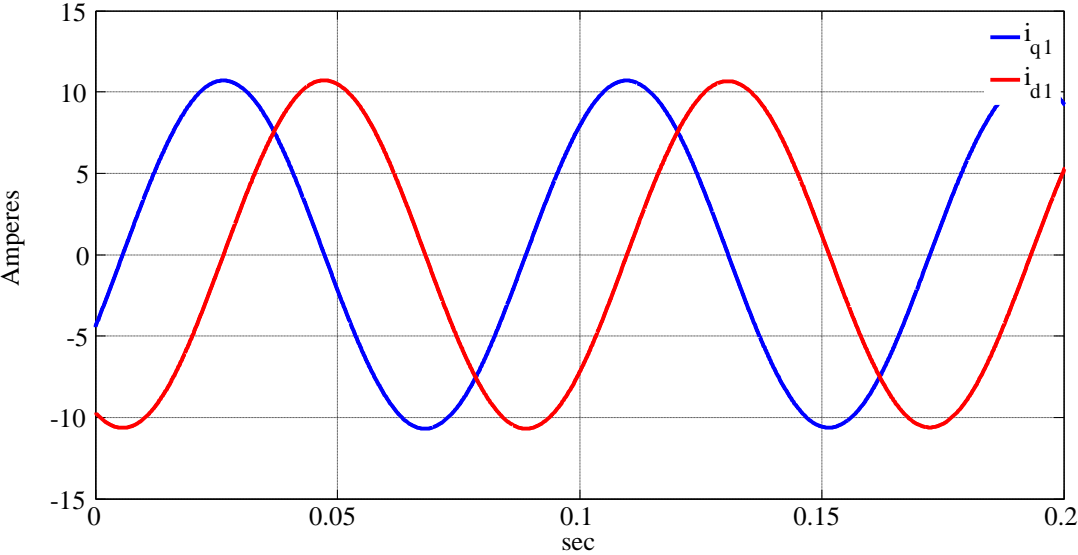


Figure 5.20: Simulation results for fundamental sequence current in stationary reference frame (i_{q1} , i_{d1}).

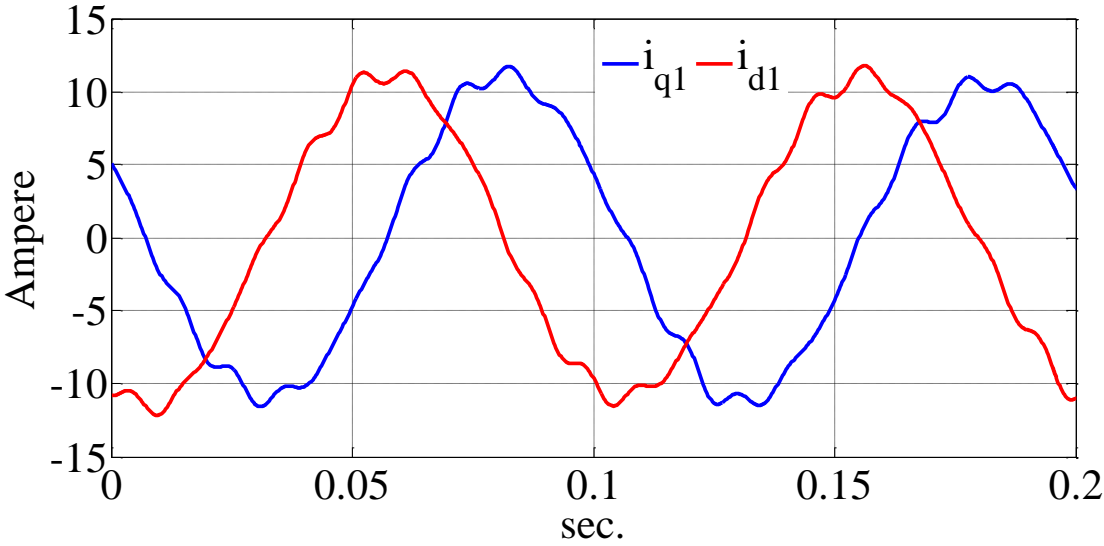


Figure 5.21: Experimental results for fundamental sequence current in stationary reference frame (i_{q1} , i_{d1}).

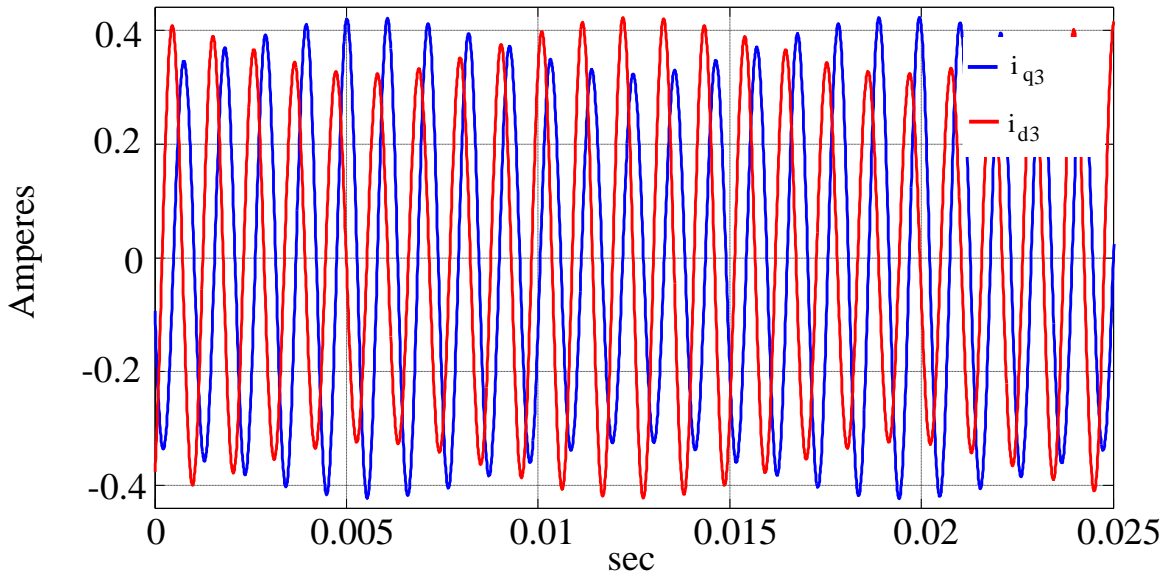


Figure 5.22: Simulation results for third sequence current in the stationary reference frame
(i_{q3} , i_{d3}).

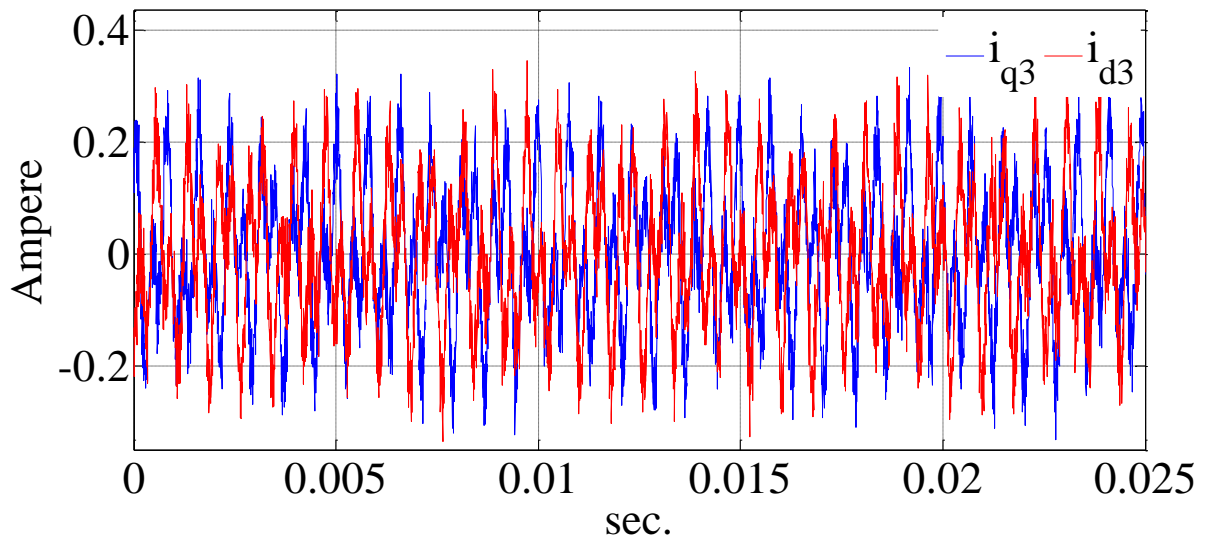


Figure 5.23: Experimental results for third sequence current in the stationary reference frame
(i_{q3} , i_{d3}).

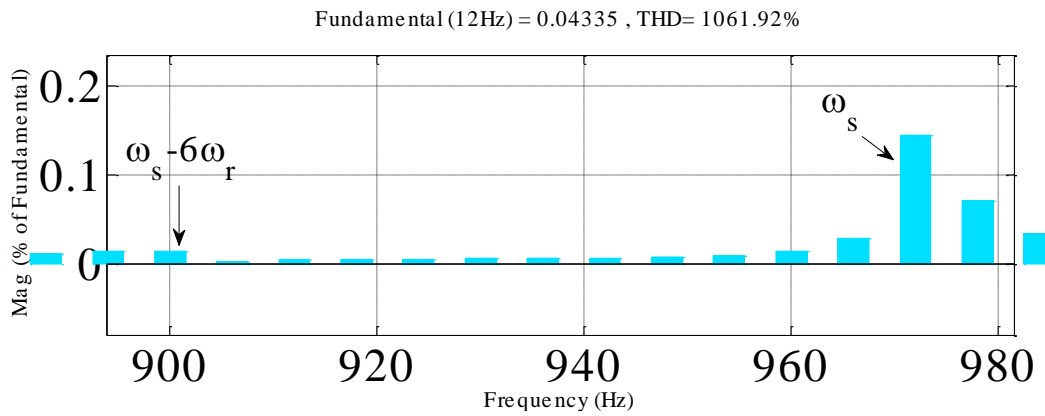


Figure 5.24: The spectrum phase 'a' current (simulation results).

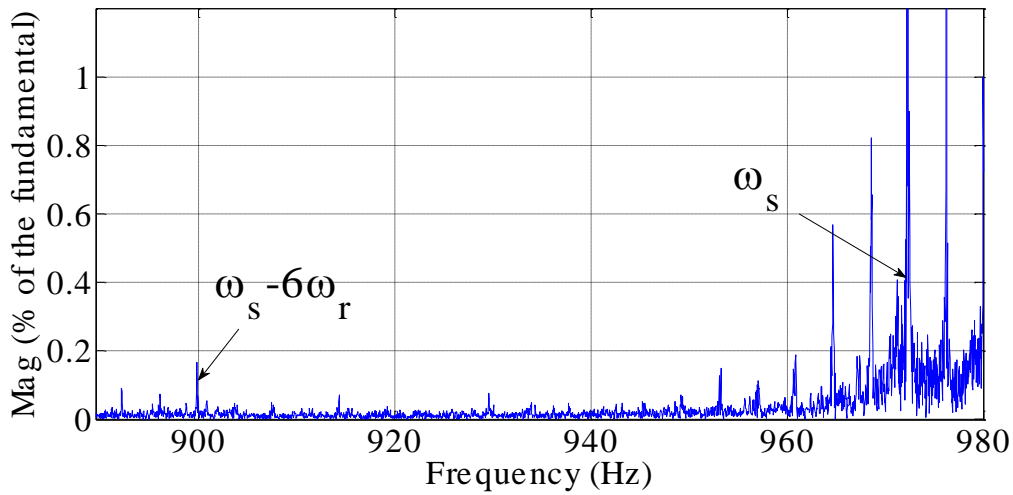


Figure 5.25: The spectrum phase 'a' current (experimental results).

The spectrum of the stator phase currents in the high frequency ranges are shown in the Figures 5.24 and 5.25 for simulation and experiment respectively. The spectrums show the presence of the current component with the same frequency as the frequency of the injected voltages (980 Hz).

Beside the 980 Hz signal, there is another signal with a lower frequency ($\omega_s - 6\omega_r$) related to the rotor speed (pointed in the figures). The signals pointed in the figures can be extracted and

used for the position estimation. The electromagnetic torque of the machine for simulation and experiment are shown in the Figure 5.26 and 5.27 respectively.

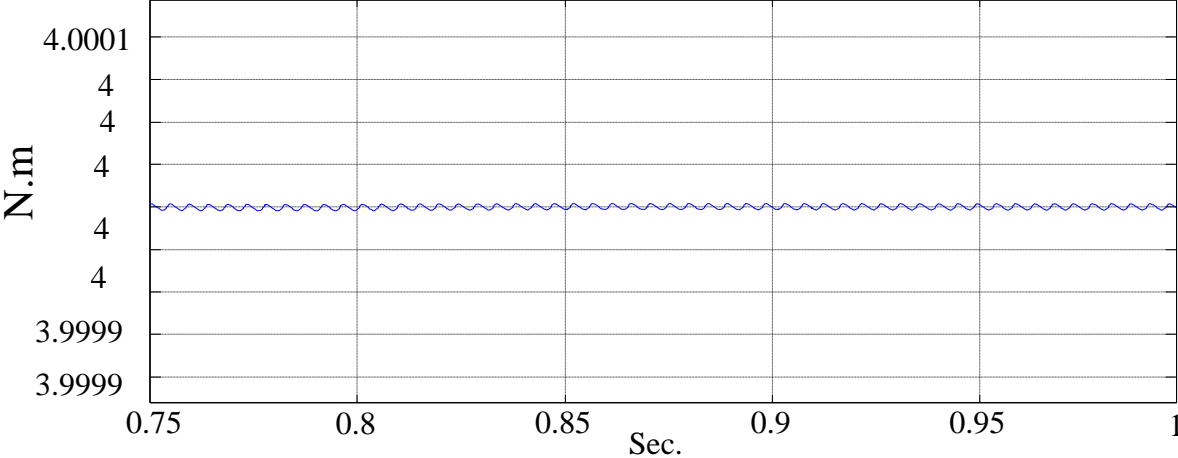


Figure 5.26: The developed electromagnetic torque showing a low ripple content in electromagnetic torque (simulation results).

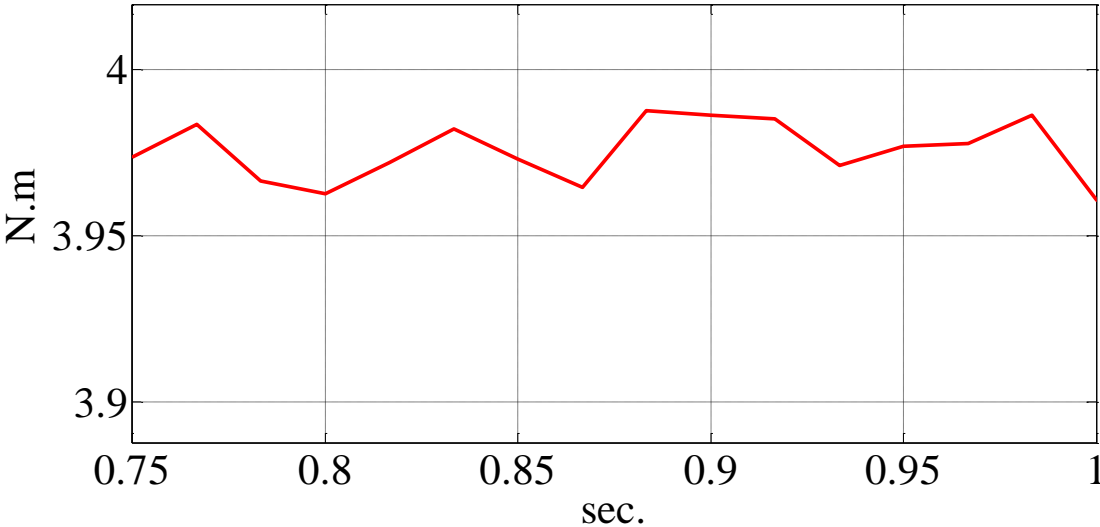


Figure 5.27: The developed electromagnetic torque (experimental results).

The third sequence currents, after heterodyning, are shown in the Figures 5.28 and 5.29 for simulation and experimental results respectively. These currents are filtered to remove their extra

high frequency parts and also they are normalized to have unity magnitude to be compatible with the observer.

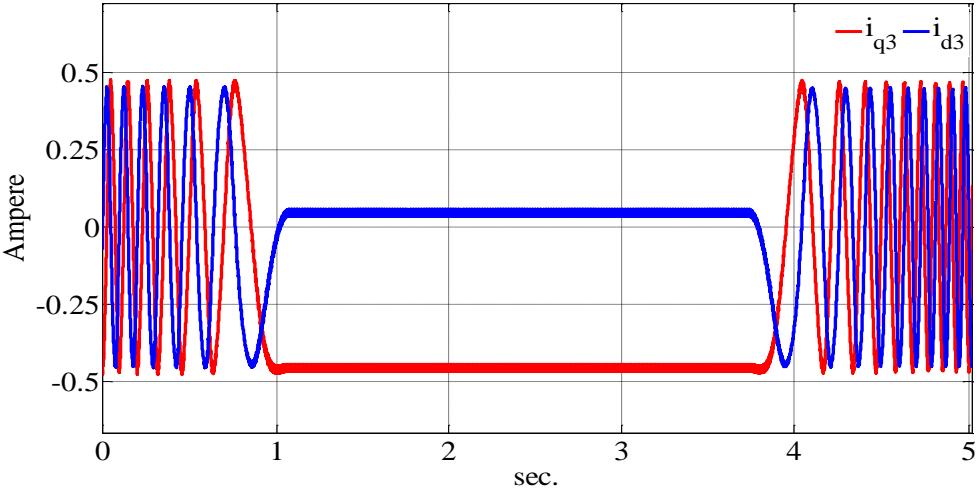


Figure 5.28: The third sequence of the current in stationary reference frame (i_{q3} , i_{d3}) after heterodyning and filtering (simulation results).

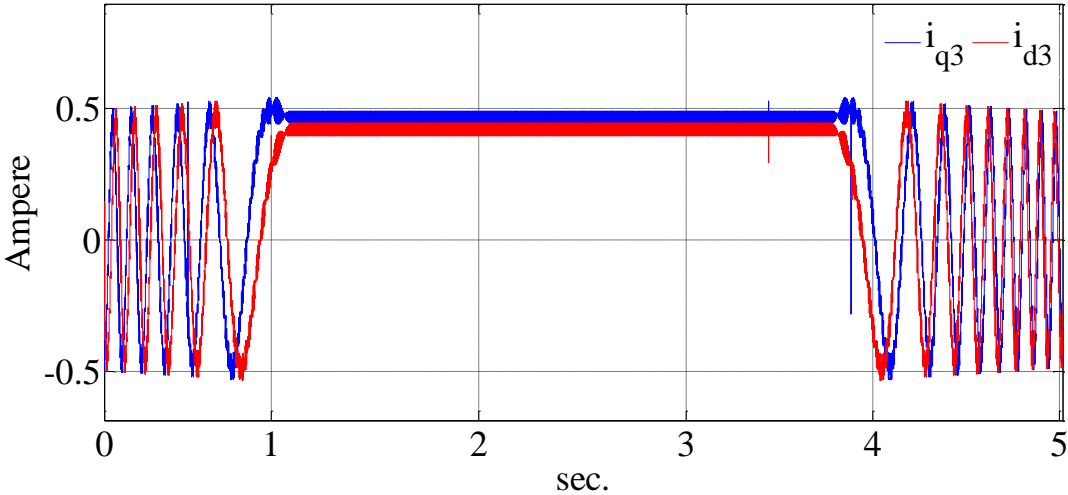


Figure 5.29: The third sequence of the current in stationary reference frame (i_{q3} , i_{d3}) after heterodyning and filtering (experimental results).

The resulting currents after, filtering and normalizing, are shown in the Figure 5.30 and 5.31 for simulation and experimental results, respectively.

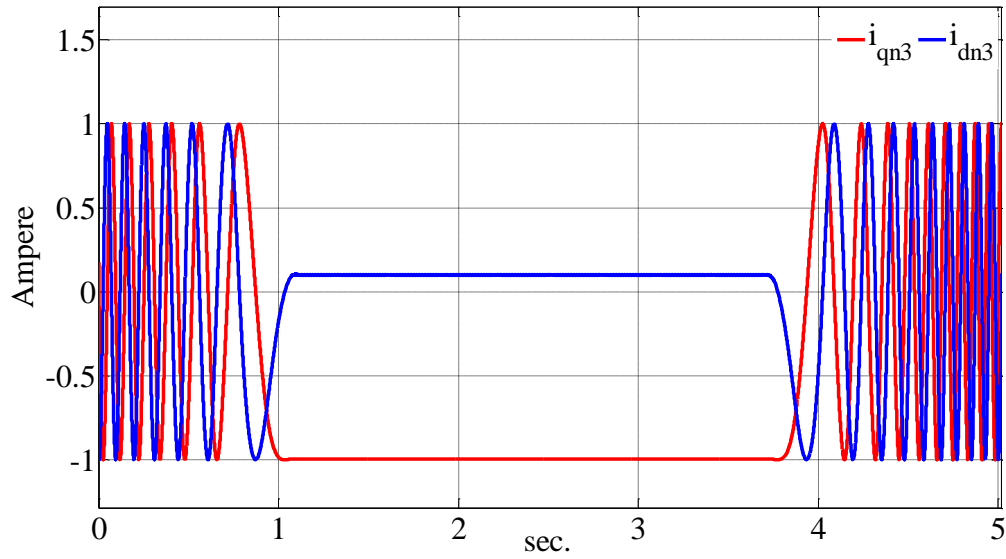


Figure 5.30: The third sequence of the current in stationary reference frame (i_{qn3} , i_{dn3}) after normalizing (simulation results).

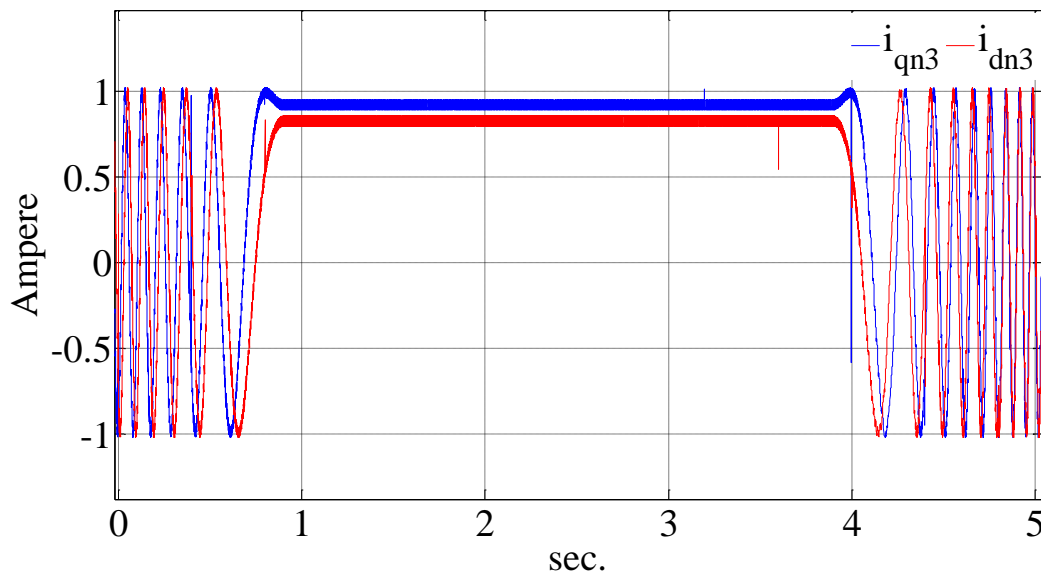
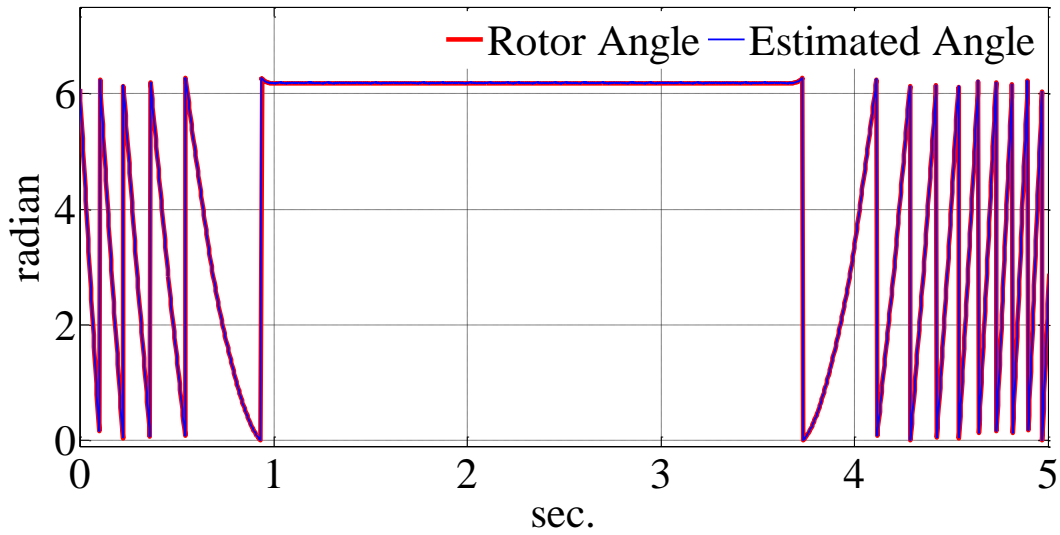
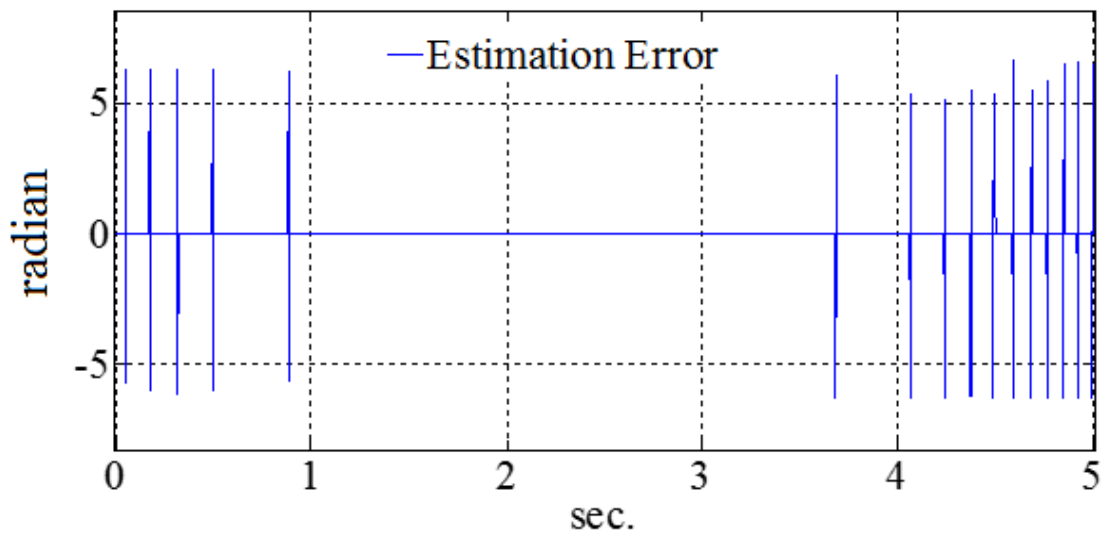


Figure 5.31: The third sequence of the current in stationary reference frame (i_{qn3} , i_{dn3}) after normalizing (experimental results).

In the third harmonic currents, the measured currents show more ripples than the simulated ones. The ripples are mostly coming from sampling noise of the prototype.



(a)

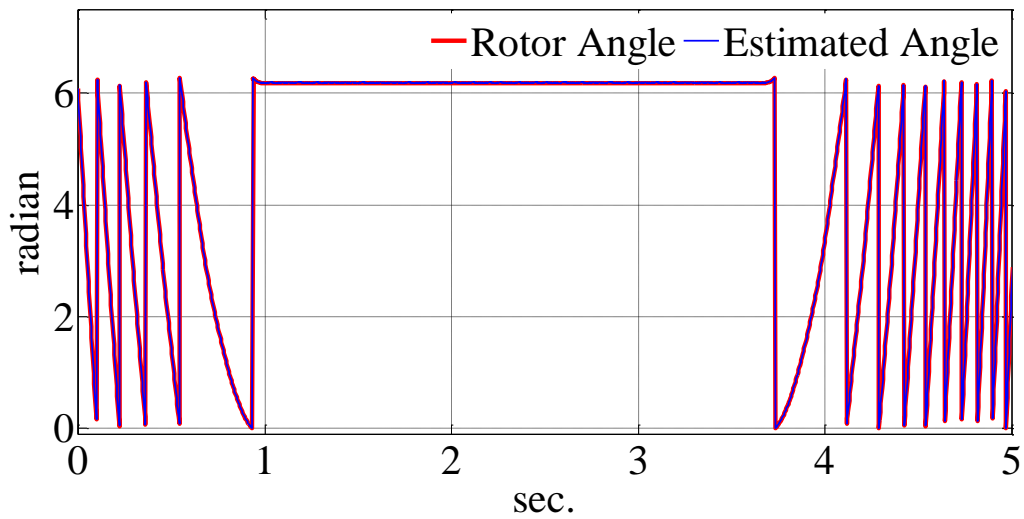


(b)

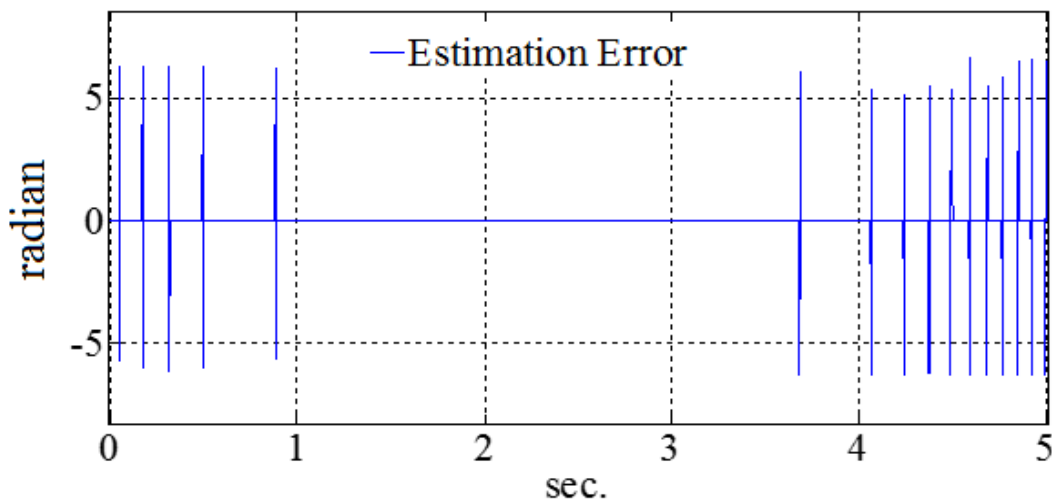
Figure 5.32: (a) The estimated and simulated rotor angle (simulation results), (b) The position estimation error (simulation results).

These currents are injected to the observer to obtain the position of the rotor. The plots of the estimated and actual rotor angles along with the estimation error are shown in Figures 5.32 and 5.33 for full order machine model simulation and experiment respectively. It is observed that, in

the negative, positive and also zero rotor speed regions the rotor position observer follows the rotor position precisely.



(a)

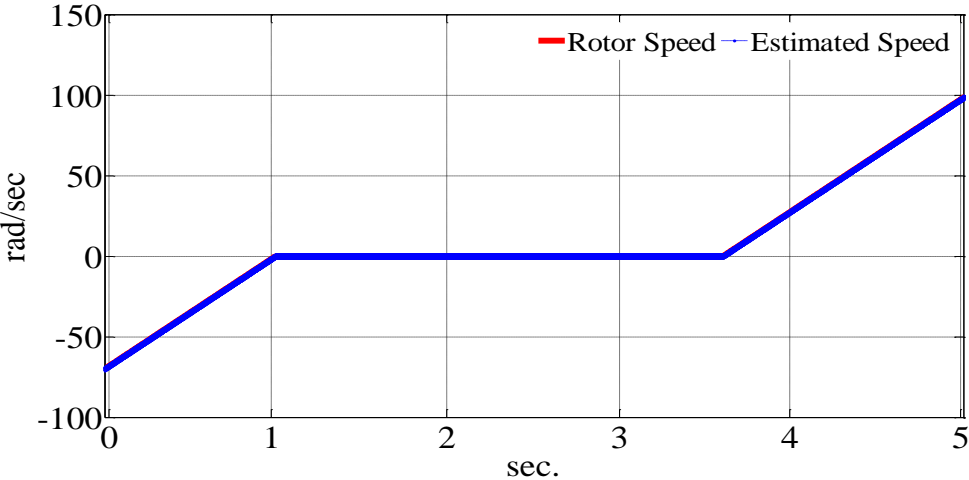


(b)

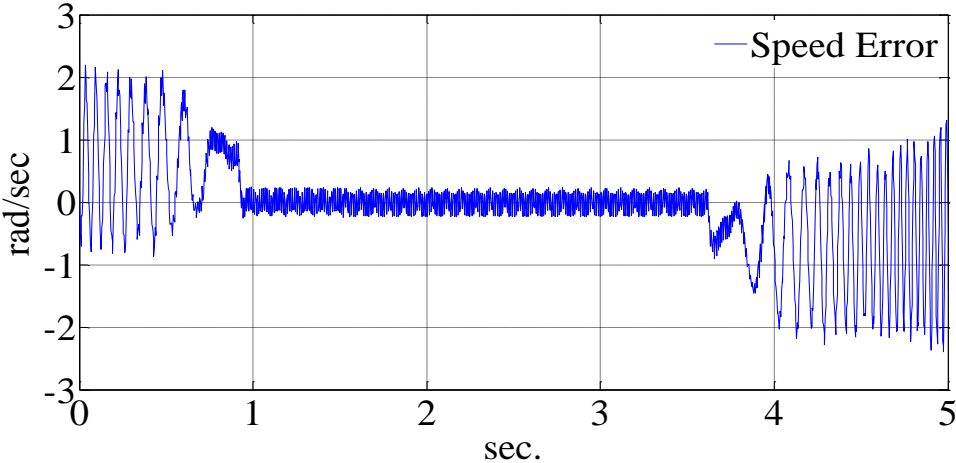
Figure 5.33: (a) The estimated and measured rotor angle (experimental results), (b) The estimation error (experimental results).

The error of the position in Figures 5.32 (b) and 5.33 (b), are mostly due to the natural delay of the observer and the filters. It can be seen more clearly at the moments when the angle jumps between '0' and ' 2π '. At these moments the error appears as big spikes. At zero speed, when there is no jumping, the spikes cannot be seen. Figures 5.34 (a) and 5.35 (a) also show the estimated

speed and rotor speed for the simulation and experiment respectively. It can be seen that the estimator can follow the rotor speed accurately. The errors of the estimated speed are shown in the Figures 5.34 (b) and 5.35 (b) for simulation and experimental results, respectively.



(a)



(b)

Figure 5.34: (a) The simulated and estimated rotor speed (simulation results), (b) The speed estimation error (simulation results).

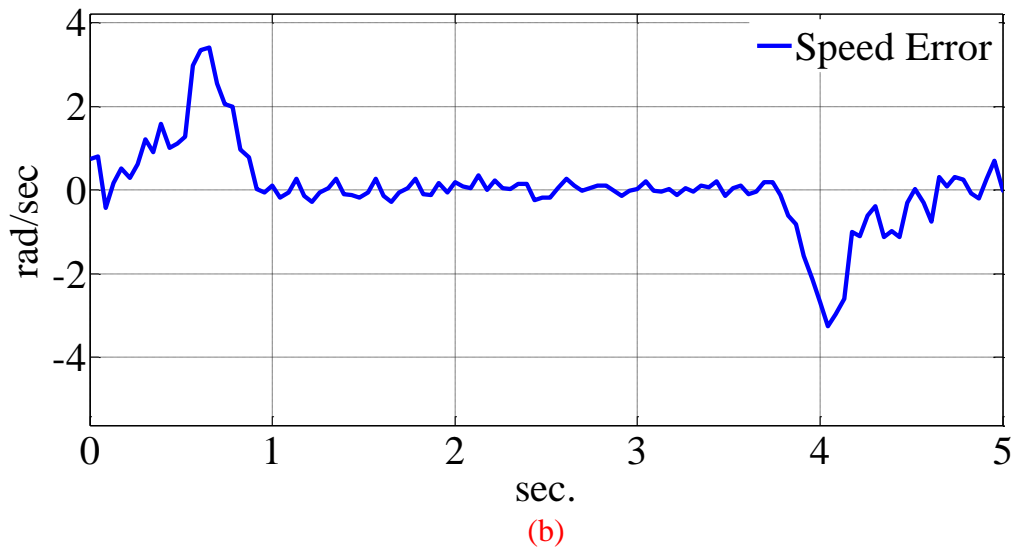
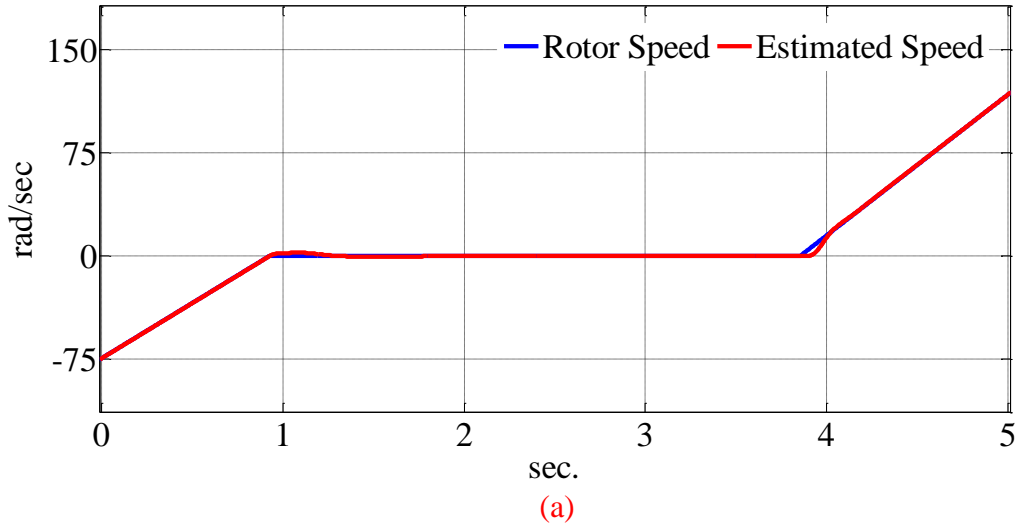


Figure 5.35: (a) The measured and estimated rotor speed (experimental results), (b) The speed error (experimental results).

5.6.2 Vector Control Simulation and Experimental Results

The second test performed on the nine phase machine is a vector control drive in the rotor reference frame. The designed controller (designed in section 5.2) is coupled with the position estimator according to Figure 5.36. As it can be seen in the Figure 5.36, the high frequency signals are injected in the third channel of the machine circuit. The high frequency injection is done in controller level before transforming the voltages in stationary reference frame to natural variables.

The simulation and experimental results for vector control are presented in this section. The simulation and experiment run for 20 seconds and the load is a damping load according to equation (5.164). The speed reference is a trapezoidal one that starts from zero and covers positive and negative rotor speeds.

$$T_L = 0.01\omega_r \quad (5.164)$$

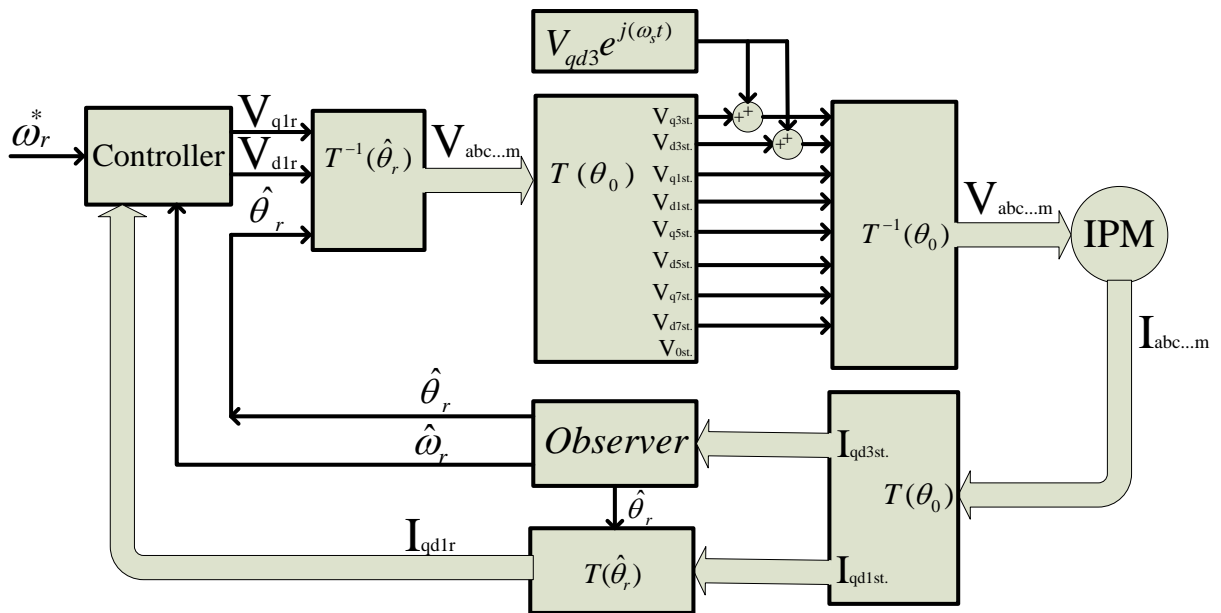
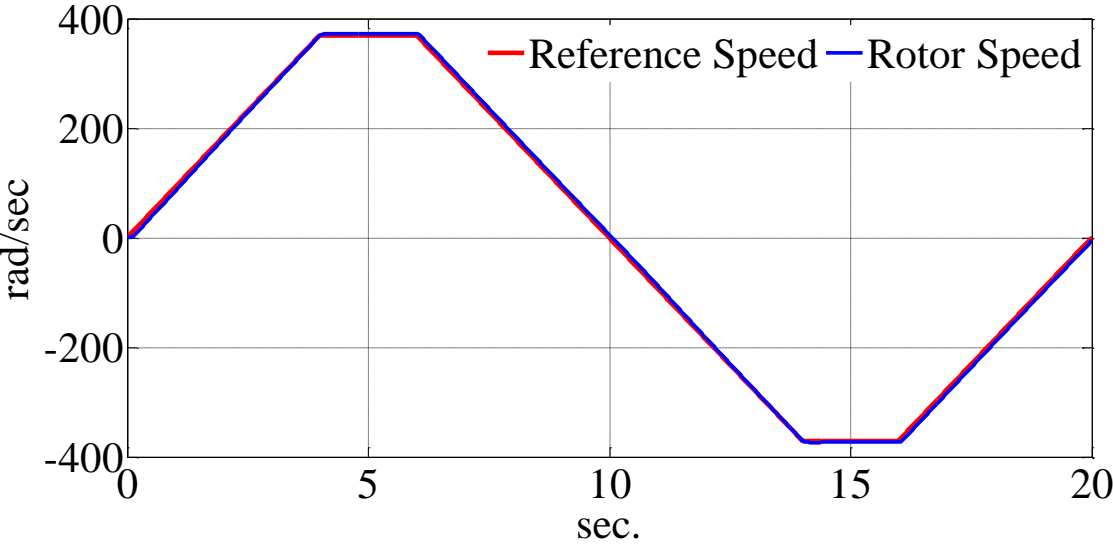


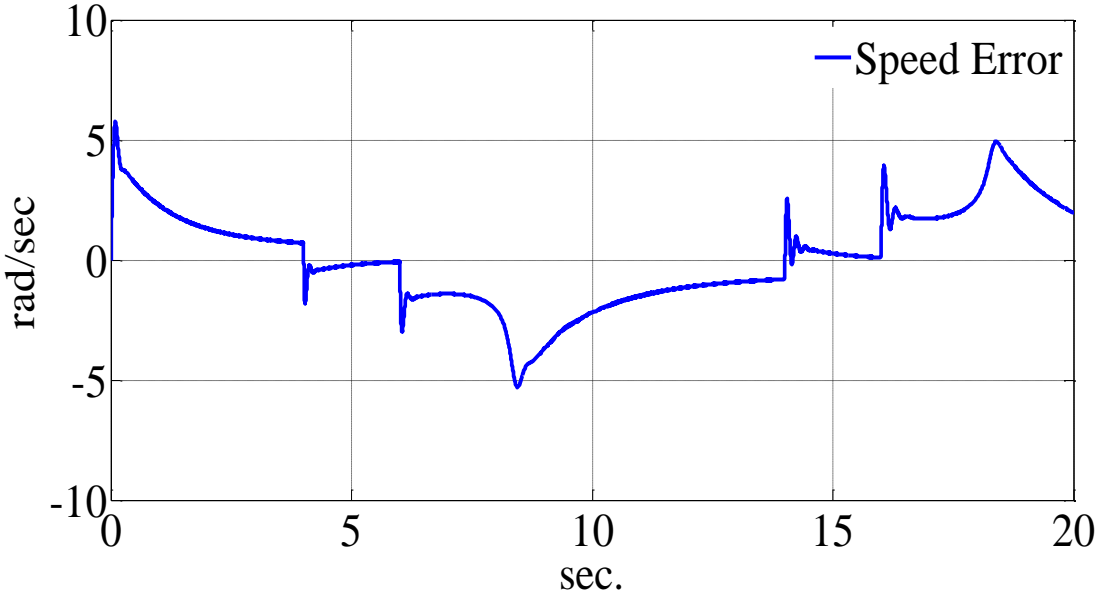
Figure 5.36: The controller of the IPM machine with observer.

The following figures show the drive results. The rotor speeds for simulation and experiment are shown in Figures 5.37 and 5.38 respectively. Figure 5.37 (a) shows the reference speed and the rotor speed together. The speed error is also shown in the Figure 5.37 (b). It can be seen that the drive can track the reference speed while operating in negative and positive ranges. Figure 5.38 (a) shows the reference and feedback rotor speed from the experiment. The speed error is also shown in the Figure 5.38 (b). The drive uses the controller in the rotor reference frame to control the machine speed according to the trapezoidal speed reference of the Figure 5.38. In this

drive the q axis reference current is generated from the speed error and the d axis reference current is coming from the minimum copper loss strategy.

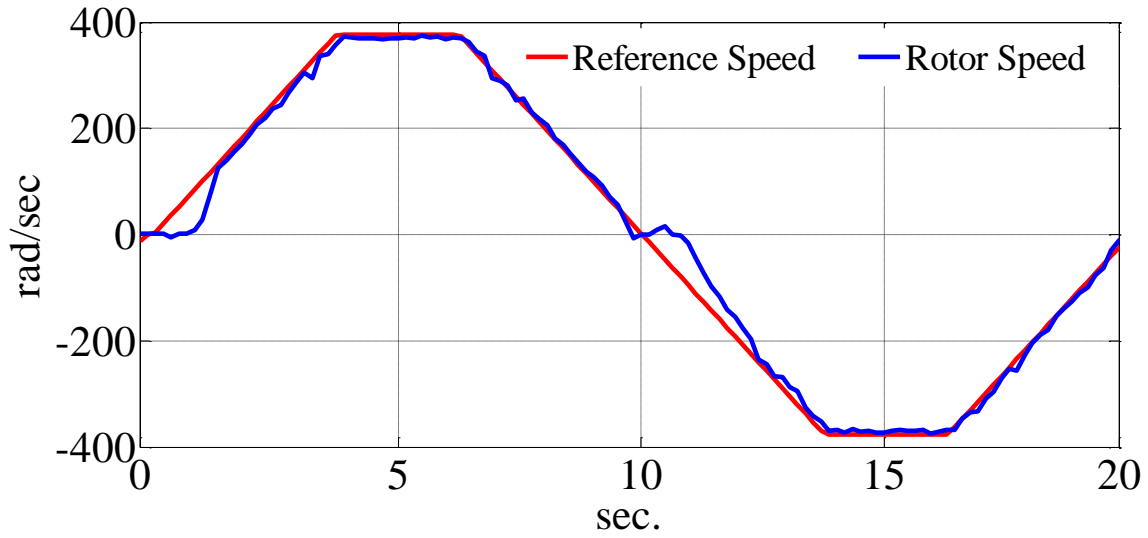


(a)

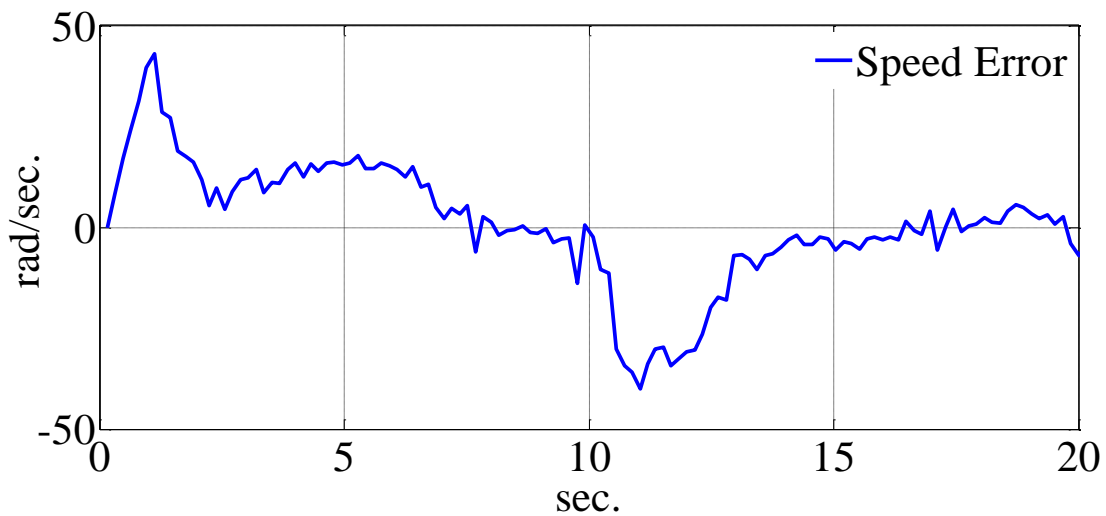


(b)

Figure 5.37: (a) The rotor speed and the reference speed (simulation results), (b) The speed error (simulation results).



(a)



(b)

Figure 5.38: (a) Reference and rotor speed (experimental results), (b) The speed error (experimental results).

Figure 5.39 show the simulation result of the q axis voltage in rotor reference frame. The experimental result of the same voltage is also shown in Figure 5.40. It can be seen that by increasing the rotor speed, when the load torque and consequently q axis current increases, the q axis voltage also increases to let the machine supply the load. Figures and 5.41 and 5.42 show the

output voltages of the controller loops for d axis in rotor reference frame for simulation and experimental results respectively. The q and d axis voltages are transformed to real quantities and the resulting nine phase voltages are used to generate appropriate nine-phase PWM signals.

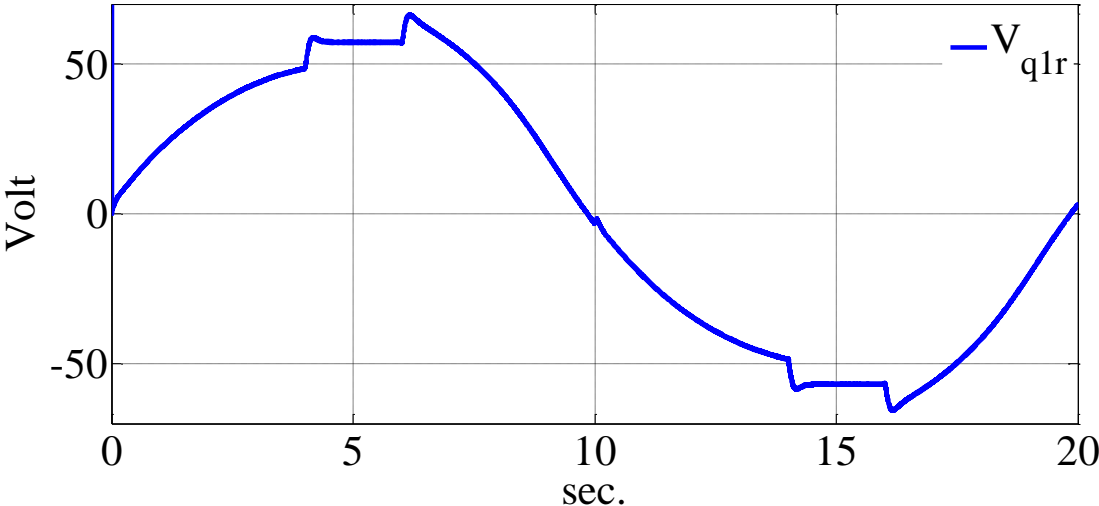


Figure 5.39: The q axis voltage in the rotor reference frame (simulation result).

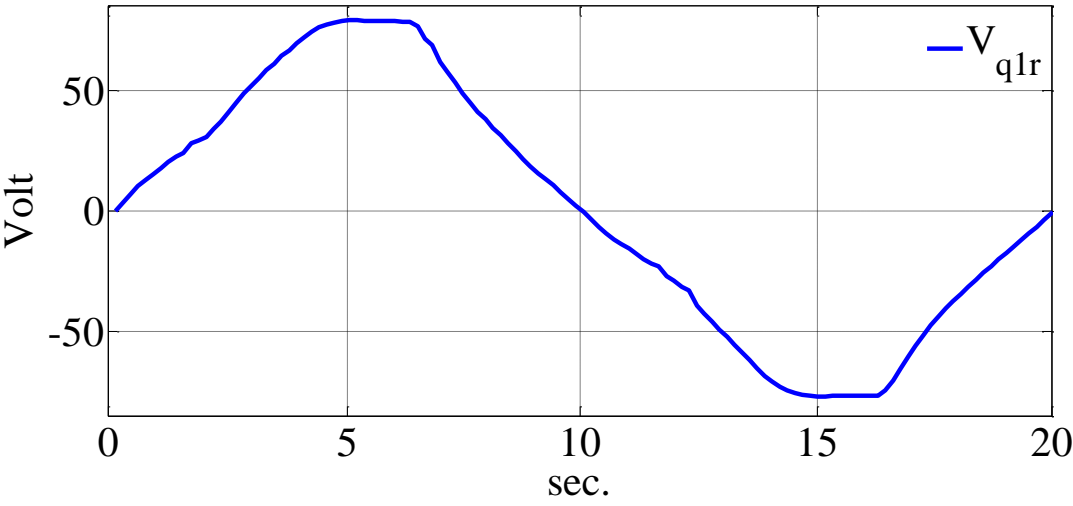


Figure 5.40: The q axis voltage in the rotor reference frame (experimental result).

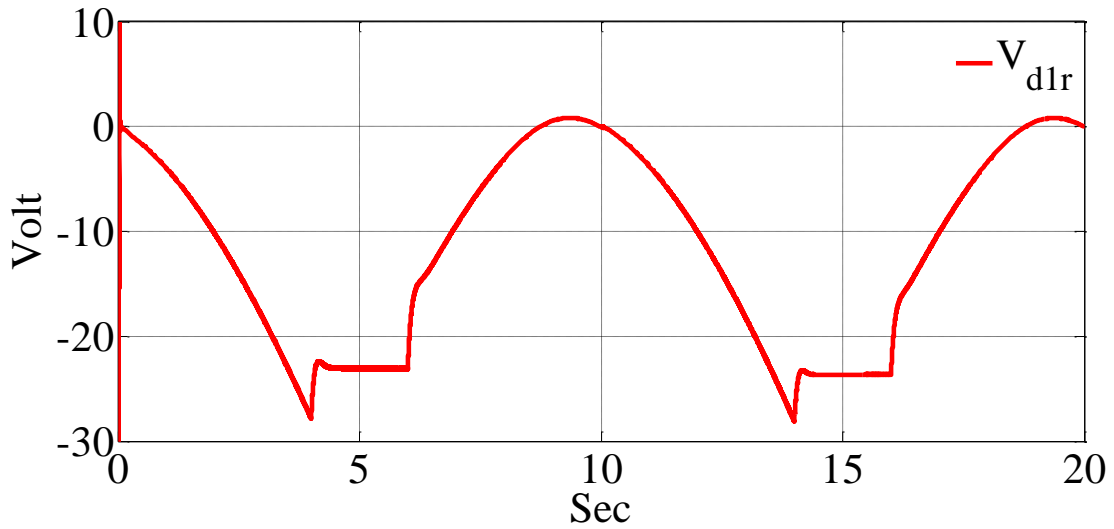


Figure 5.41: The d axis voltage in the rotor reference frame (simulation result).

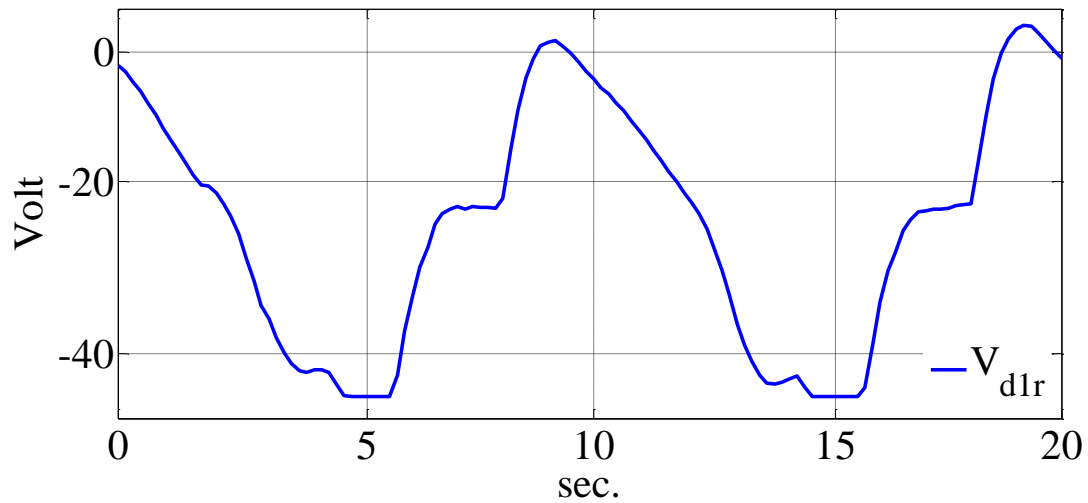
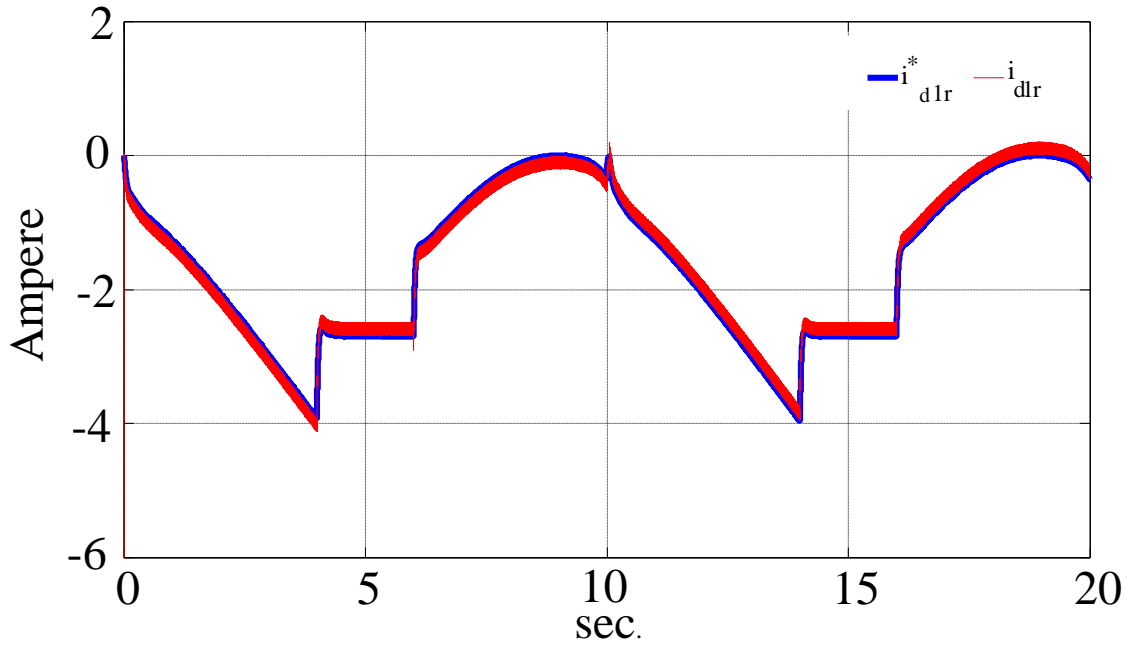
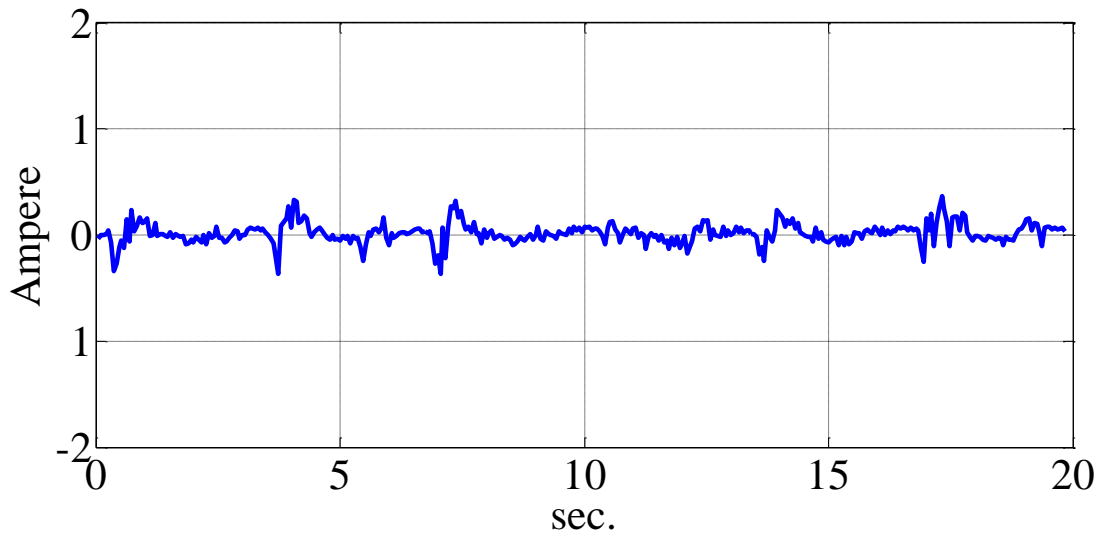


Figure 5.42: The d axis voltage in the rotor reference frame (experimental result).

The reference and simulated current of the d axis in rotor reference frame are shown in the Figure 5.43. The reference current is generated from the q axis current according to minimum copper loss strategy. It can be seen that the machine current tracks the reference. The reference and feedback of the d axis current for experiment are also shown in Figure 5.44. In both of the figures the reaction of the current regulators to the load torque can be seen from the changes of the current magnitudes.

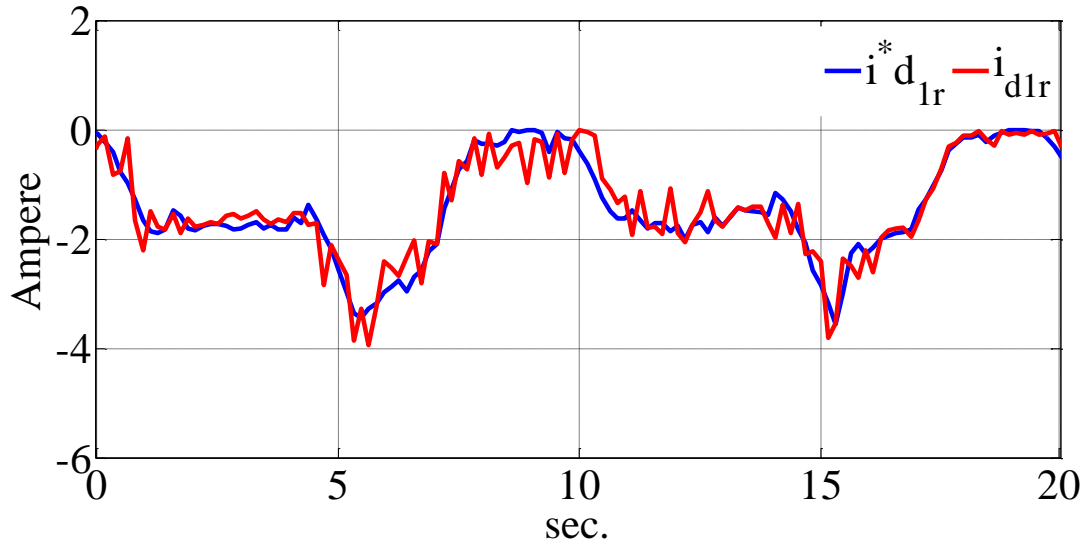


(a)

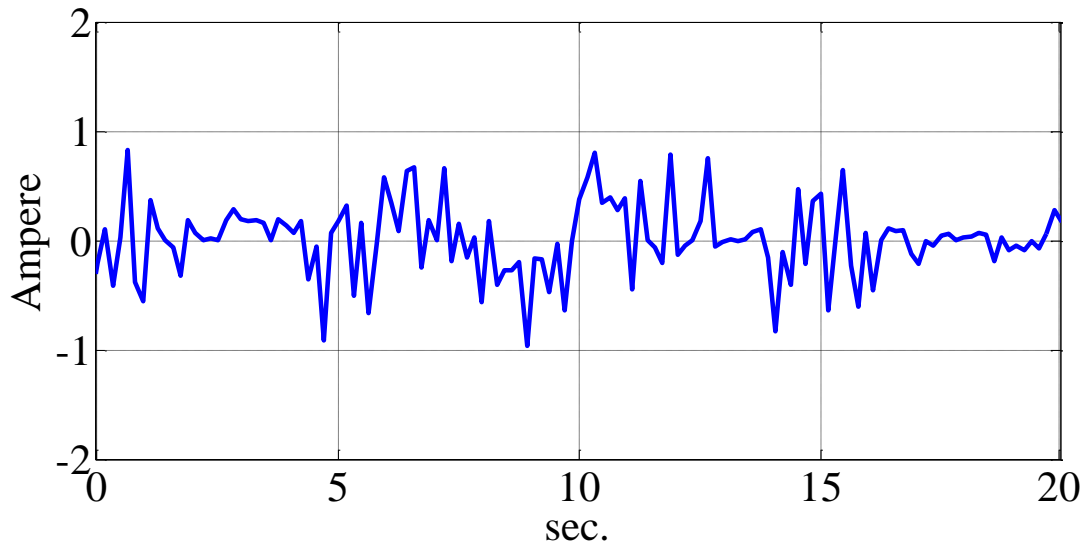


(b)

Figure 5.43: (a) The d axis currents, reference and actual (simulation results), (b) The current controller error (simulation results).



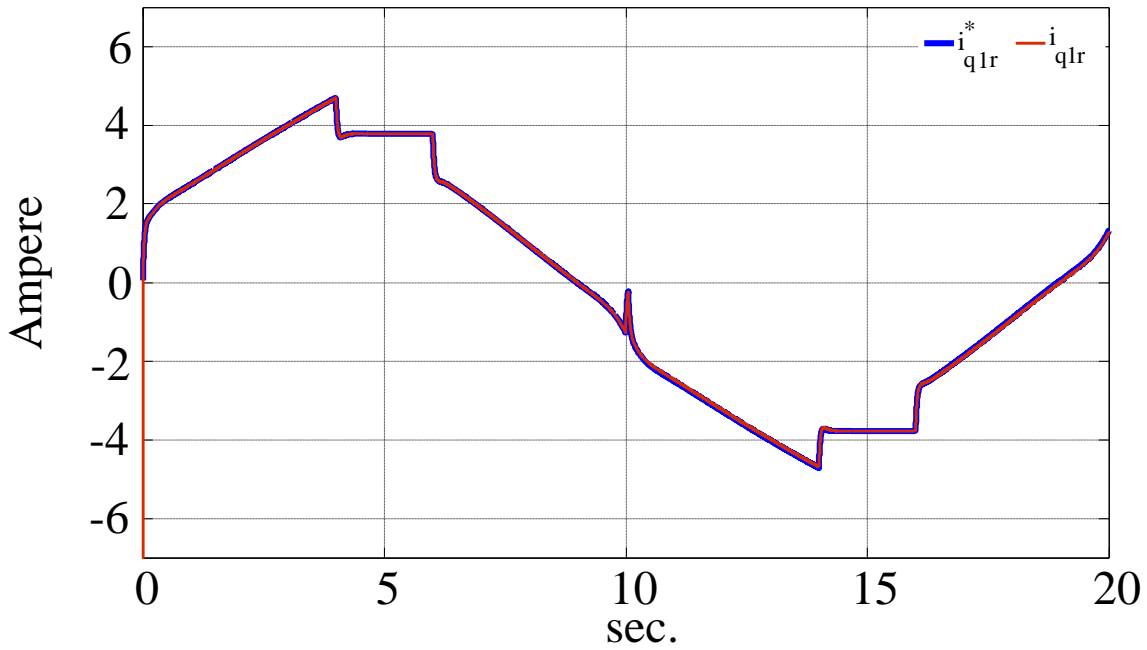
(a)



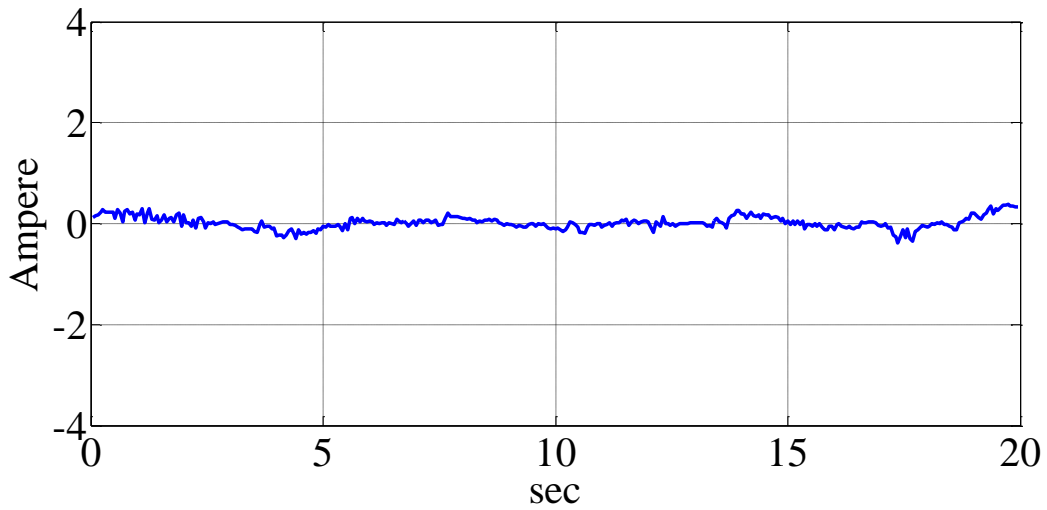
(b)

Figure 5.44: (a) Reference and actual currents for the d axis in the rotor reference frame (experimental results), (b) The error between the reference and feedback currents (experimental results).

The reference and simulated current of the q axis in rotor reference frame are also shown in the Figure 5.45. The reference current is generated from the speed control loop and it is clear that the machine current tracks the reference.



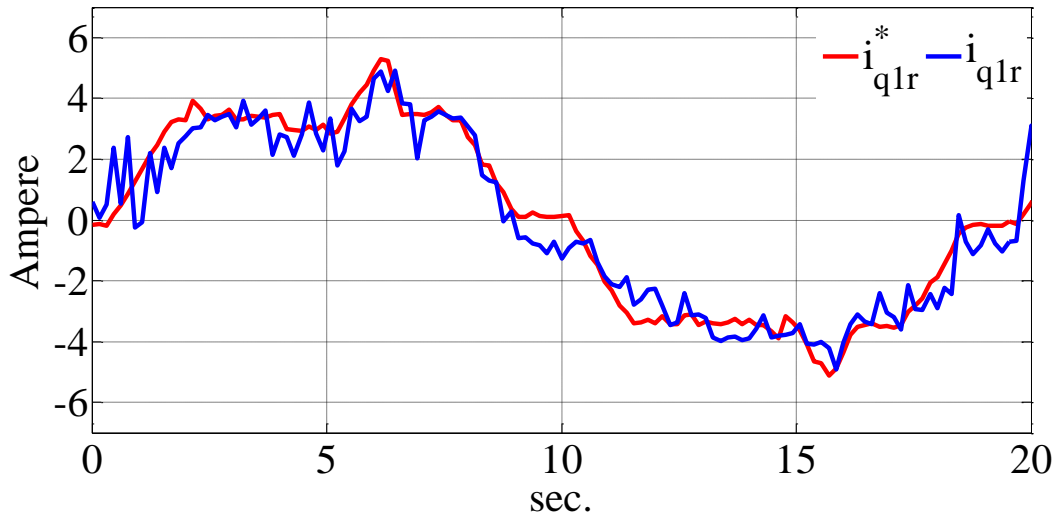
(a)



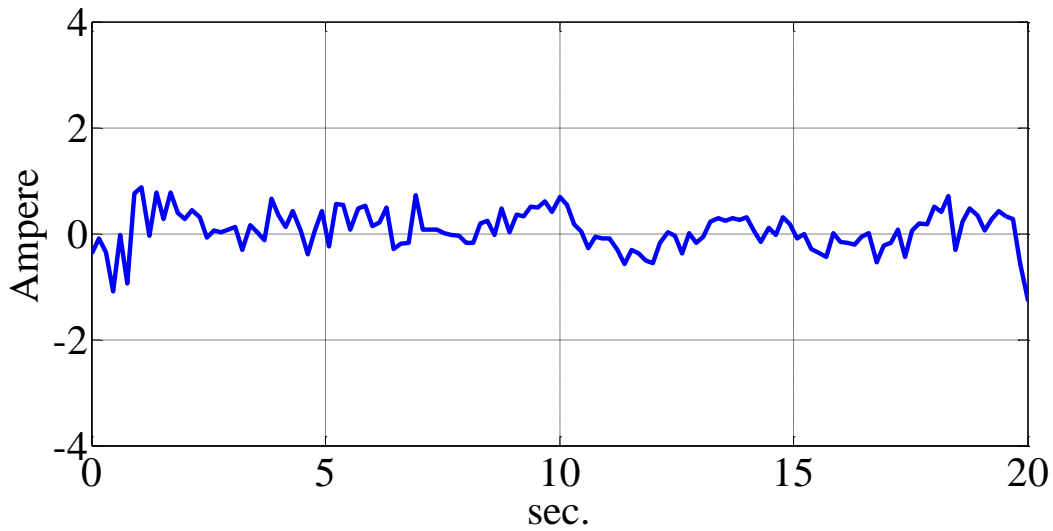
(b)

Figure 5.45: (a) Reference and actual currents for the q axis in the rotor reference frame (simulation results), (b) The error between the reference and feedback currents (simulation results).

The experimental results for q axis current is also shown in Figure 5.46. In both of the figures, the q axis current varies with the rotor speed that changes the load torque.



(a)



(b)

Figure 5.46: (a) Reference and actual currents for the q axis in the rotor reference frame (experimental results), (b) The error between the reference and feedback currents (experimental results).

The simulation and experimental results for electromagnetic torque of the machine are shown in the Figures 5.47 and 5.48 respectively. The experimental results for the torque is measures from the coupling shaft between the machine and the load. The load torque is generated by a DC machine that operates as load. The DC machine has a fixed field current and the armature is

connected to a load resistance. Figures 5.49 shows the simulation results of the nine phase currents and Figures 5.50 and 5.51 show experimental results of the stator currents for speeds of 377 and 180 rad/sec respectively. Again from these figures, the effect of some non-modeled effects such as stator magnetic saturation can be seen. The saturation causes some rotor position dependent variations in the stator inductances and consequently results in low frequency ripples in the currents.

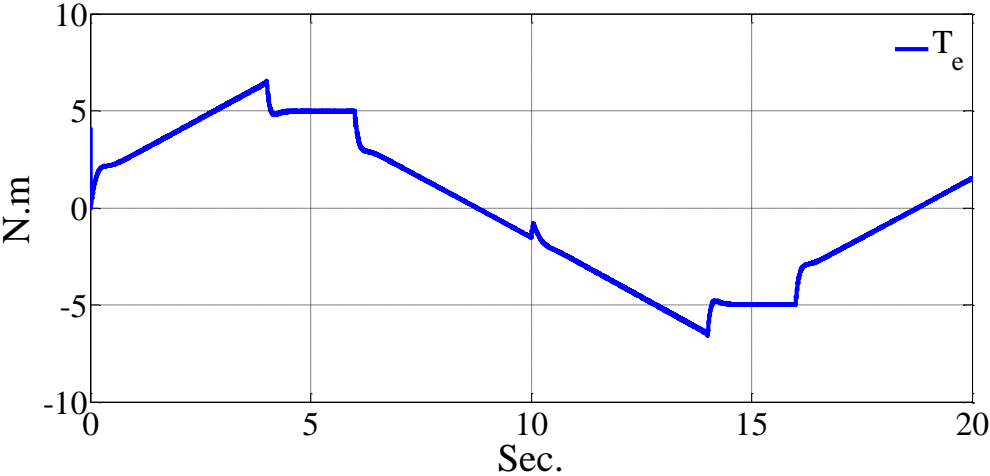


Figure 5.47: The electromagnetic torque of the IPM machine (simulation results).

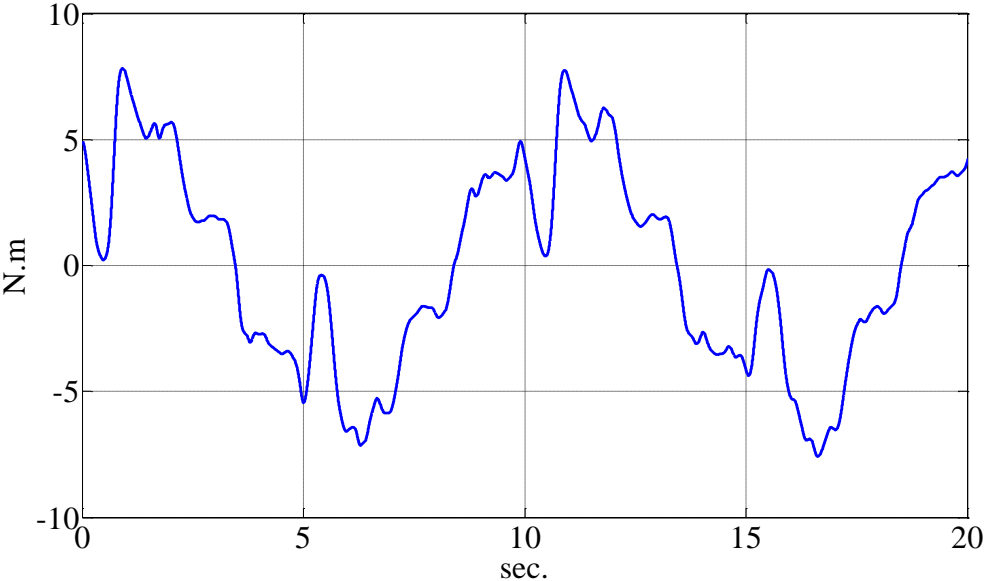
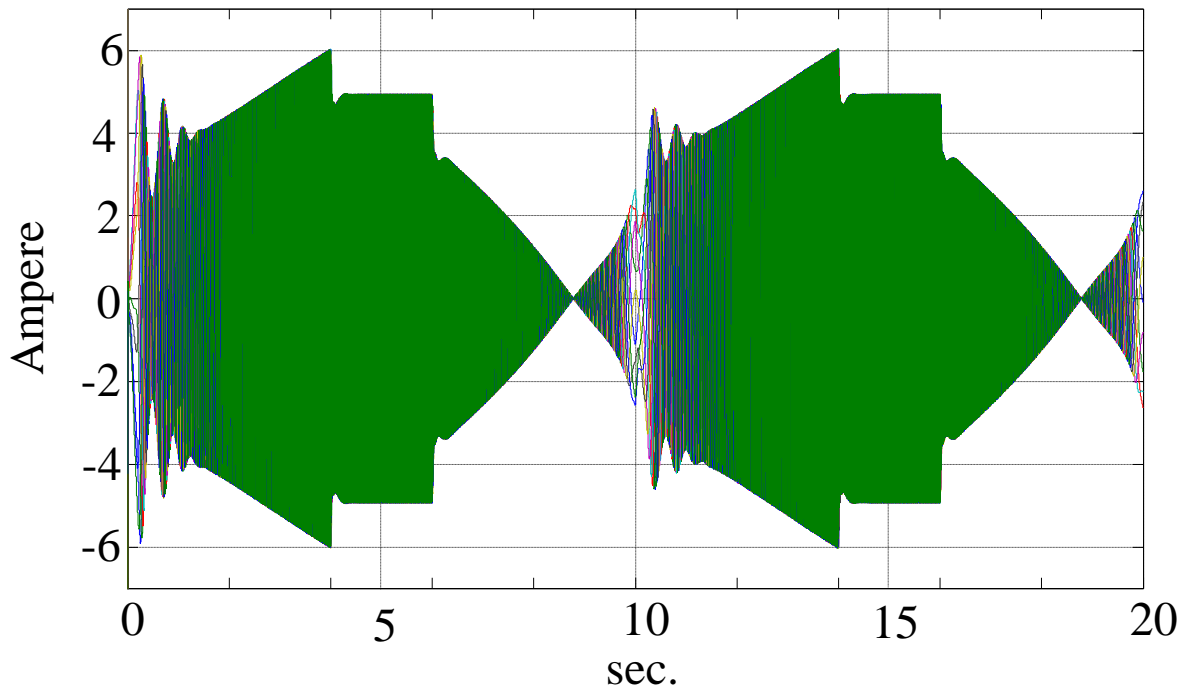
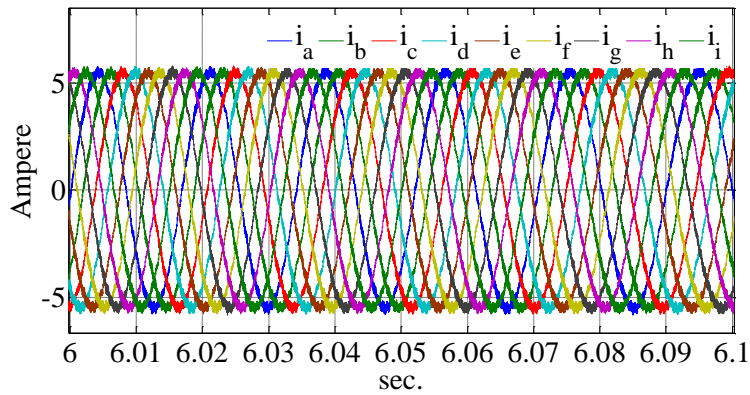


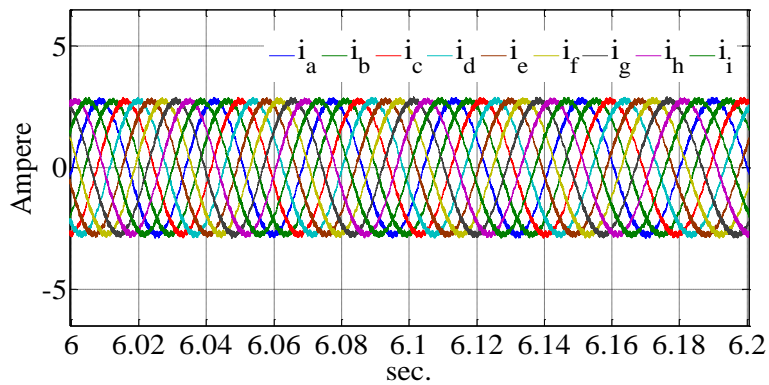
Figure 5.48: The electromagnetic torque of the IPM machine (experimental results).



(a)

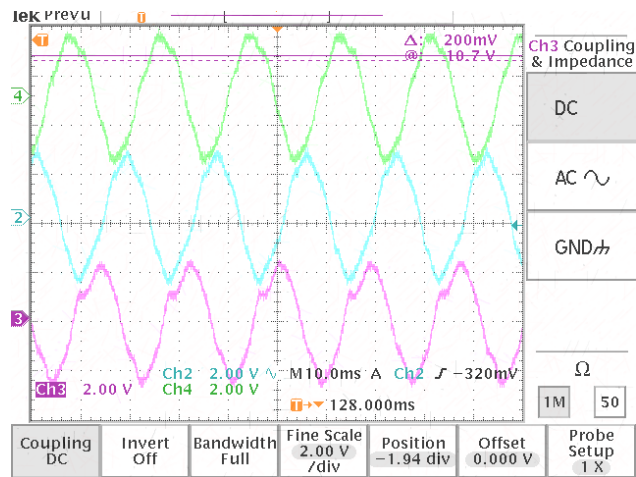


(b)

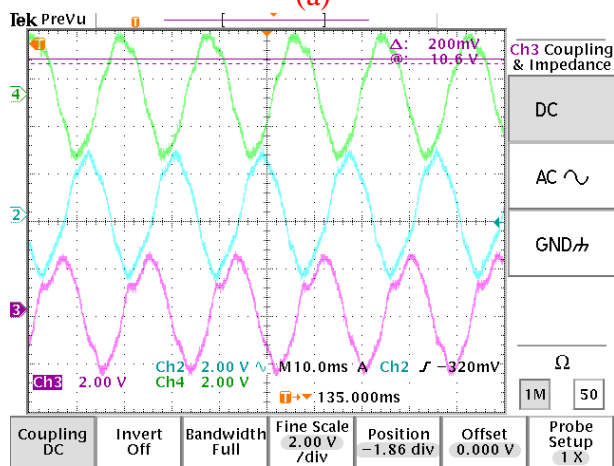


(c)

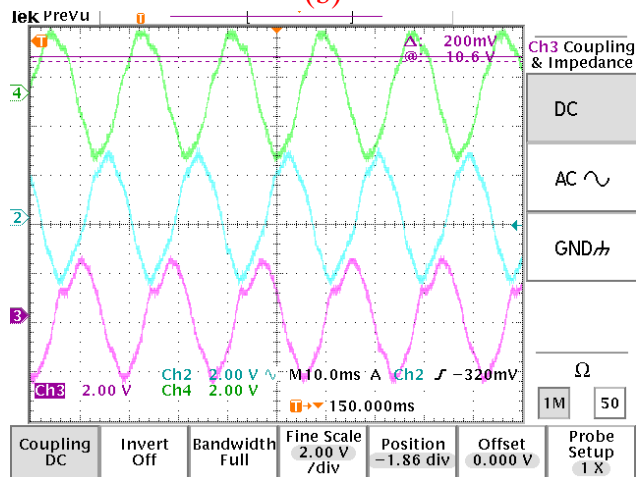
Figure 5.49: Simulation results for (a) The nine-phase currents of the machine, (b) and (c) The zoomed in view of currents for rotor speed equal to 180 and 377 rad/sec respectively.



(a)

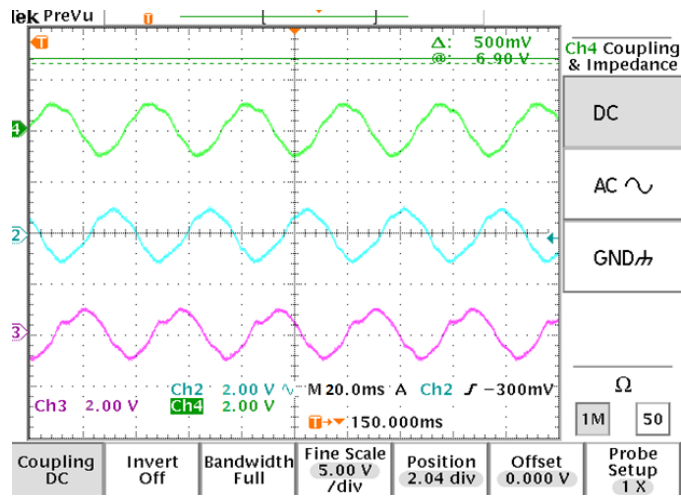


(b)

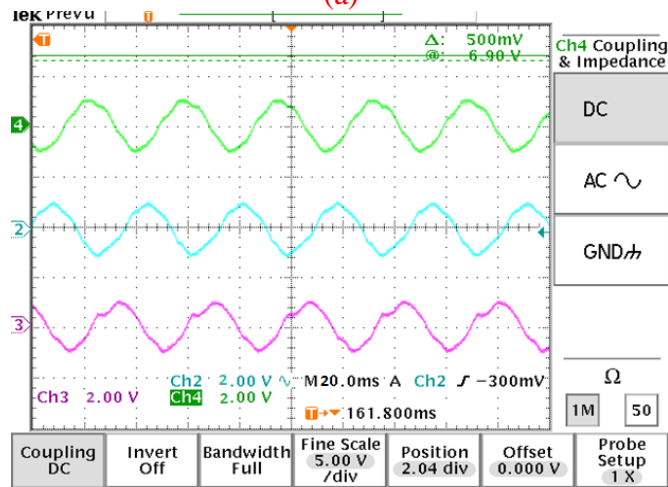


(c)

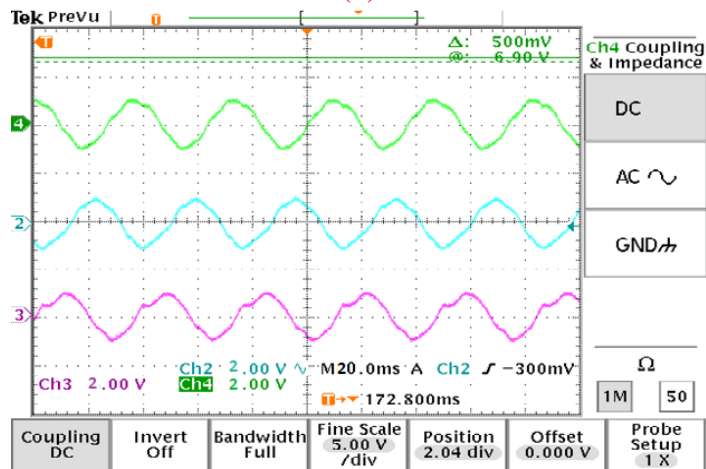
Figure 5.50: The nine-phase currents of the machine for phases, (a) 'a', 'd' and 'g', (b) 'b', 'e' and 'h', (c) 'c', 'f' and 'i', rotor speed equal to 377 rad/sec (experimental results) (5 A/scale).



(a)



(b)



(c)

Figure 5.51: The nine-phase currents of the machine for phases, (a) 'a', 'd' and 'g', (b) 'b', 'e' and 'h', (c) 'c', 'f' and 'i', rotor speed equal to 180 rad/sec (experimental results) (5 A/ scale).

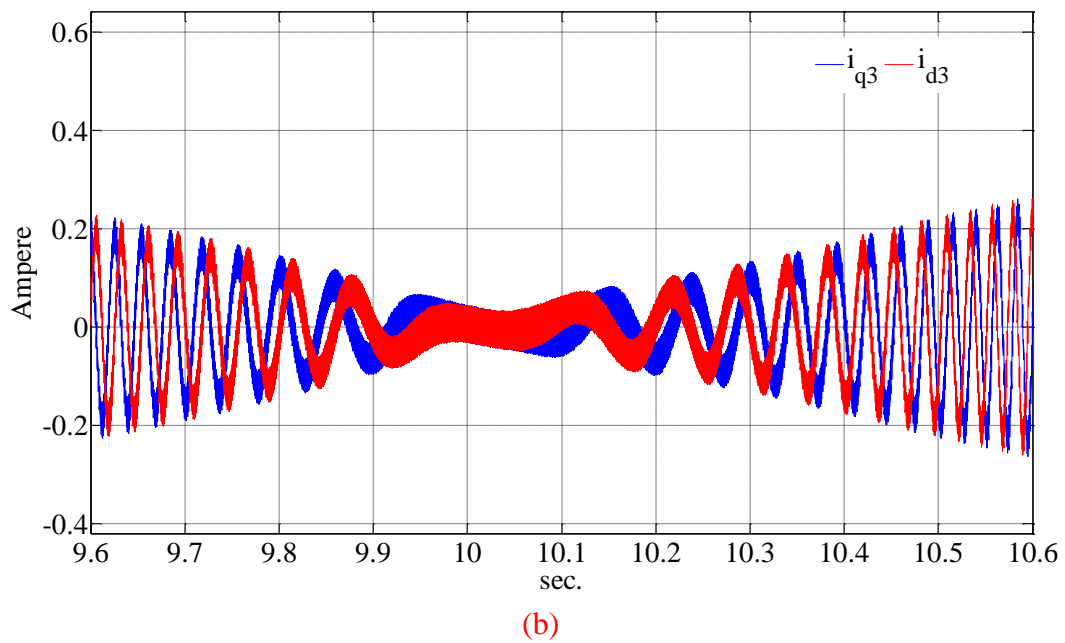
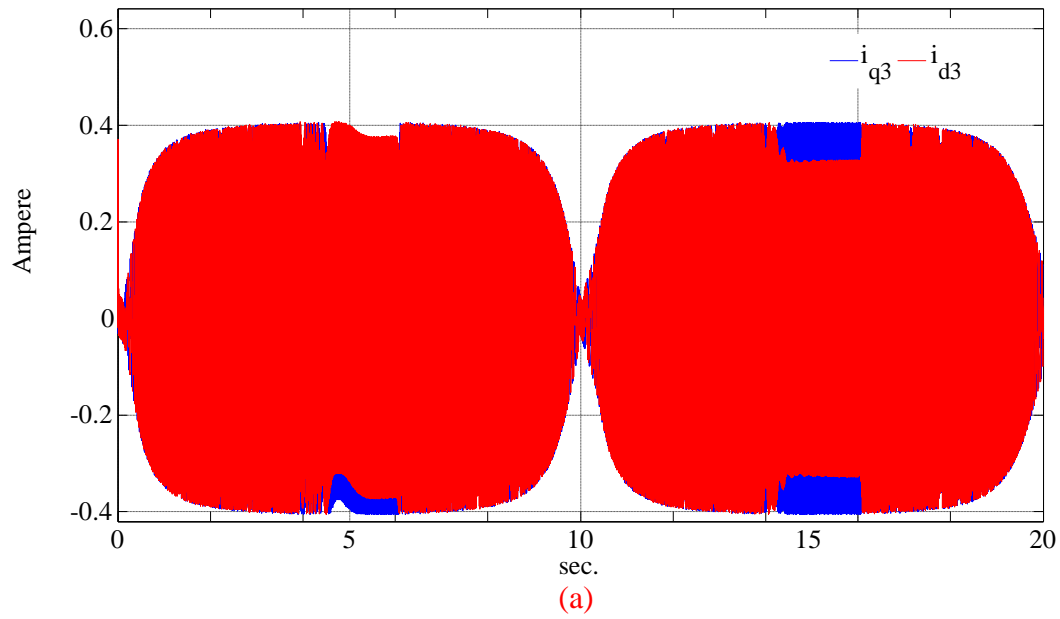
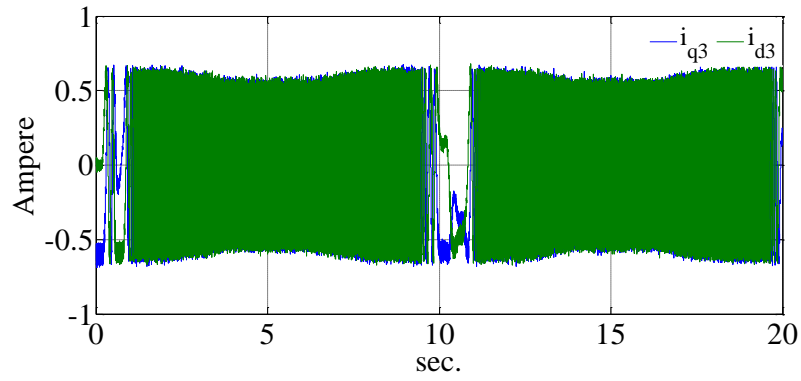
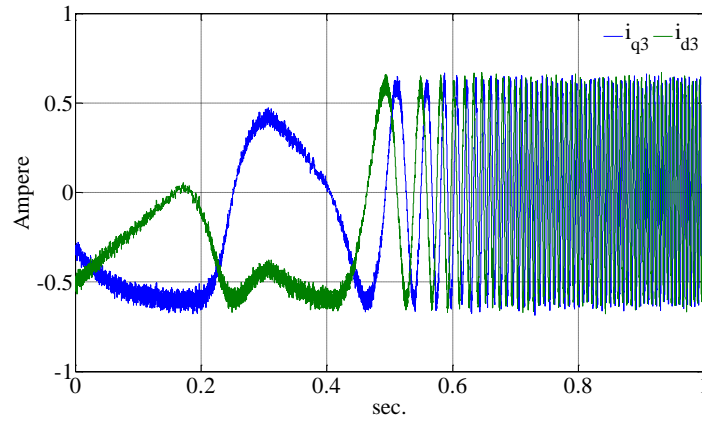


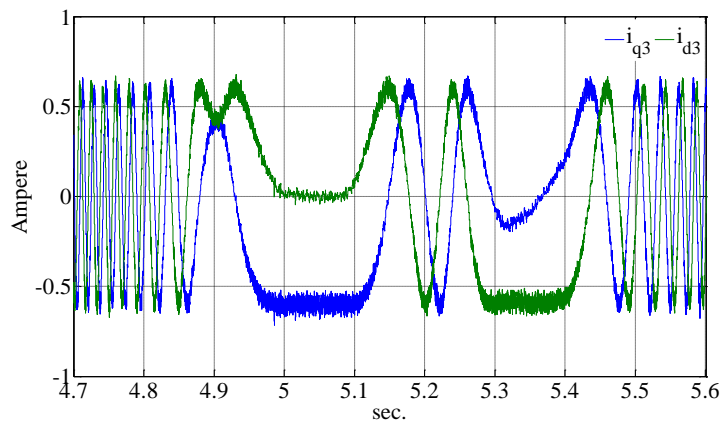
Figure 5.52: (a) The dq_3 currents before heterodyning (simulation results), (b) The dq_3 currents before heterodyning around the zero speed (simulation results).



(a)



(b)

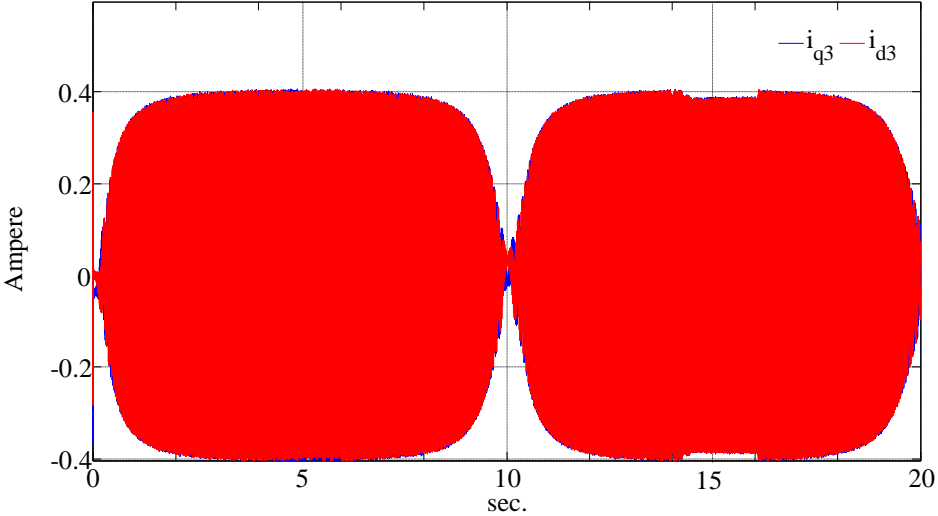


(c)

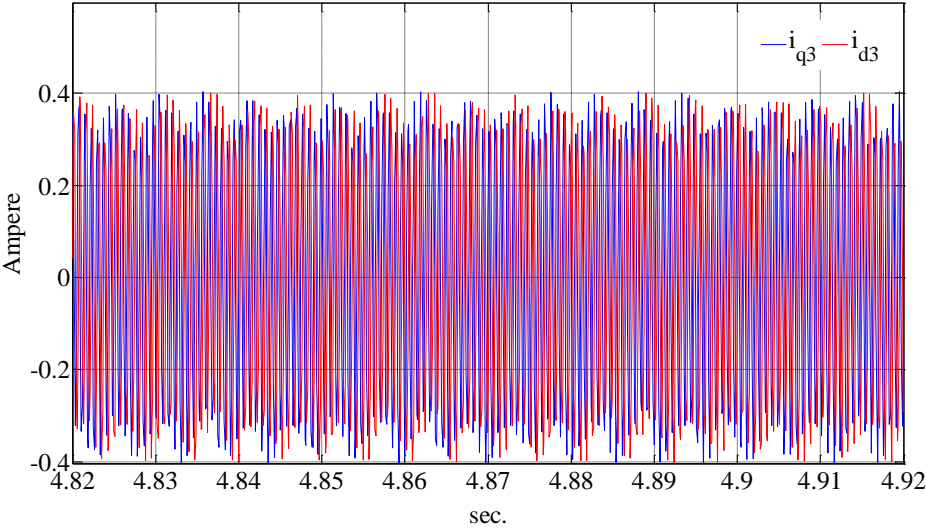
Figure 5.53: (a) The third sequence currents in q and d axis of the stationary reference frame after heterodyning and filtering (experimental results), (b), (c) The zoomed view (experimental results).

The third sequence of the nine-phase currents need to be extracted to be used for position detection. The third sequence can be extracted using the transformation matrix of equation (5.63)

in stationary reference frame. The third sequence currents from simulation and experimental results are shown in Figures 5.52 and 5.53 respectively. The high frequency components, shown in the Figures 5.52 and 5.53, have a low frequency component which is related to the position of the machine. This component can be extracted and used for estimation.

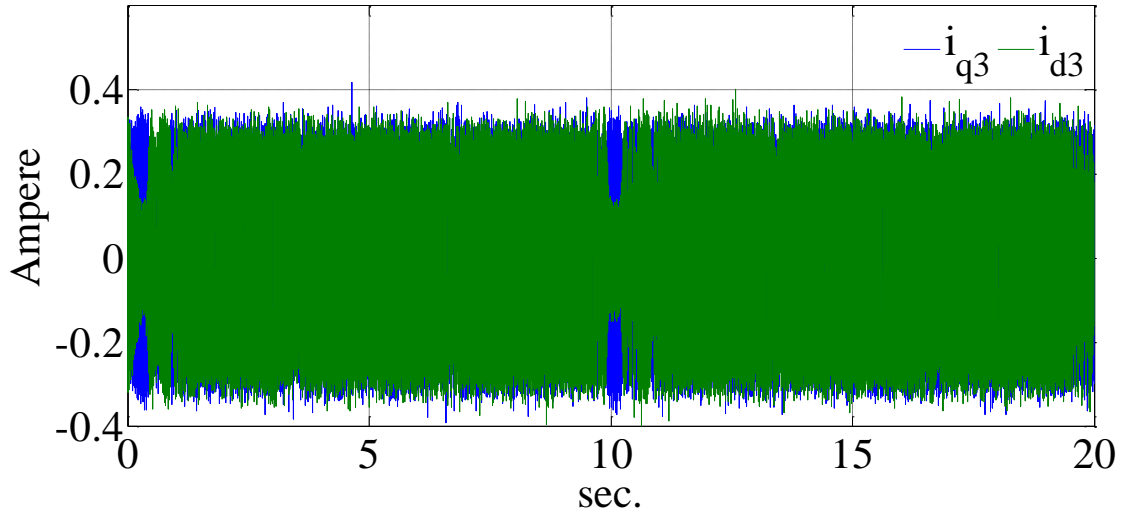


(a)

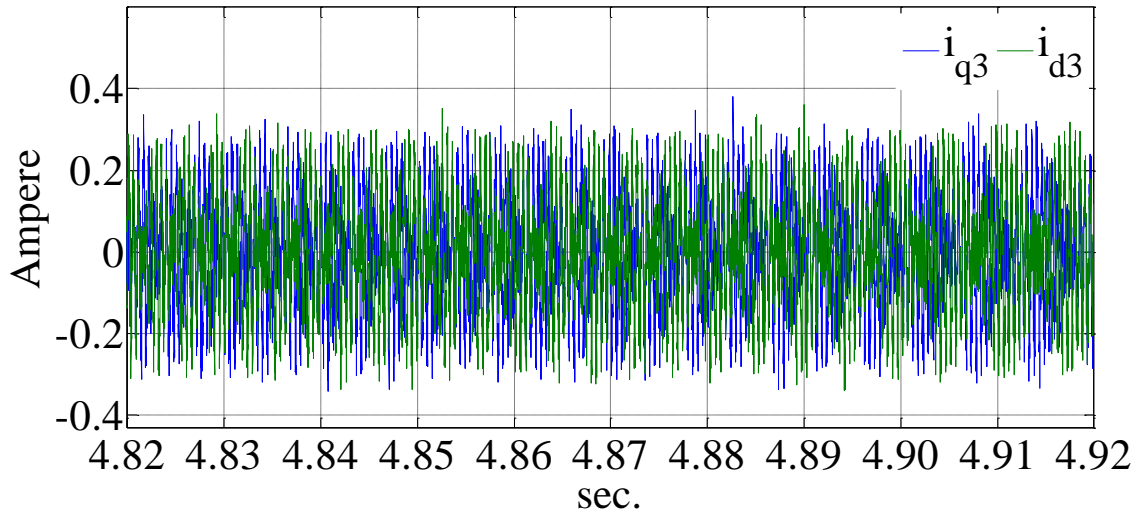


(b)

Figure 5.54: (a) The dq_3 currents after heterodyning (simulation results), (b) The dq_3 currents after heterodyning, zoomed view (simulation results).



(a)



(b)

Figure 5.55: (a) The dq_3 currents after heterodyning (experimental results), (b) The dq_3 currents after heterodyning, zoomed view (experimental results).

To extract the low frequency component, the generated signals are multiplied to term $e^{-j\omega_s t}$ the result signals are shown in the Figure 5.54 and 5.55 for simulation and experimental results respectively. It can be seen that the currents have a low frequency part which can be extracted using a low pass filter.

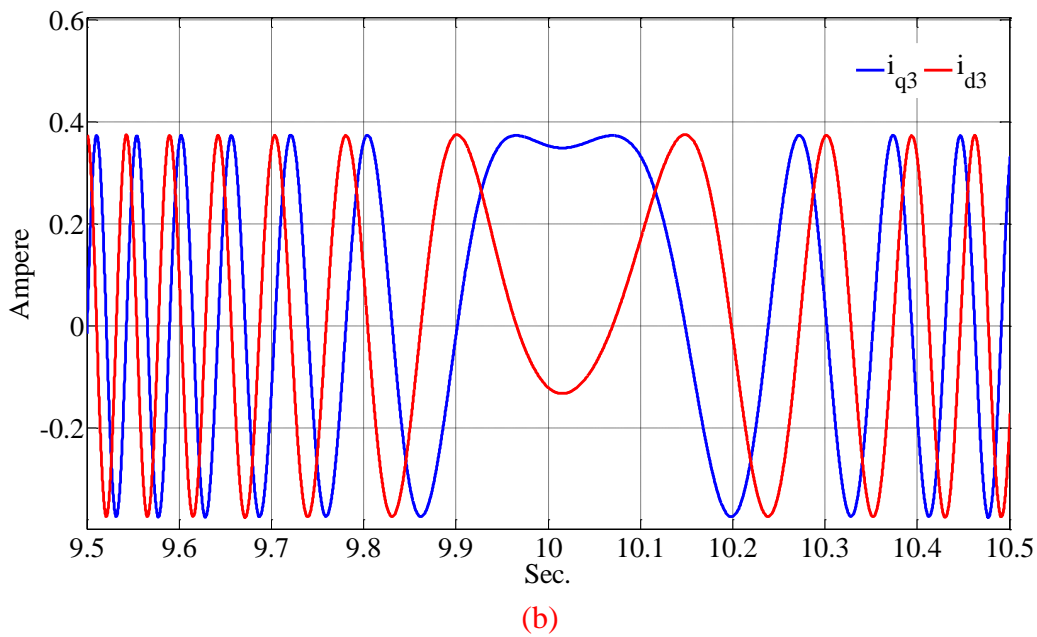
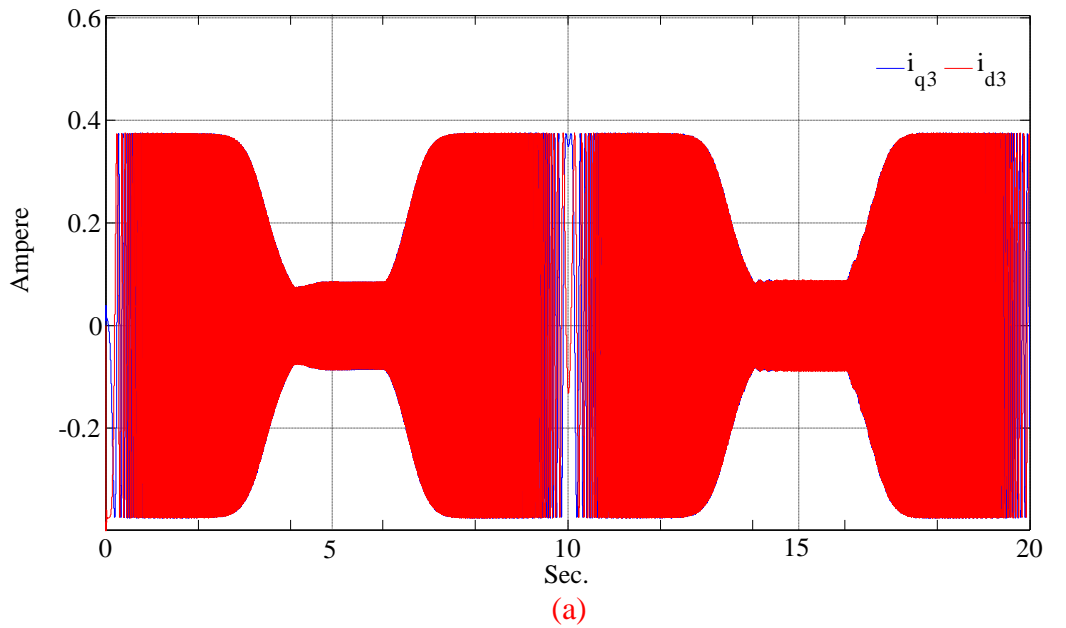
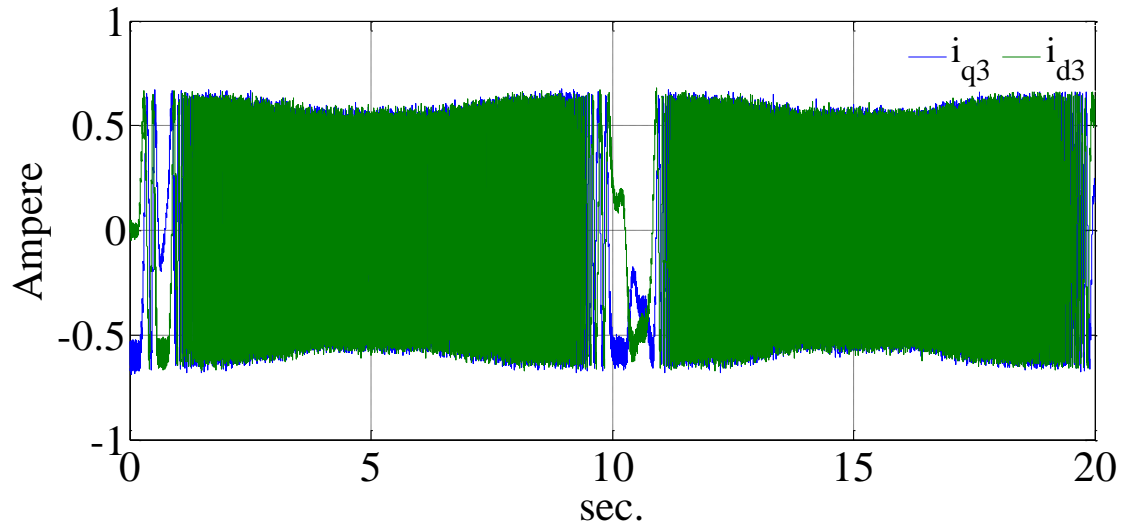
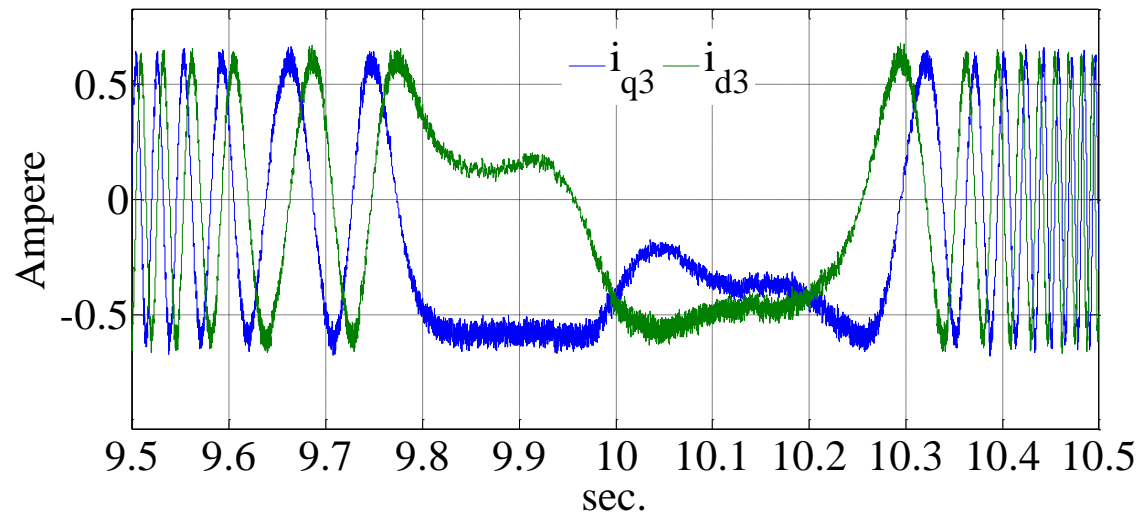


Figure 5.56: (a) The dq_3 currents after filtering (simulation results), (b) The zoomed view (simulation results).

The signals of Figures 5.54 and 5.55 can be filtered to remove their remaining high frequency components. Figures 5.56 and 5.57 show the simulation and experimental results for the third sequence currents after filtering for simulation and experiment respectively.



(a)



(b)

Figure 5.57: (a) The dq_3 currents after filtering (experimental results), (b) The zoomed view (experimental results).

It can be seen that the high frequency parts are removed by low pass filter and the position dependent low frequency signals are remained.

The signals of Figures 5.56 and 5.57 are the signals that carry the information of the rotor position. According to these figures, the signals have variable magnitude. To be able to use them to feed the observer, they should be normalized (using equation (5.87)) to have unity magnitude. Figures 5.58 and 5.59 show the normalized currents for simulation and experimental results.

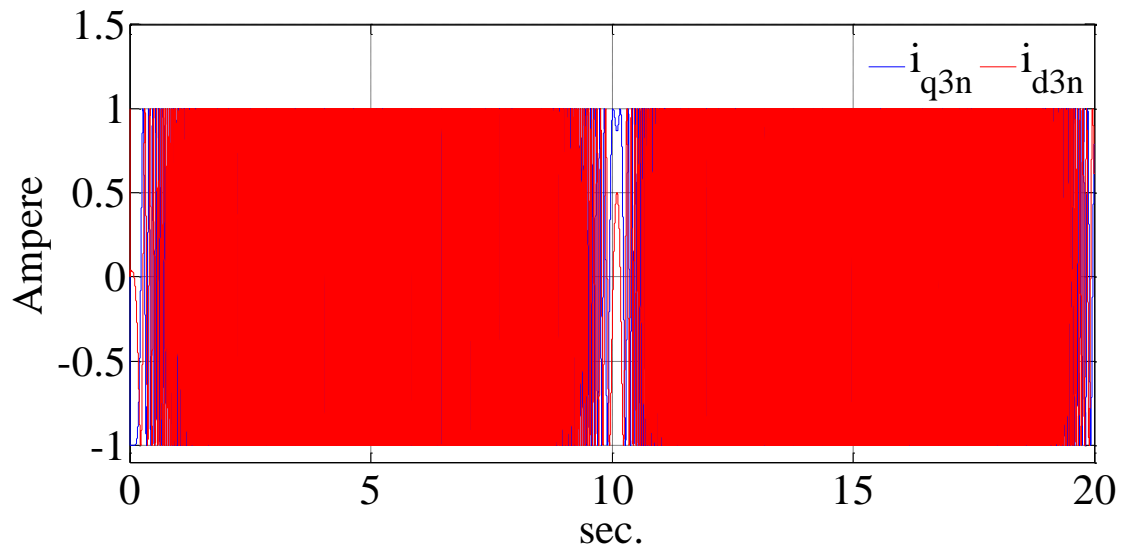


Figure 5.58: The normalized currents fed to observer. (simulation results).

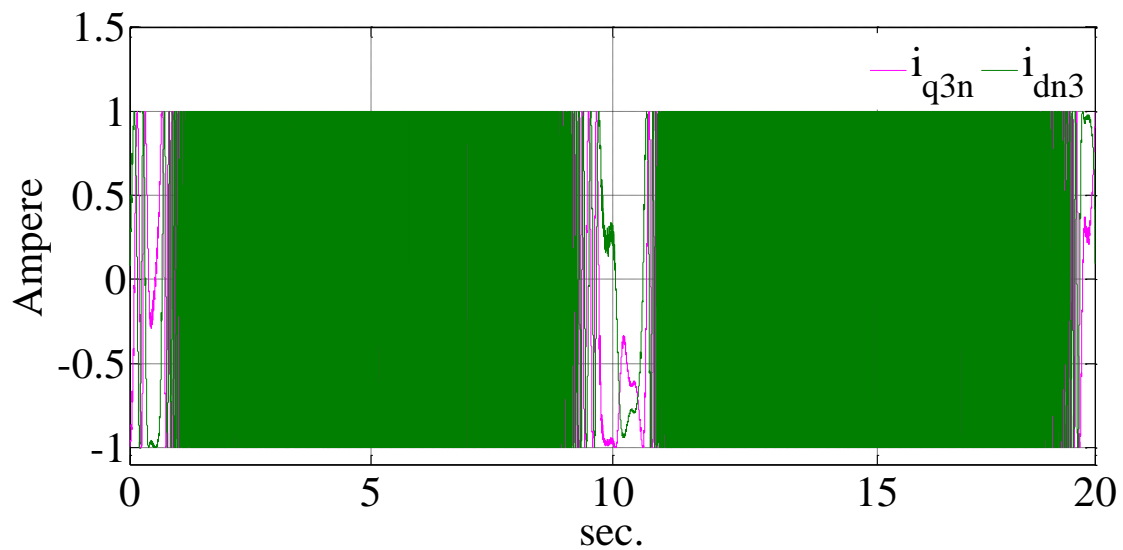
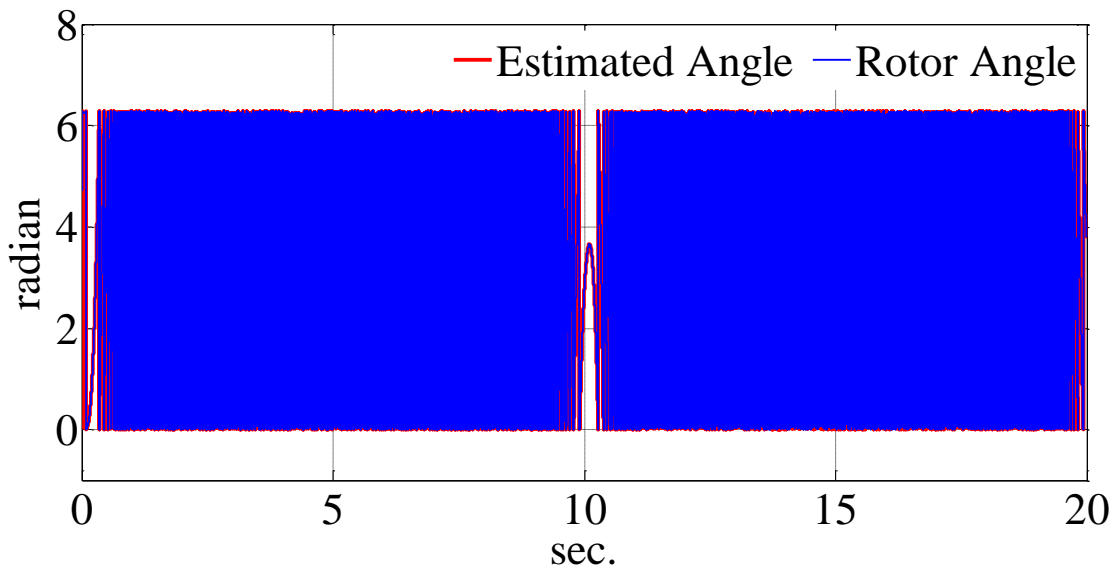
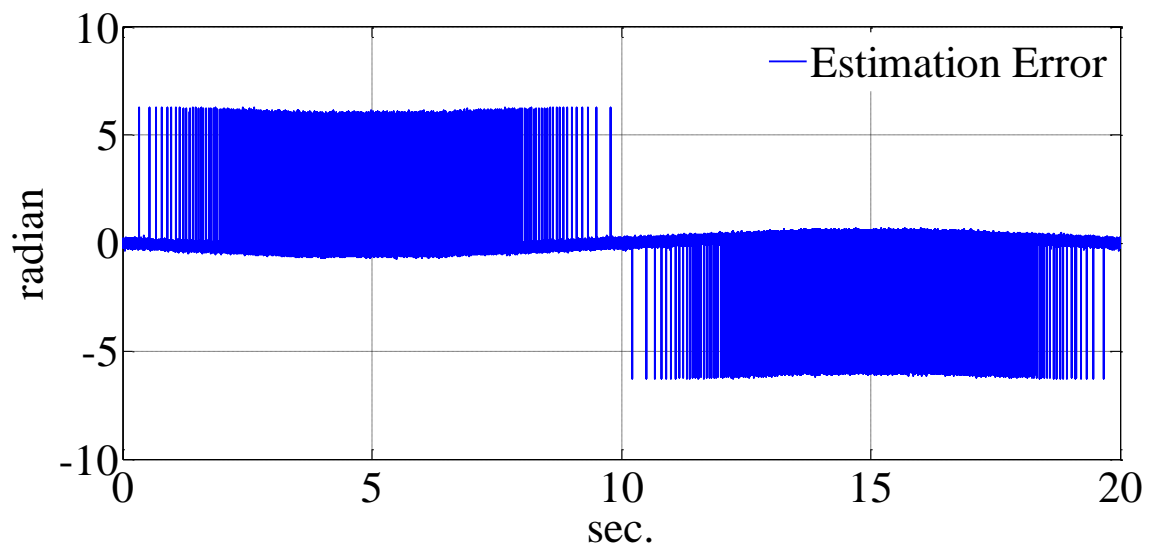


Figure 5.59: The normalized currents fed to observer. (experimental results).

From Figures 5.58 and 5.59, it can be seen that the magnitudes of the currents are fixed to unity. Now the currents are suitable to be fed to the Lunberger observer that was designed in pervious sections. The currents are fed to the Lunberger observer to estimate the rotor angle.



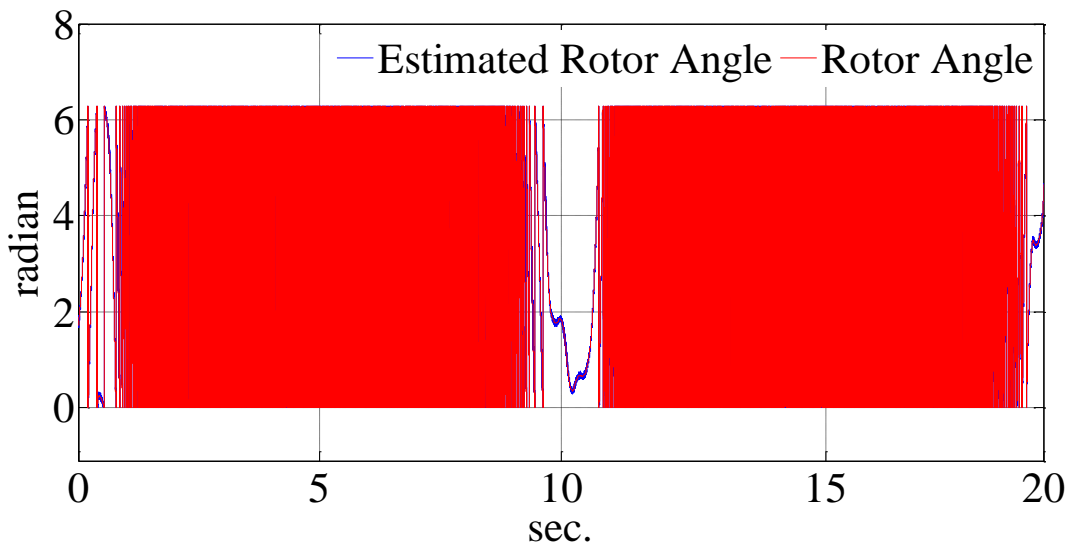
(a)



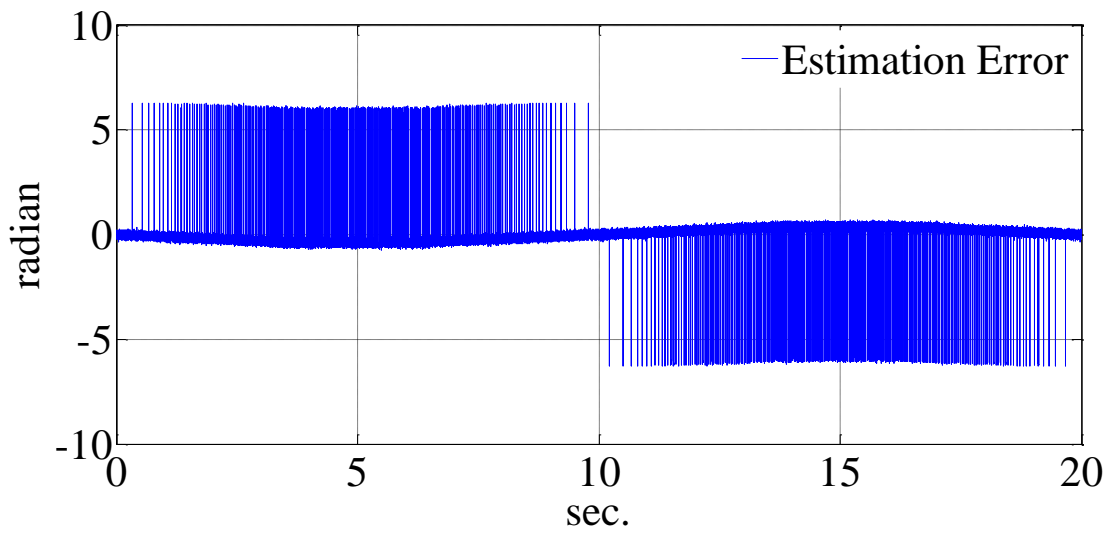
(b)

Figure 5.60: (a) Estimated and simulated rotor angle (simulation results), (b) Estimation error (simulation results).

Figures 5.60 and 5.61 show the estimated and rotor angle for simulation and experiment along with the estimation error.



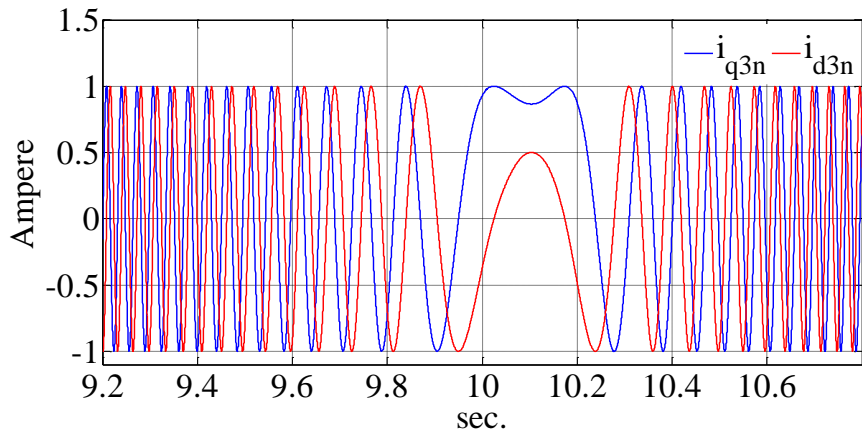
(a)



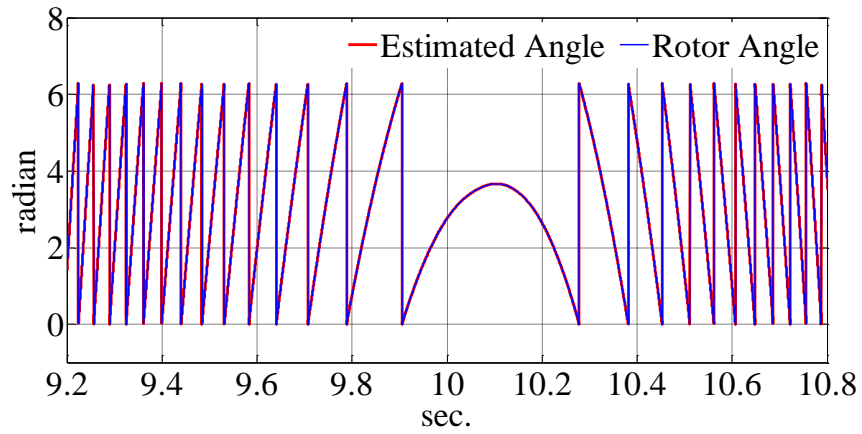
(b)

Figure 5.61: (a) Estimated and measured rotor angle (experimental results), (b) Estimation error (experimental results).

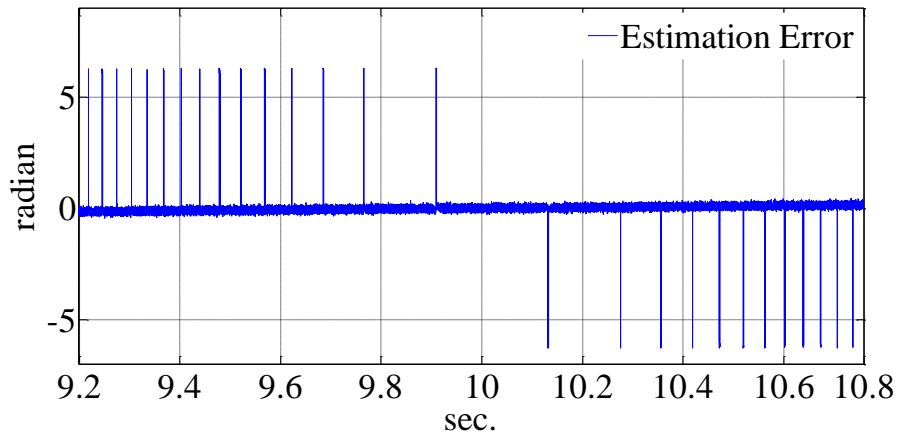
The Figures 5.58 to 5.61 are repeated in the Figures 5.62 and 5.63 to show the zoomed views of zero crossing intervals. The estimated and simulated rotor angles can be seen more clearly in these figures.



(a)

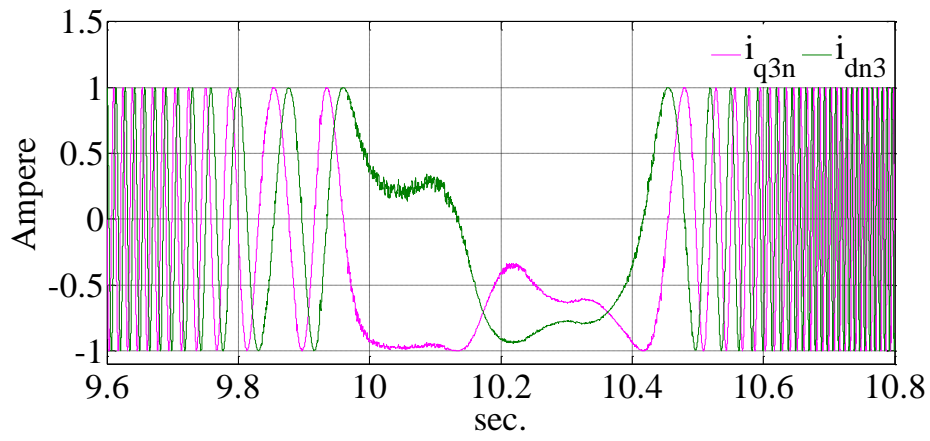


(b)

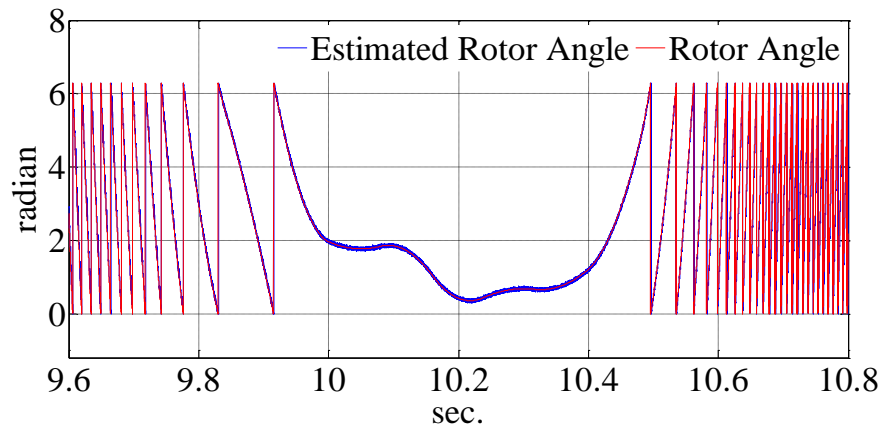


(c)

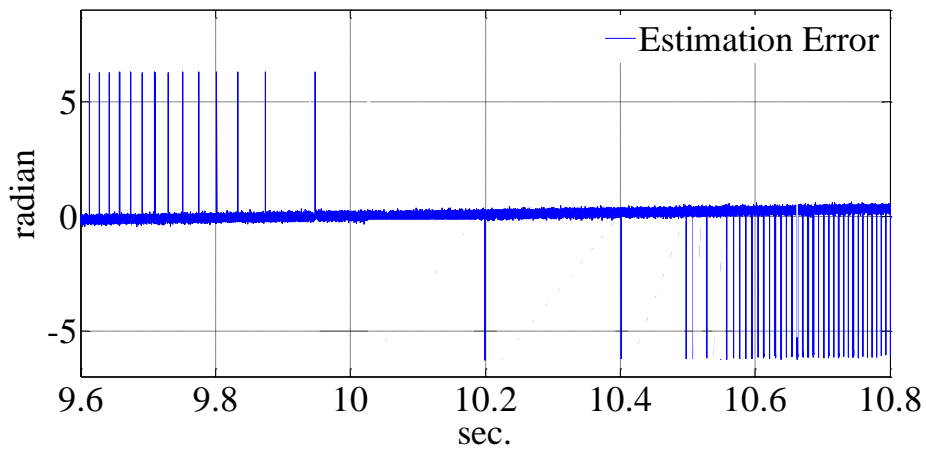
Figure 5.62: (a) The normalized currents fed to observer around rotor speed zero crossing (simulation results), (b) Estimated and measured rotor angle (simulation results), (c) The estimation error (simulation results).



(a)



(b)

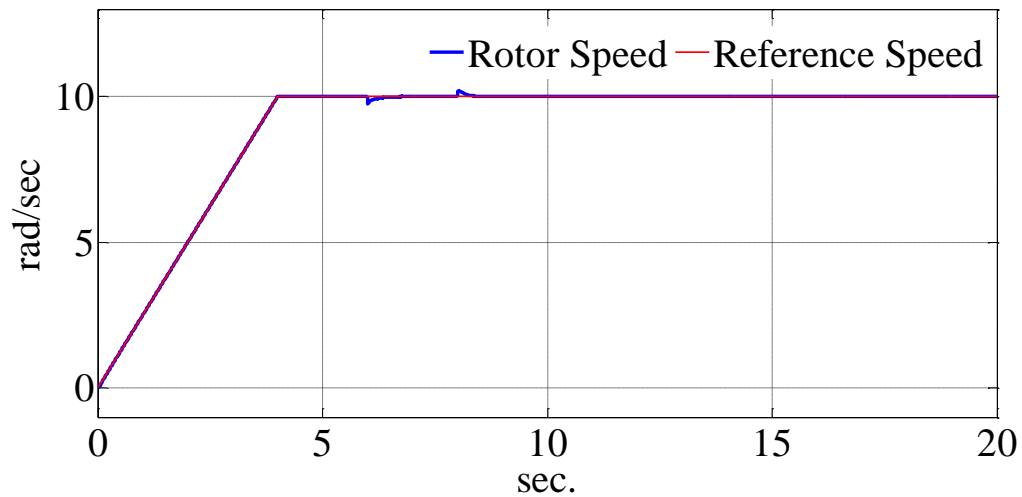


(c)

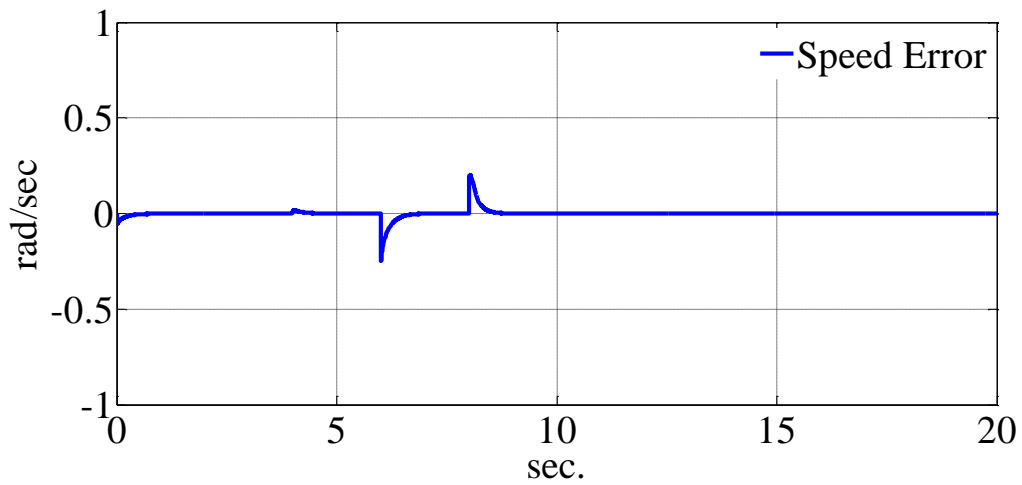
Figure 5.63: (a) The normalized currents fed to observer around rotor speed zero crossing (experimental results), (b) Estimated and measured rotor angle (experimental results), (c) The estimation error (experimental results).

5.6.3 Low Speed Run

In this section the controller is tested for a low speed reference as the input command. The speed reference starts from the zero and goes to a fixed speed at 10 (rad/sec) after drive settles down to the steady state conditions a step load torque is applied to the rotor for 2 seconds. The simulation and experimental results are shown in this section.

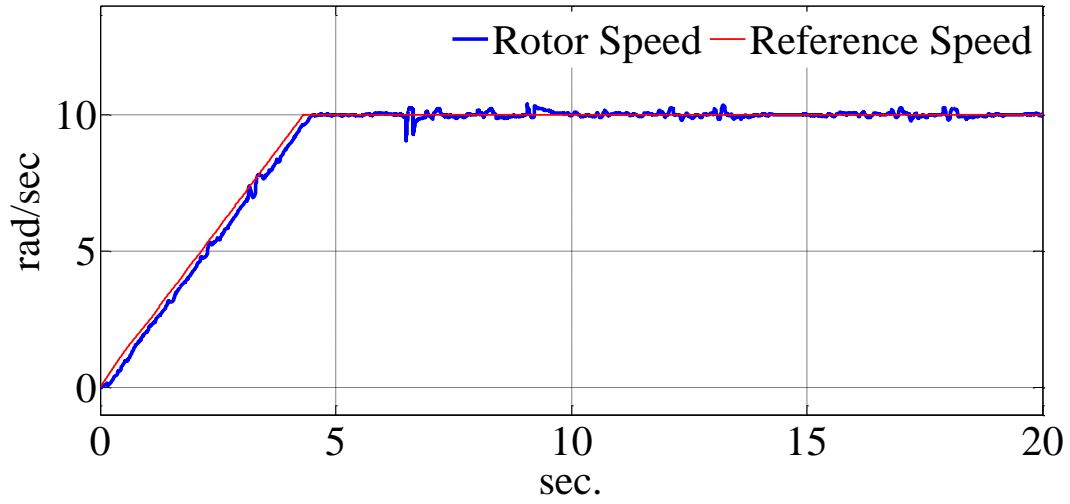


(a)

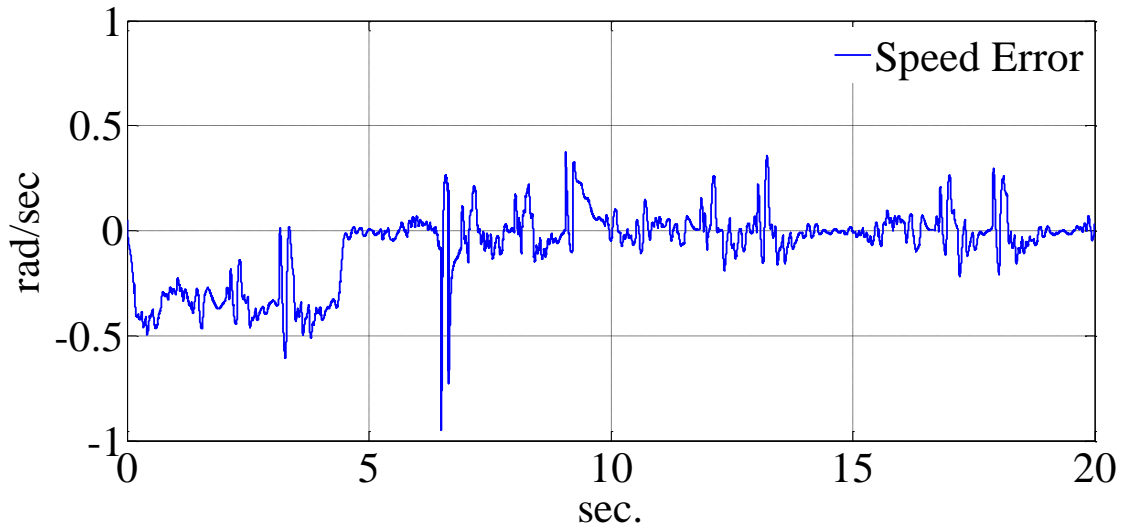


(b)

Figure 5.64: (a) The reference and rotor speed (simulation results), (b) Speed error (simulation results).



(a)



(b)

Figure 5.65: (a) The reference and rotor speed (experimental results), (b) Speed error (experimental results).

Figures 5.64 and 5.65 show the reference speed and the rotor speed together along with the speed error for simulation and experiment respectively. From Figures 5.64 (a) and 5.65 (a) it can be seen that the drive can accurately follow the reference speed.

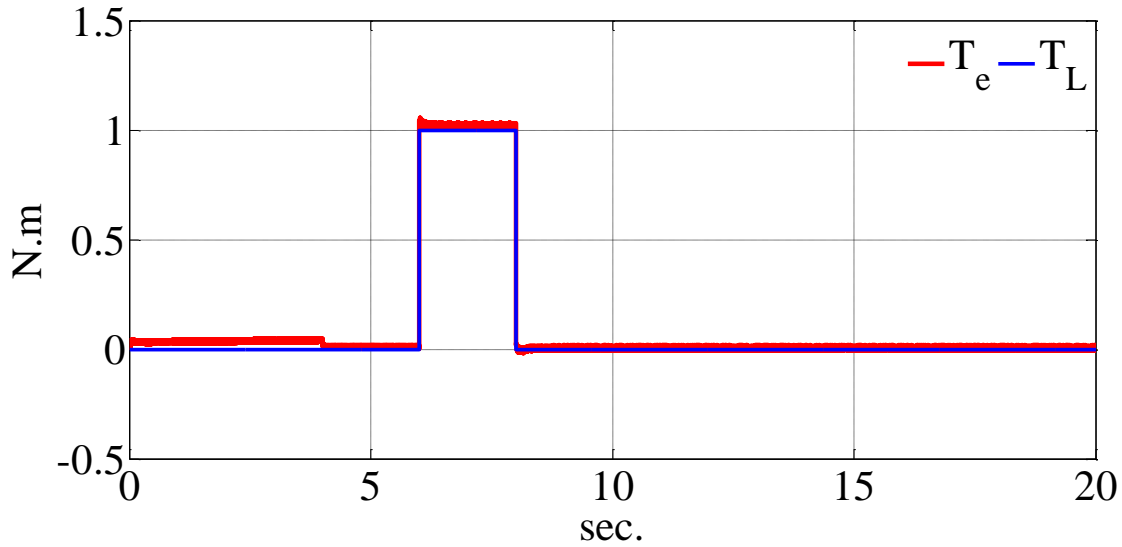


Figure 5.66: The electromagnetic torque of the machine (simulation results).

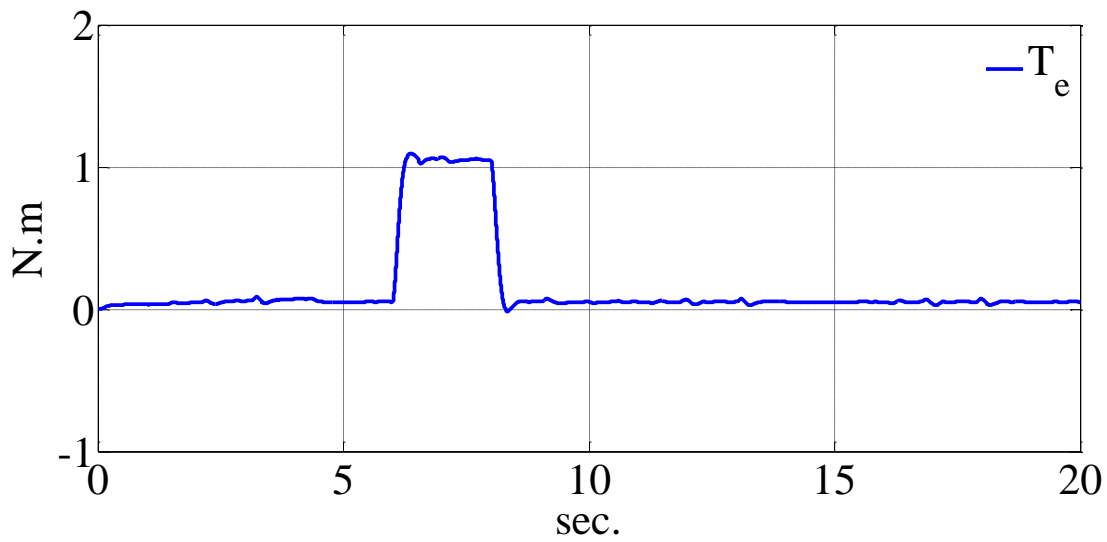


Figure 5.67: The electromagnetic torque of the machine (experimental results).

The Figure 5.64 (b) and 5.65 (b) show the speed error for simulation and experiment respectively. Figures 5.66 shows the electromagnetic torque of machine and the load torque for simulation and 5.67 shows the electromagnetic torque of machine for experiment. From both figures it can be seen that, by applying the load, machine generated electromagnetic torque to keep the rotor speed constant.

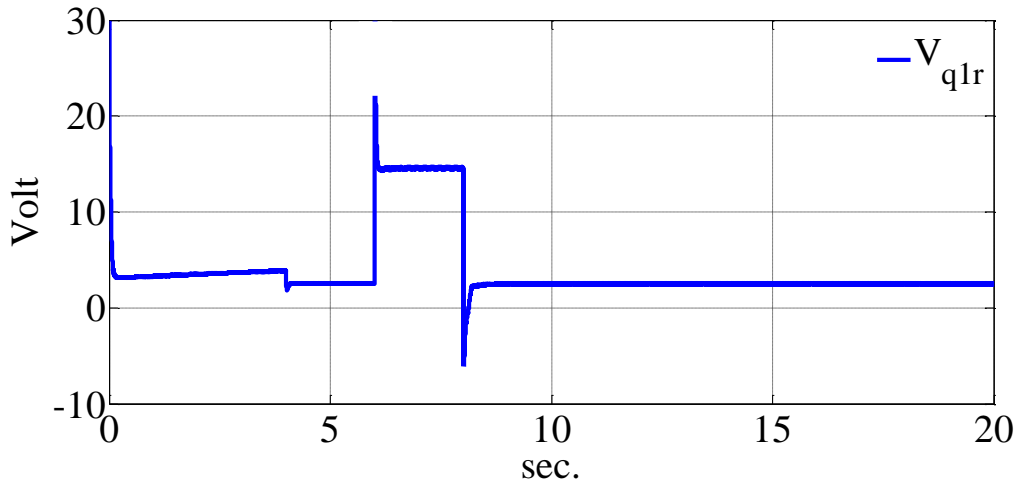


Figure 5.68: The voltage generated by the current regulators in q axis of rotor reference frame (simulation results).

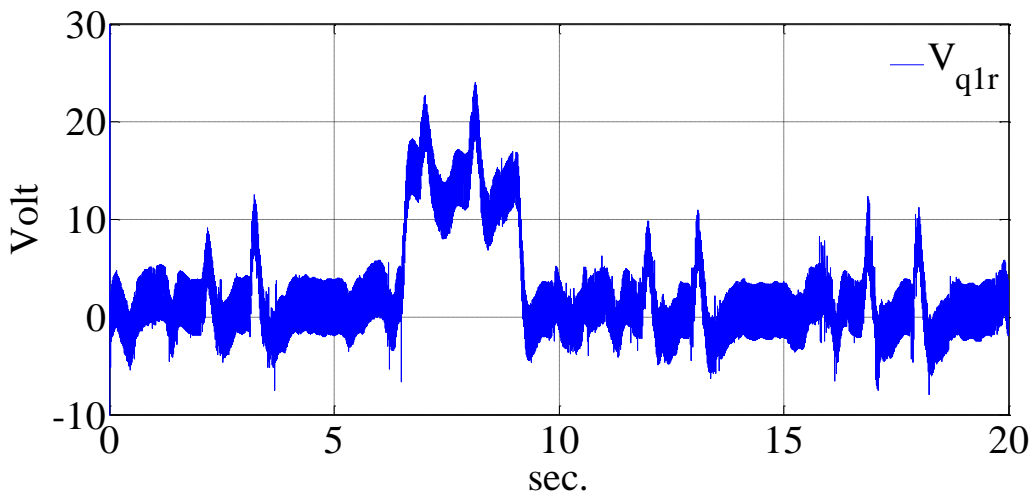


Figure 5.69: The voltage generated by the current regulators q axis of the rotor reference frame (experimental results).

Figures 5.68 and 5.69 show the output voltage of controller generated in q axis of the rotor reference frame for simulation and experimental respectively. It can be seen by applying the load torque the q axis increases to let q axis current increase and generate the electromagnetic torque.

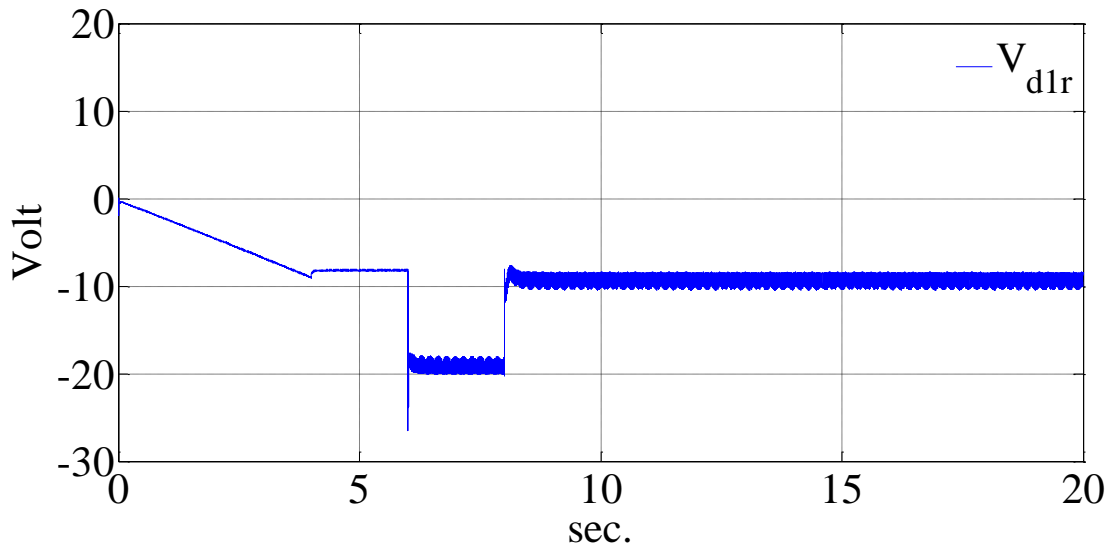


Figure 5.70: The voltage generated by the current regulators d axis of the rotor reference frame (simulation results).

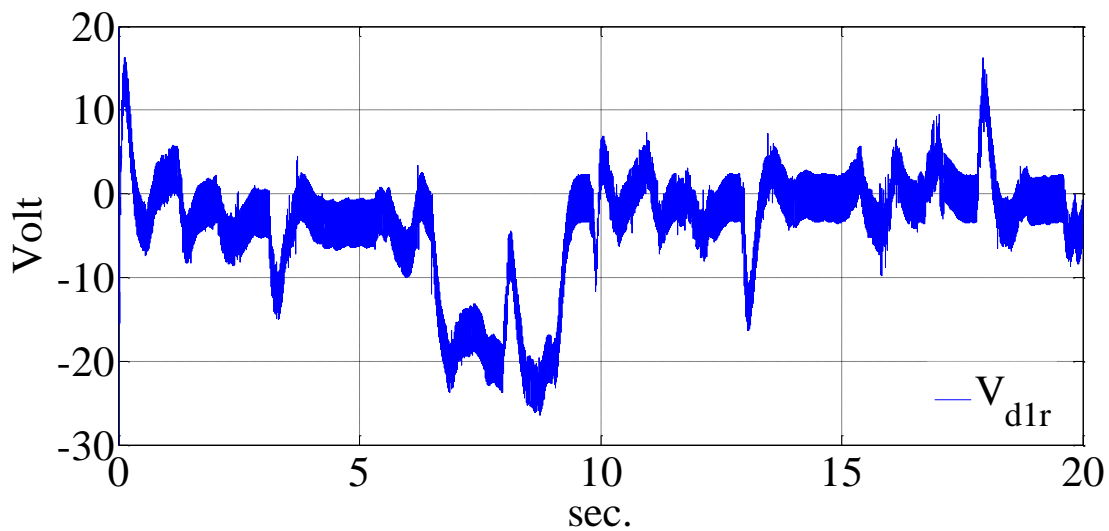


Figure 5.71: The voltage generated by the current regulators d axis of the rotor reference frame (simulation results).

Figures 5.70 and 5.71 show the output voltage of controller generated in d axis of the rotor reference frame for simulation and experimental respectively. It can be seen by increasing the q

axis current and consequently d axis current, the d axis voltage increases in negative side to let the essential d axis current flow to the machine stator.

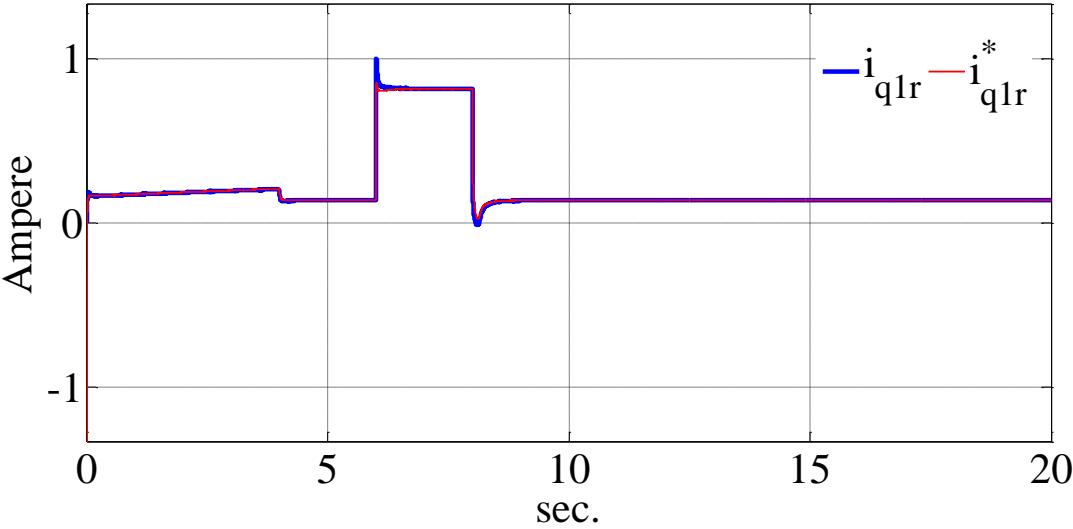


Figure 5.72: The q axis reference and feedback currents (simulation results).

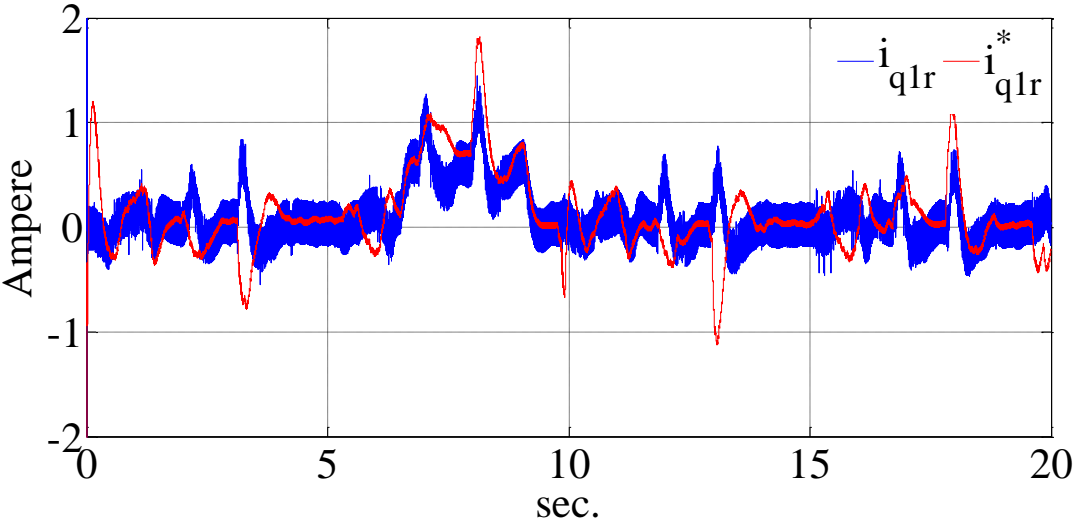


Figure 5.73: The q axis reference and feedback currents (experimental results).

Figures 5.72 and 5.73 show the reference and measured currents in q axis of the rotor reference frame for simulation and experimental respectively. The q axis current is generated from

the speed error and it can be seen that, the q axis current increases when the load torque is applied to the machine shaft.

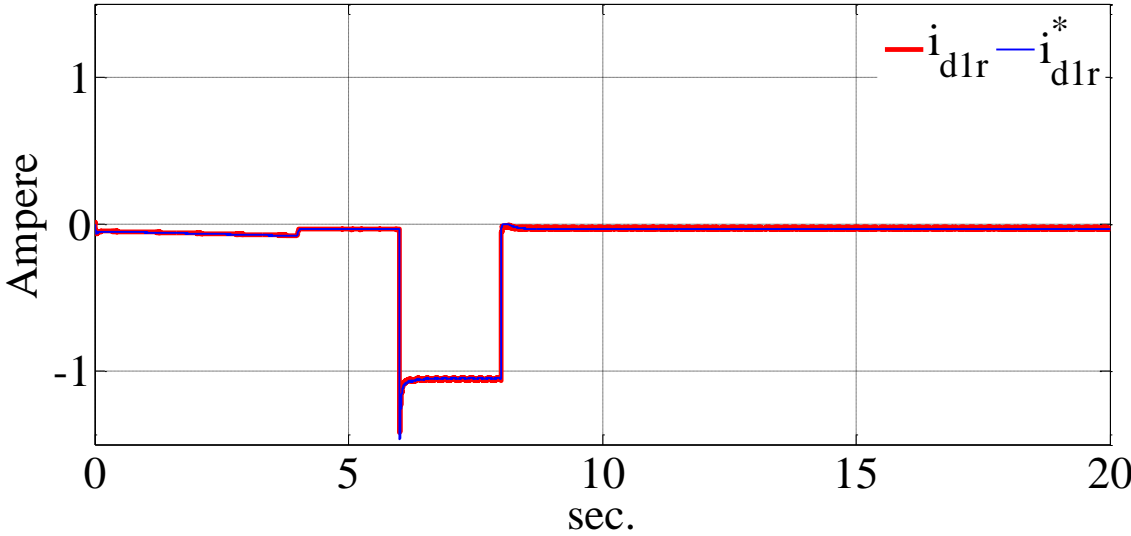


Figure 5.74: The d axis reference and feedback currents (simulation results).

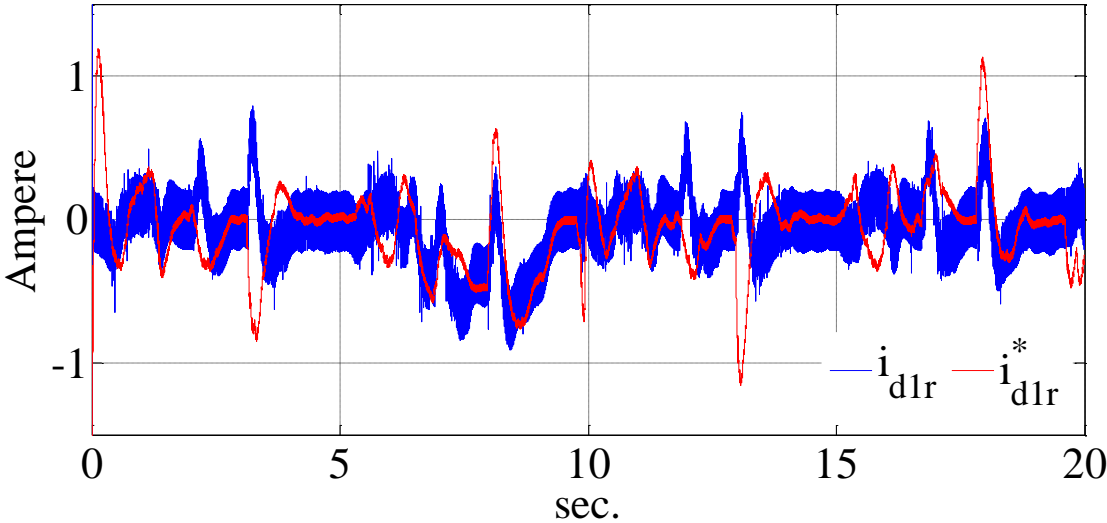
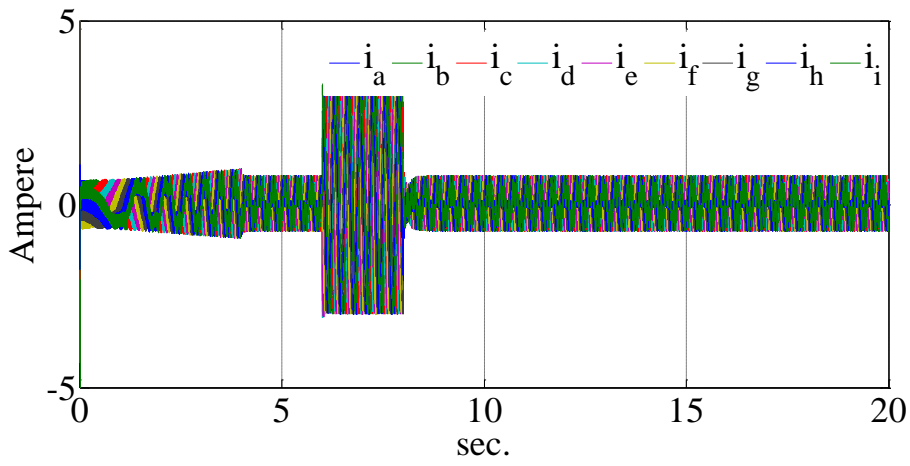
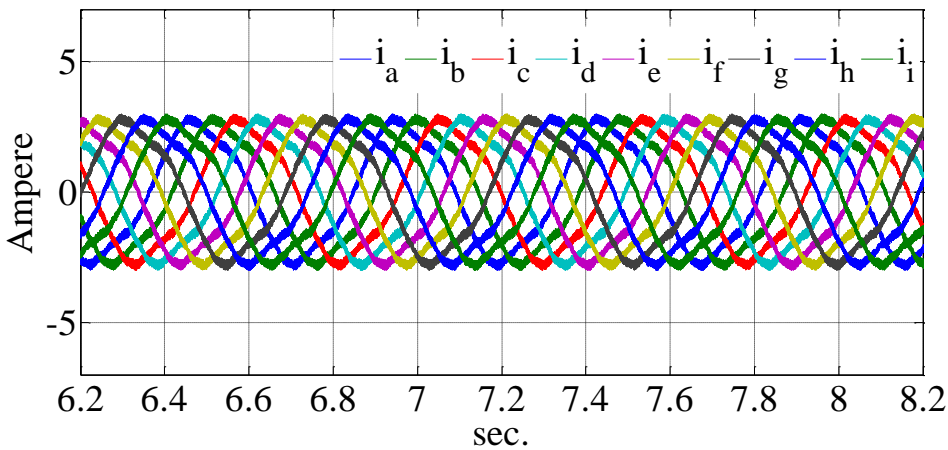


Figure 5.75: The d axis reference and feedback currents (experimental results).

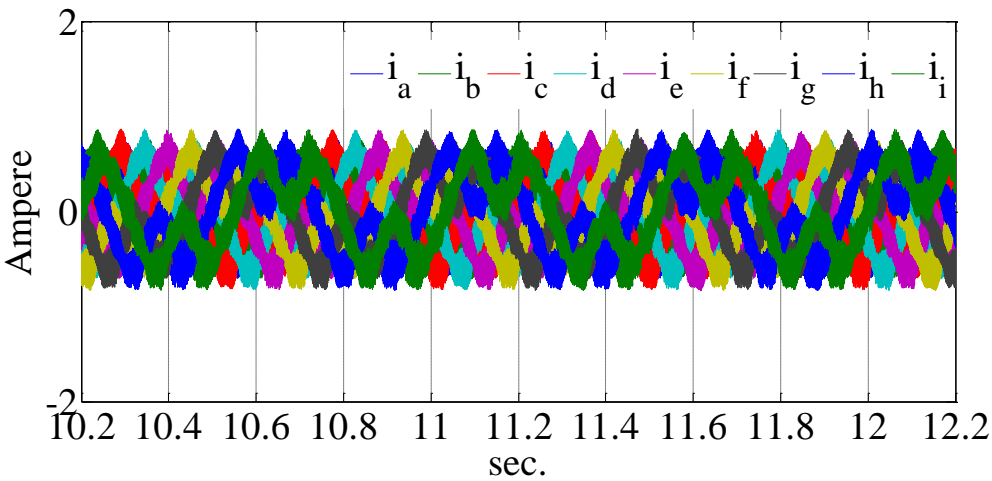
Figures 5.74 and 5.75 show the reference and the feedback values for the d axis current for simulation and experiment respectively. The reference is again generated from the q axis current using the minimum copper loss strategy.



(a)

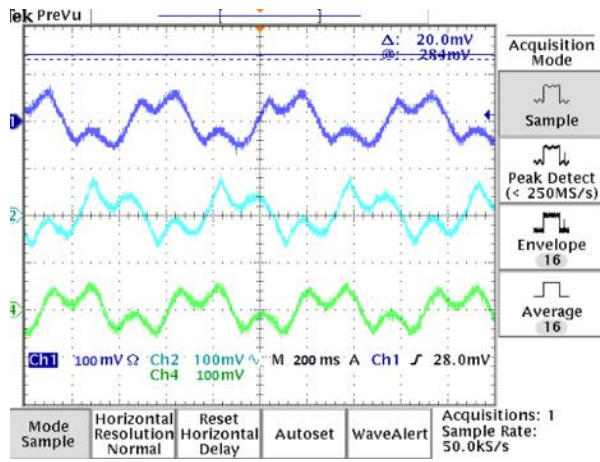


(b)

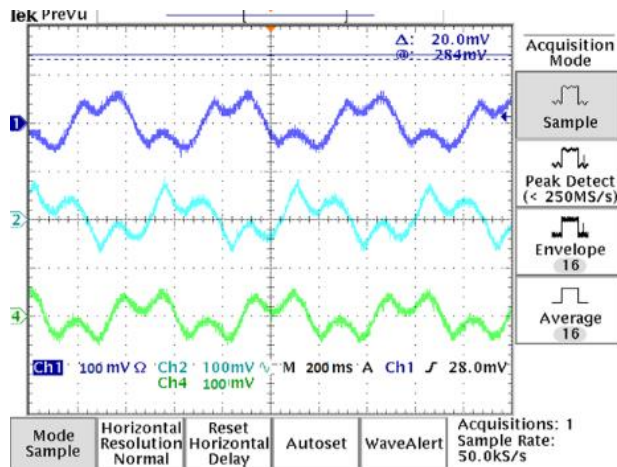


(c)

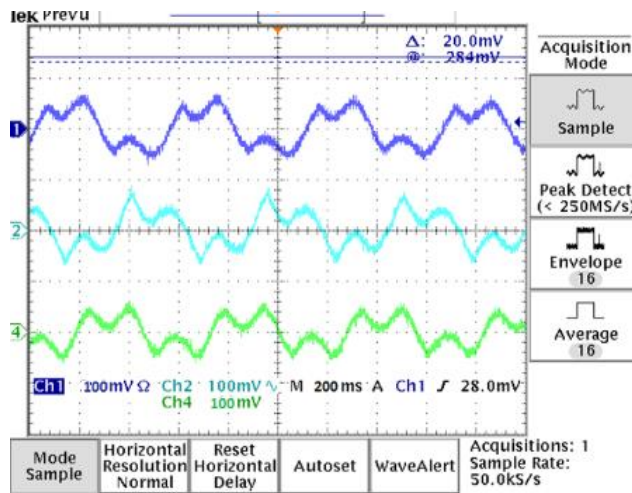
Figure 5.76: (a) The currents of the machine in natural variables (simulation results), (b) and (c) Zoomed view before and after load application respectively (simulation results).



(a)

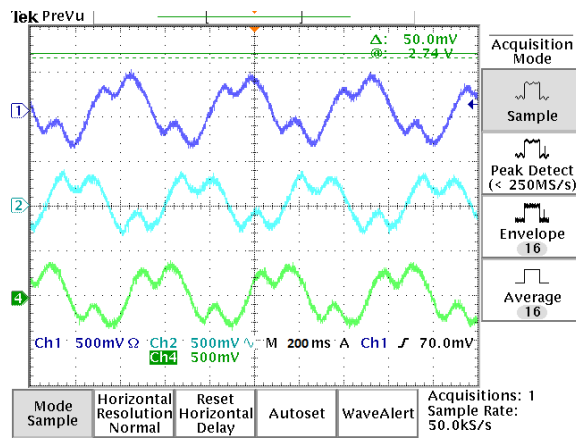


(b)

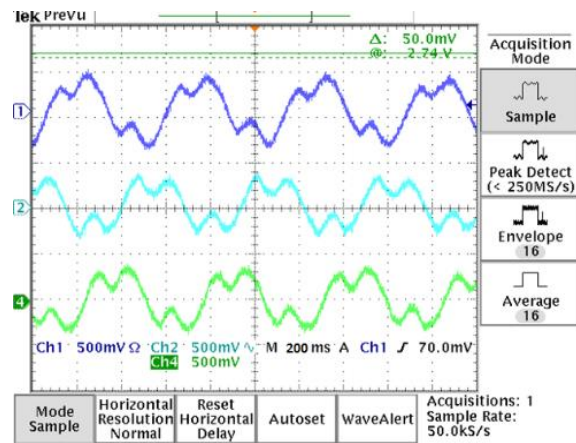


(c)

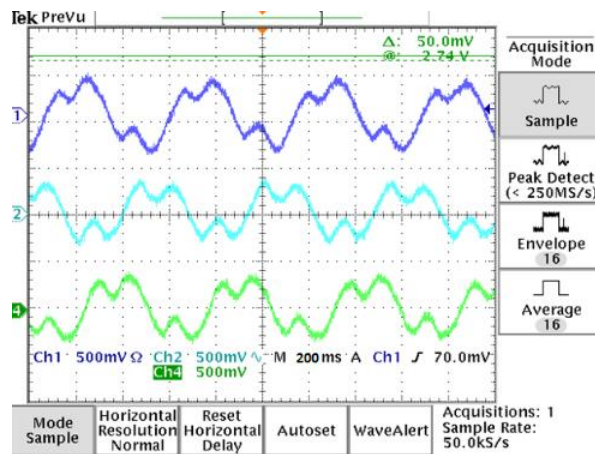
Figure 5.77: The nine-phase currents of the machine phases before applying load for phases, (a) 'a', 'd' and 'g', (b) 'b', 'e' and 'h', (c) 'c', 'f' and 'i' (experimental results) (2 A/ scale).



(a)

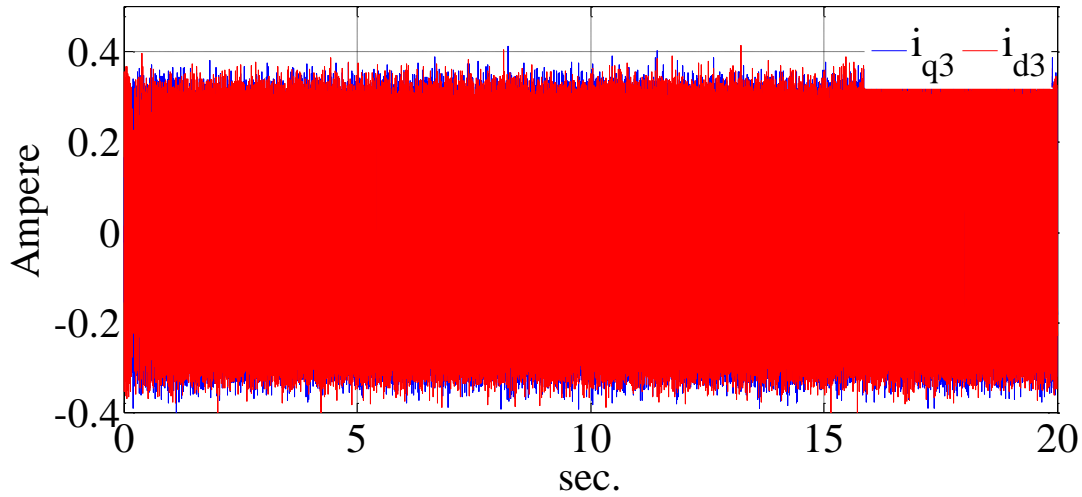


(b)

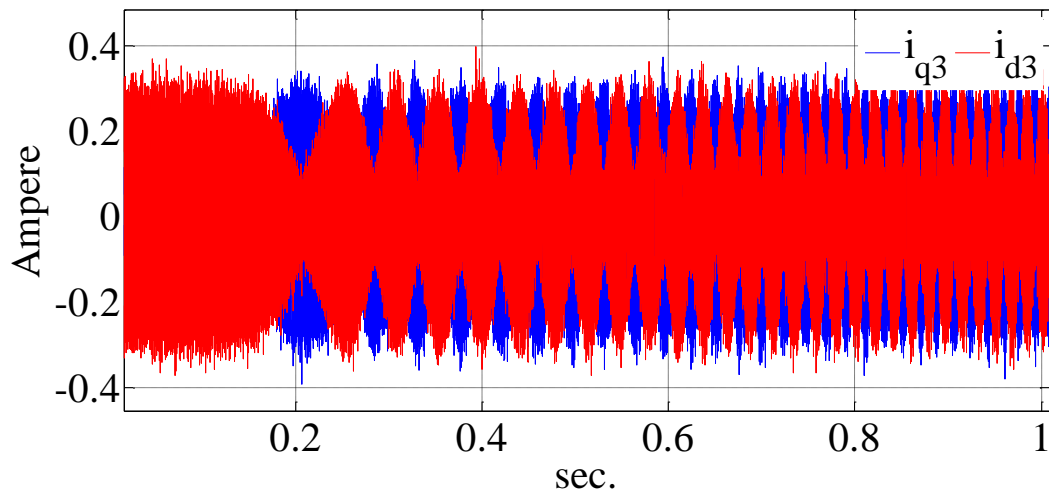


(c)

Figure 5.78: The nine-phase currents of the machine phases after applying load for phases for phases, (a) 'a', 'd' and 'g', (b) 'b', 'e' and 'h', (c) 'c', 'f' and 'i' (experimental results) (5 A/ scale).



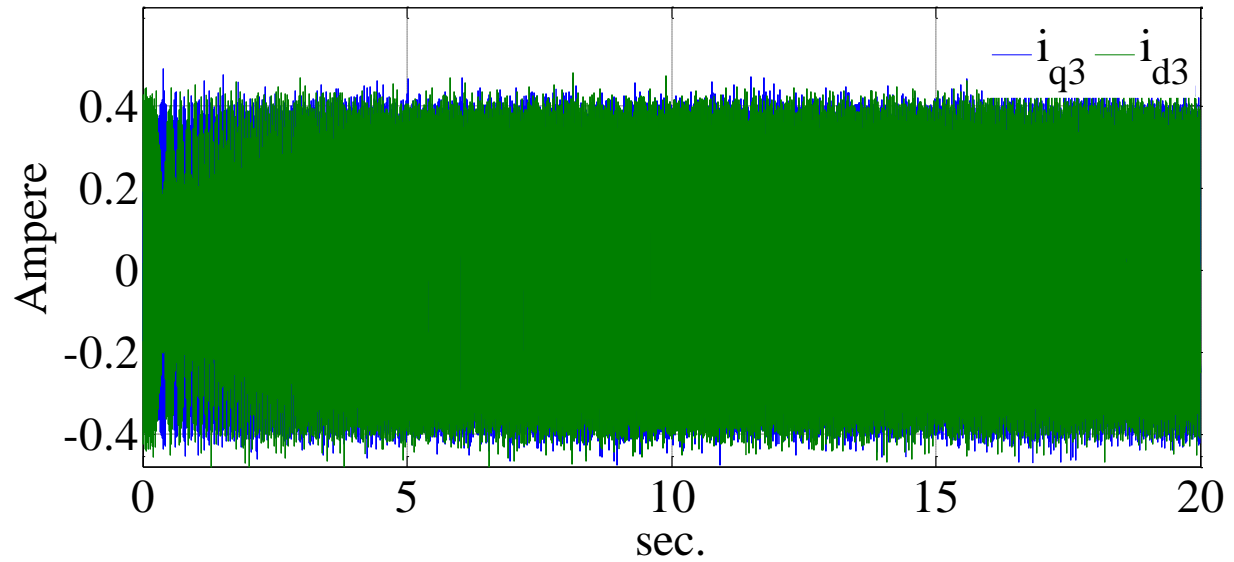
(a)



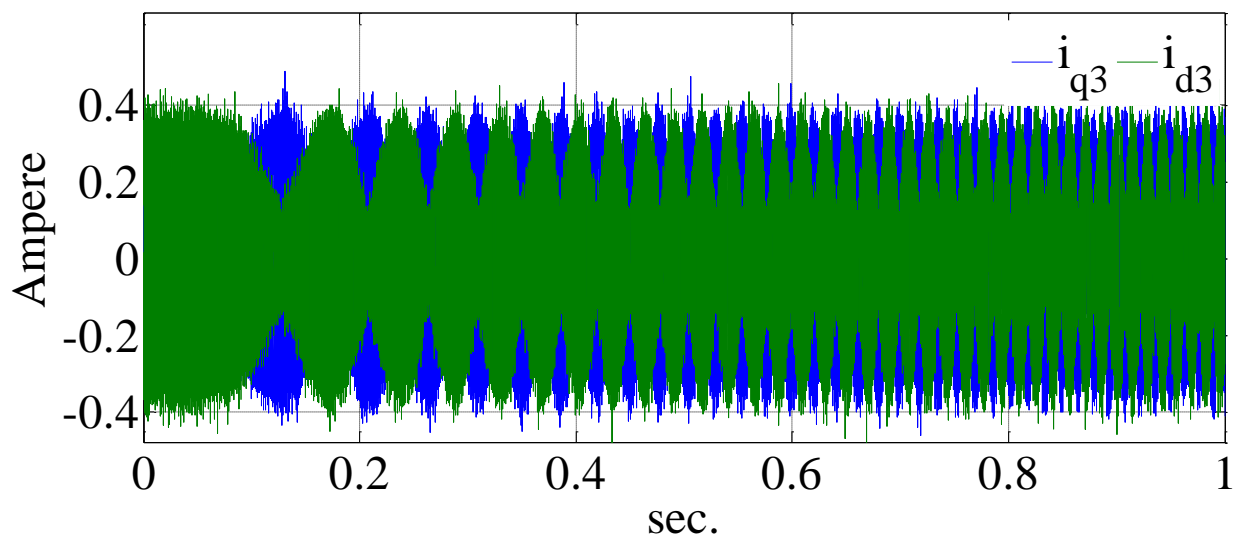
(b)

Figure 5.79: (a) The third sequence of the stator current in the stationary reference frame (simulation results), (b) The zoomed view (simulation results).

Figure 5.76 shows the simulation results of the stator currents. The effect of the increase in q and d axis current of the rotor reference frame can be seen from their peak magnitude. The stator currents of experimental results are also shown in Figures 5.77 and 5.78. Figure 5.77 shows the currents before applying load torque and Figure 5.78 shows the stator currents after applying load torque. There are some ripples on the currents of the experimental results which are due to the magnetic saturation of the machine stator and measurement noise.



(a)

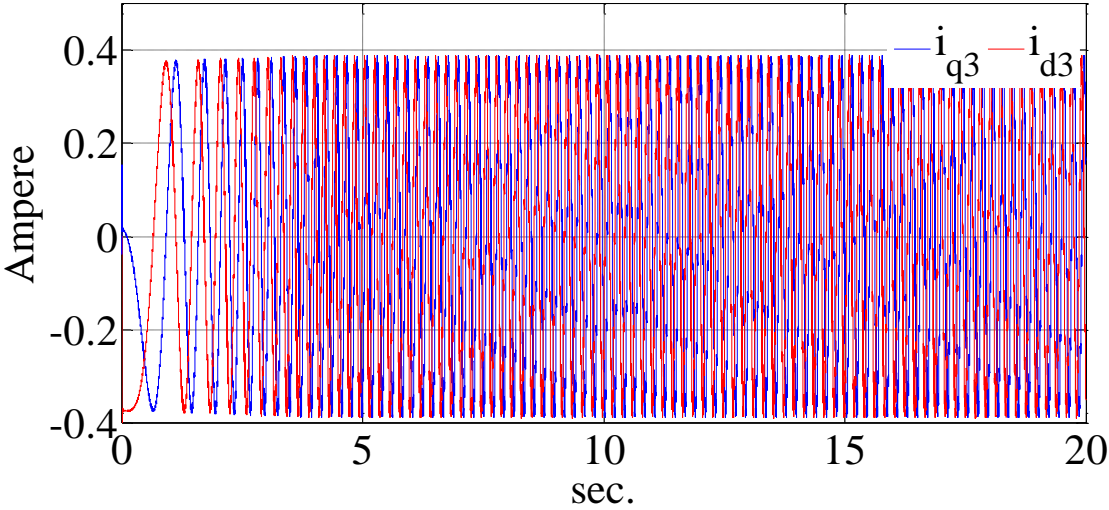


(b)

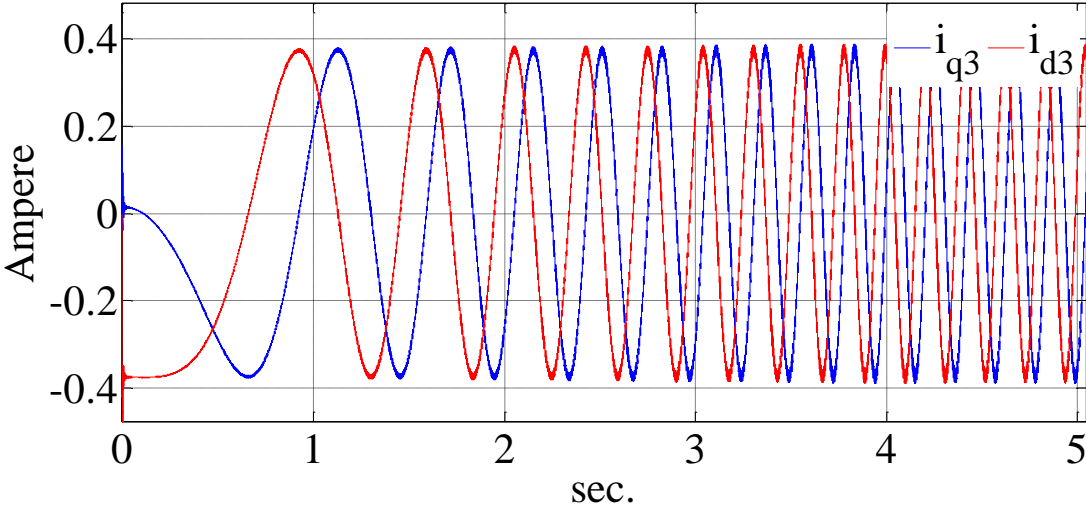
Figure 5.80: (a) The third sequence of the stator current in the stationary reference frame (experimental results), (b) The zoomed view (experimental results).

The third sequence currents of the stator are extracted and used for position estimation. The simulation and experimental results of the third sequence currents are shown in Figures 5.79 and 5.80 respectively. The currents in Figures 5.81 and 5.82 pass through a heterodyning block then

they can pass through a low pass filter to remove their redundant high frequency parts. Figures 5.83 and 5.84 show the resulting current after heterodyning and filtering for simulation and experiment respectively.

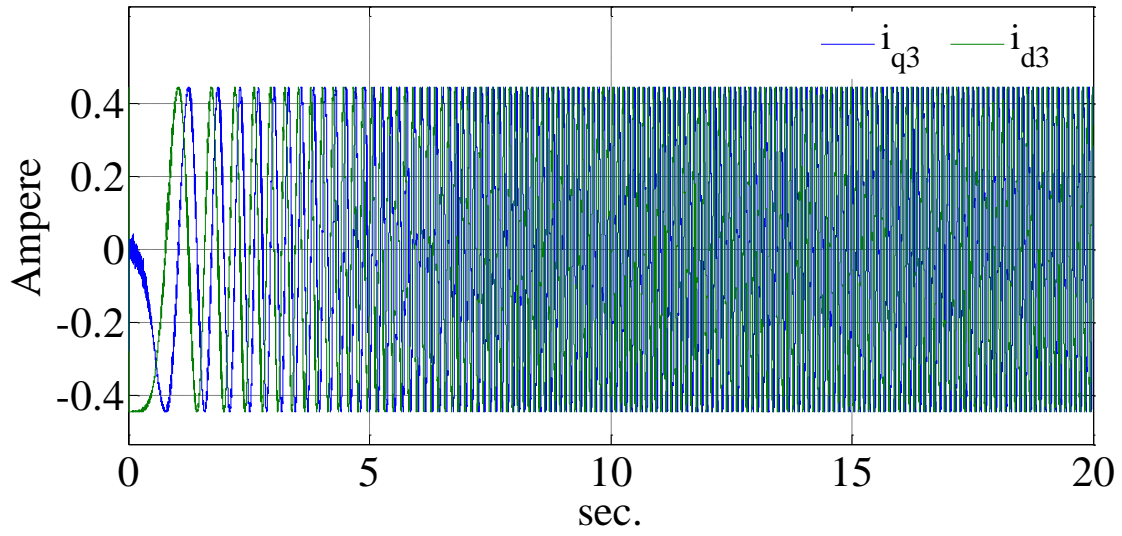


(a)

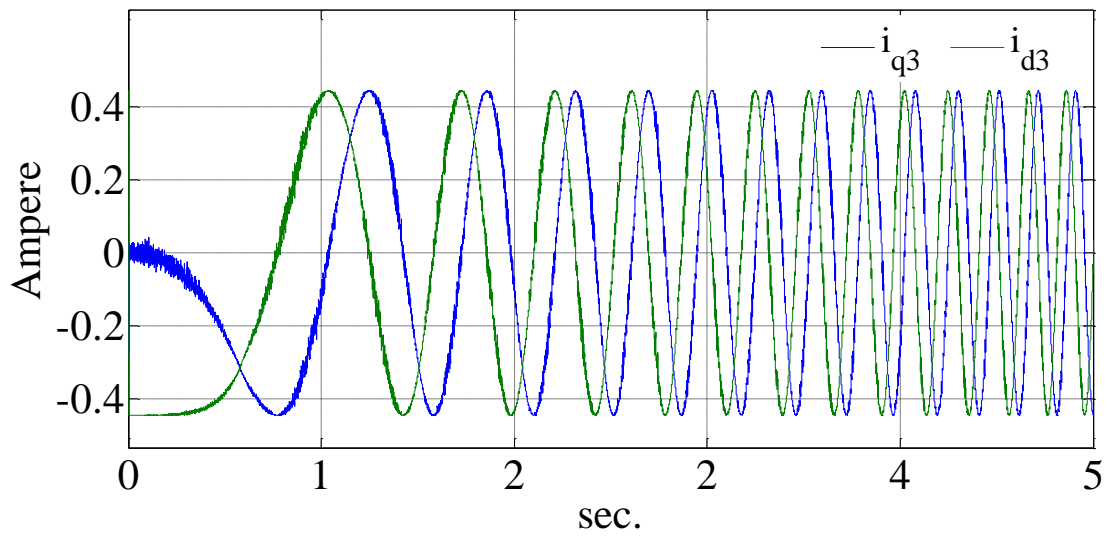


(b)

Figure 5.81: (a) The third sequence of the stator current in the stationary reference frame after heterodyning and filtering (simulation result), (b) The zoomed view (simulation result).



(a)



(b)

Figure 5.82: (a) The third sequence of the stator current in the stationary reference frame after heterodyning and filtering (experimental result), (b) The zoomed view (experimental result).

The signals of Figures 5.81 and 5.82 need to be normalized to have unity magnitude and be fed to the observer. Figures 5.83 and 5.84 show the signals after normalizing for simulation and experimental results respectively.

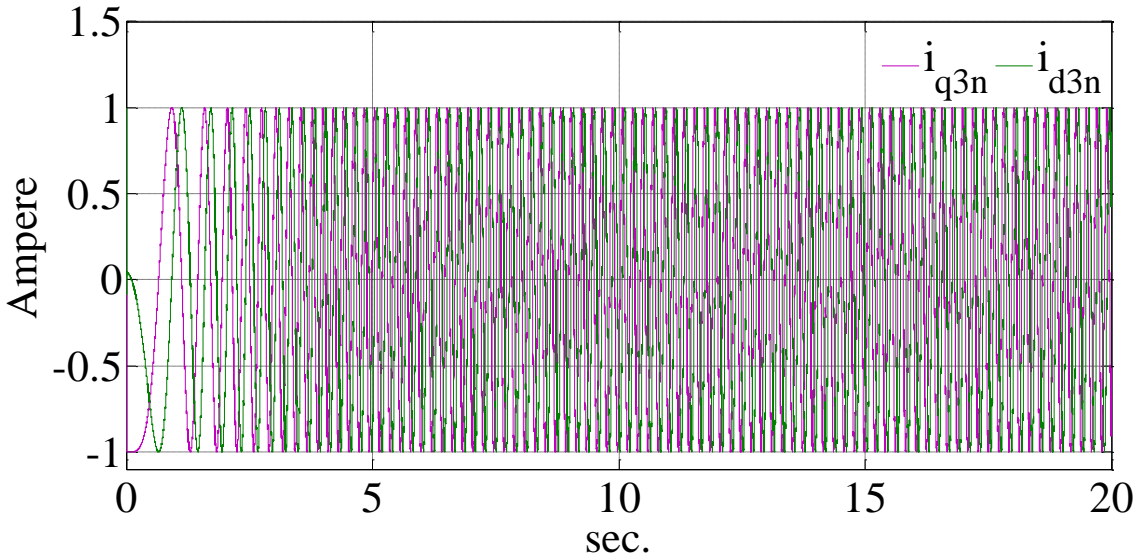


Figure 5.83: The normalized currents of the third sequence (simulation results).

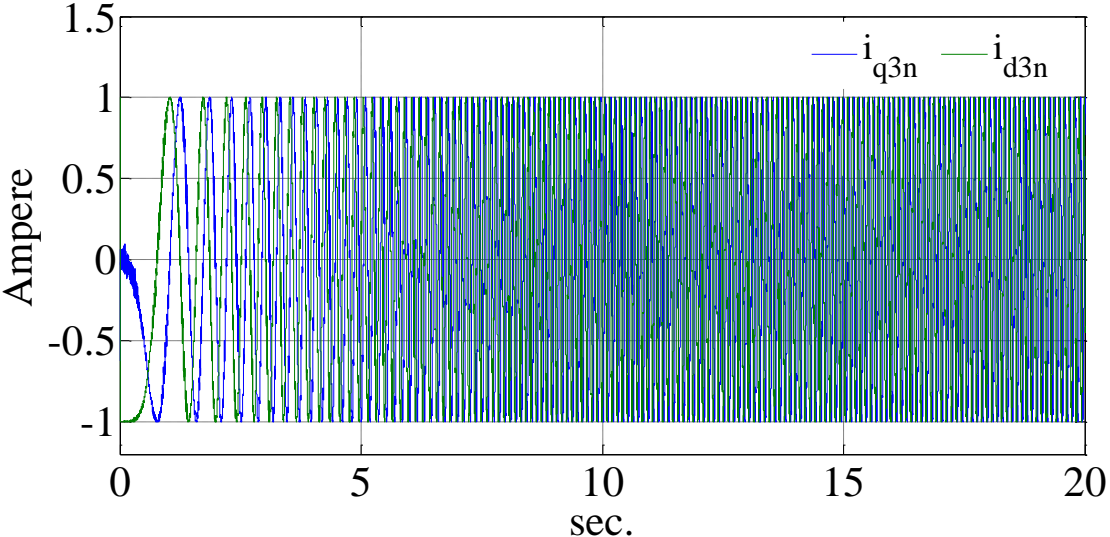
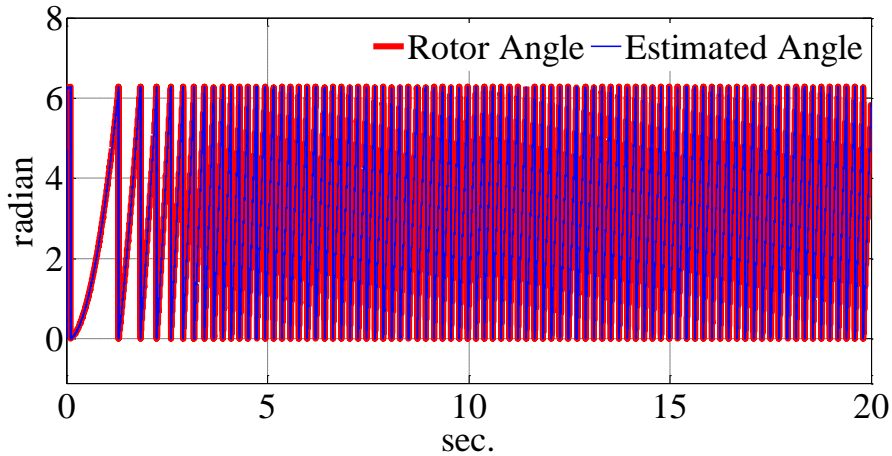
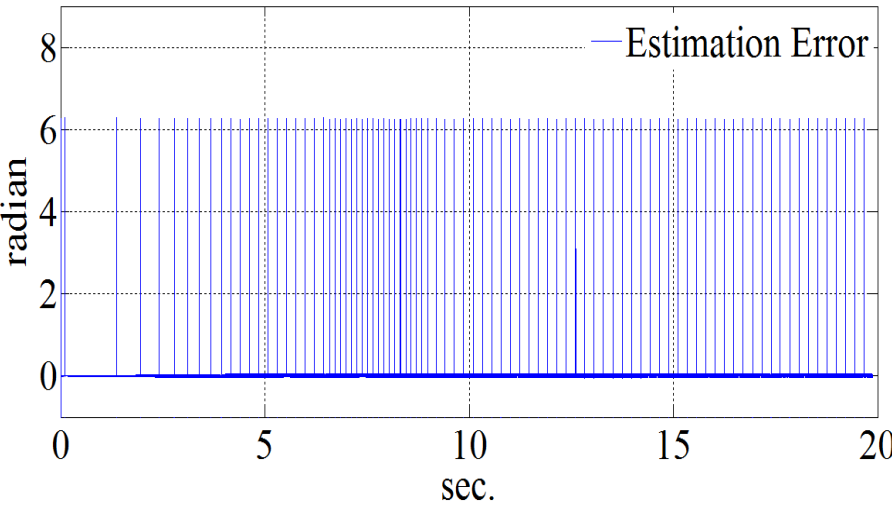


Figure 5.84: The normalized currents of the third sequence (experimental results).

The signals of Figure 5.83 and 5.84 carry the rotor position information. The rotor position now can be extracted using Luenberger observer. The signals are fed to the observer and the results are shown in Figures 5.85 and 5.86 for simulation and experiment respectively. These two figures show the rotor angle and the estimated one along with the estimation error.

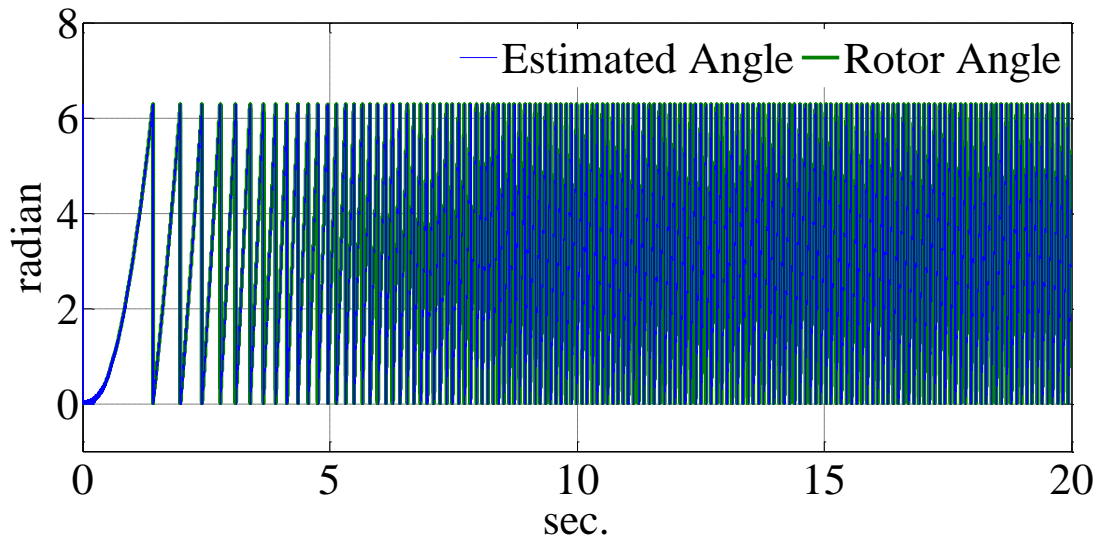


(a)

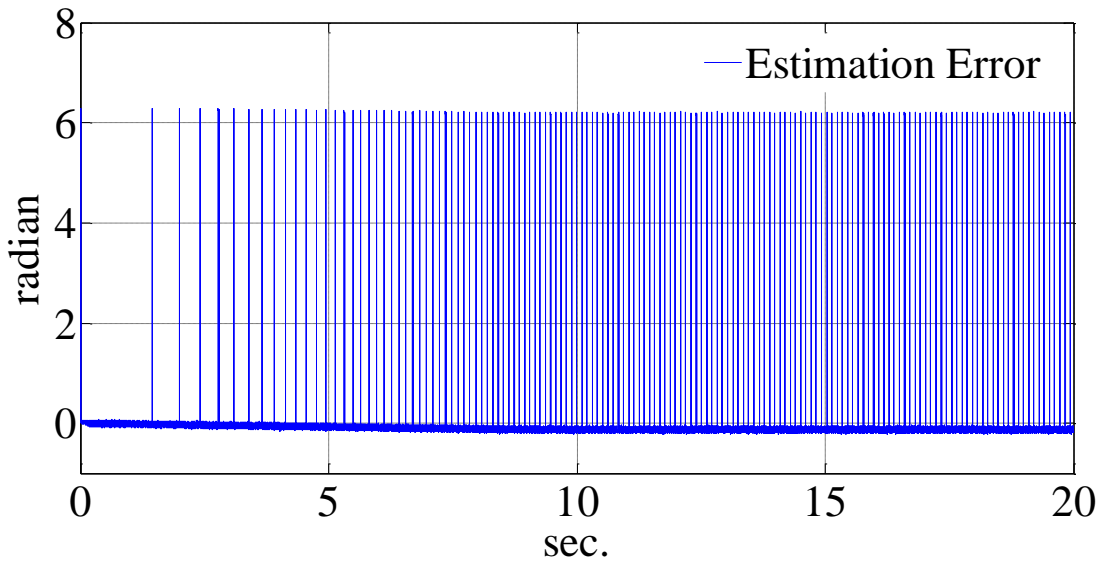


(b)

Figure 5.85: (a) The simulated and estimated angle (simulation results), (b) The estimation error (simulation results).



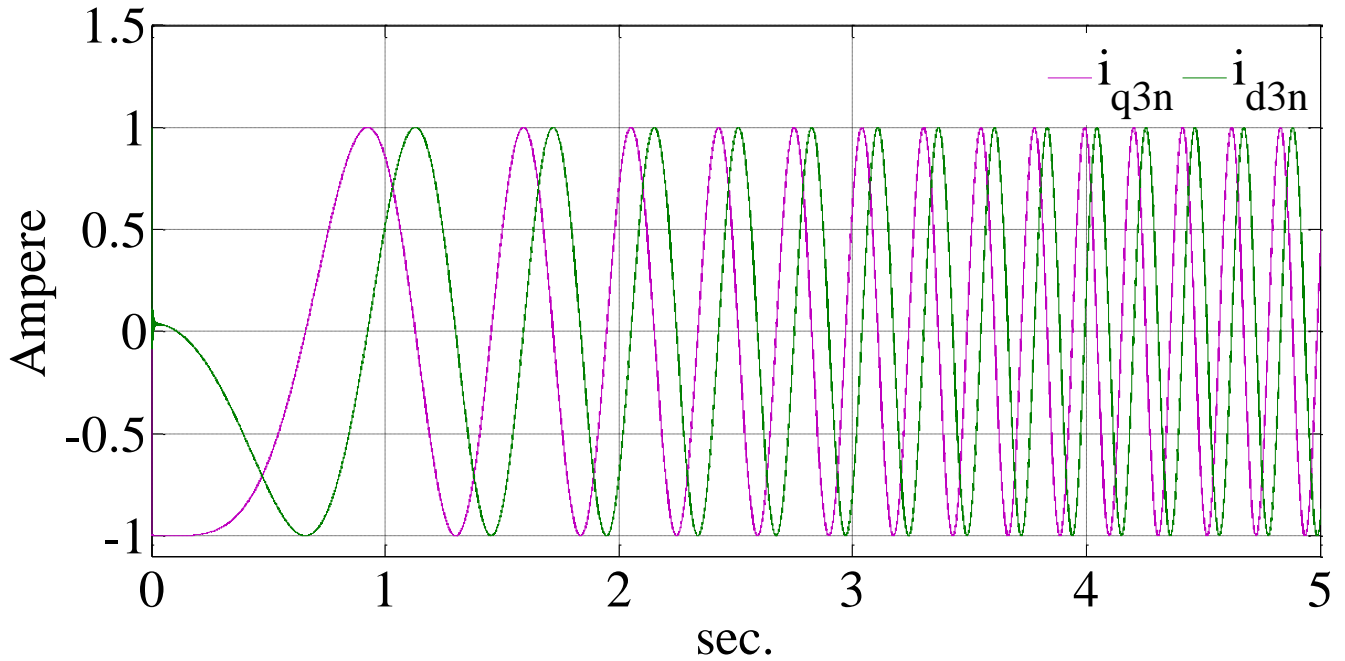
(a)



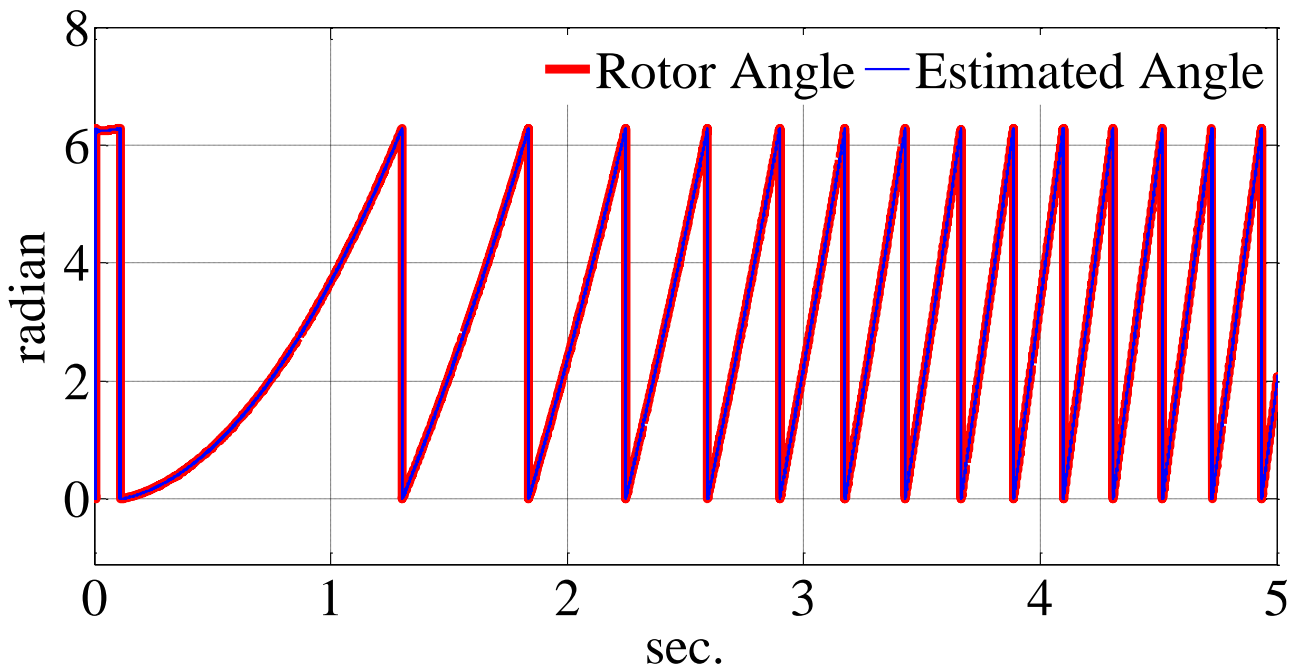
(b)

Figure 5.86: (a) The simulated and estimated angle (experimental results), (b) The estimation error (experimental results).

The Figures 8.87 to 8.88 show the zoomed view of the Figures 5.85 and 5.86 for first five seconds.

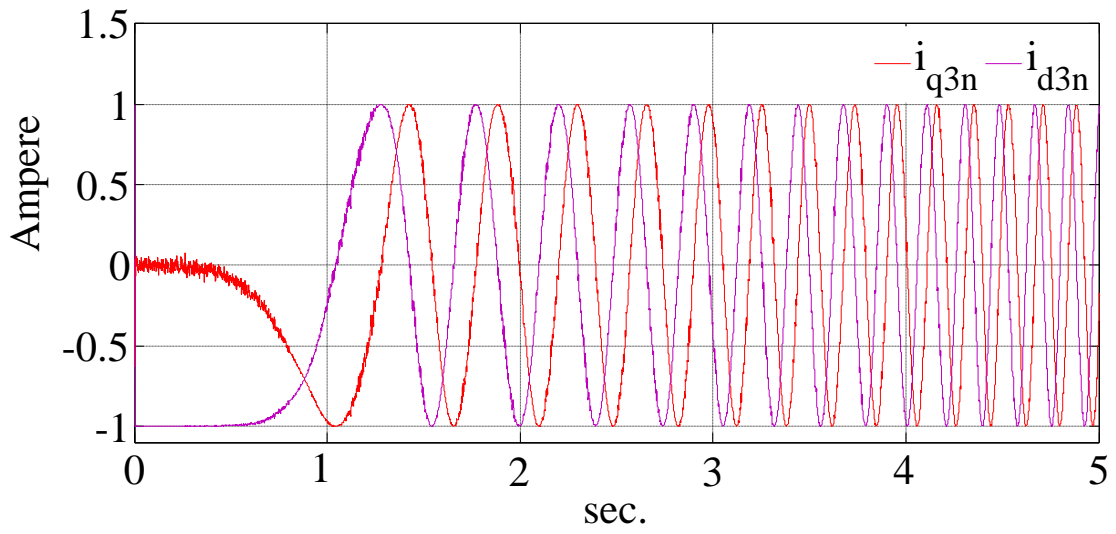


(a)

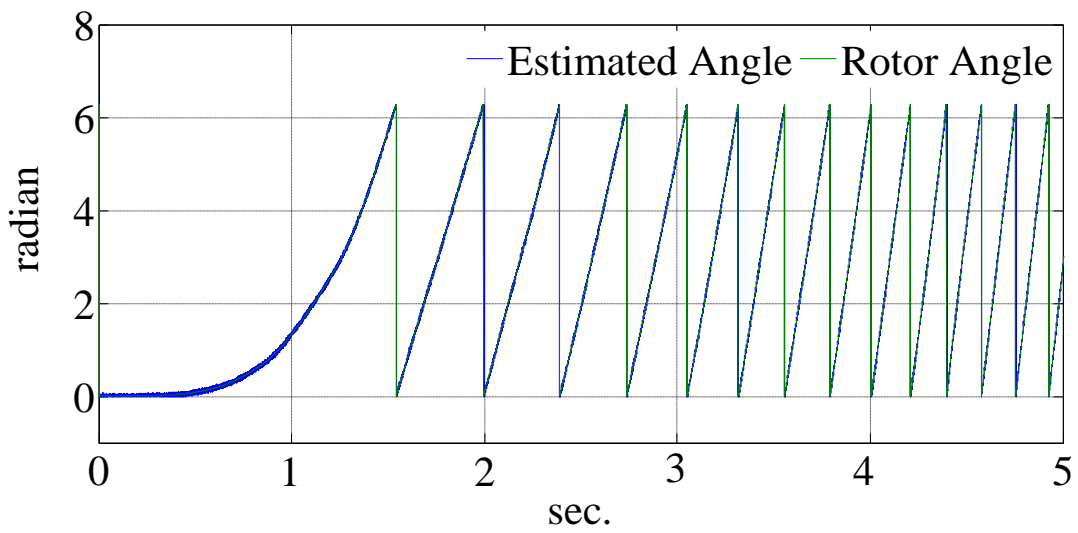


(b)

Figure 5.87: (a) The normalized currents of the third sequence (simulation results), (b) The simulated and estimated rotor angle at the starting interval (simulation results).



(a)

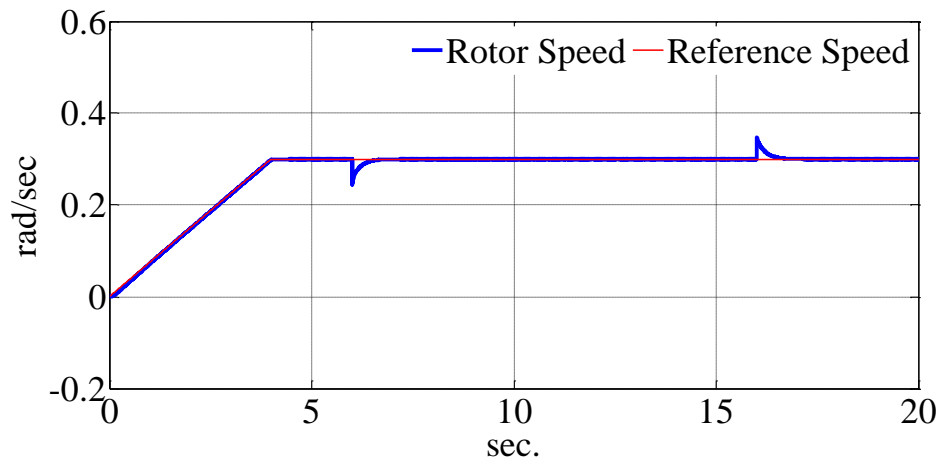


(b)

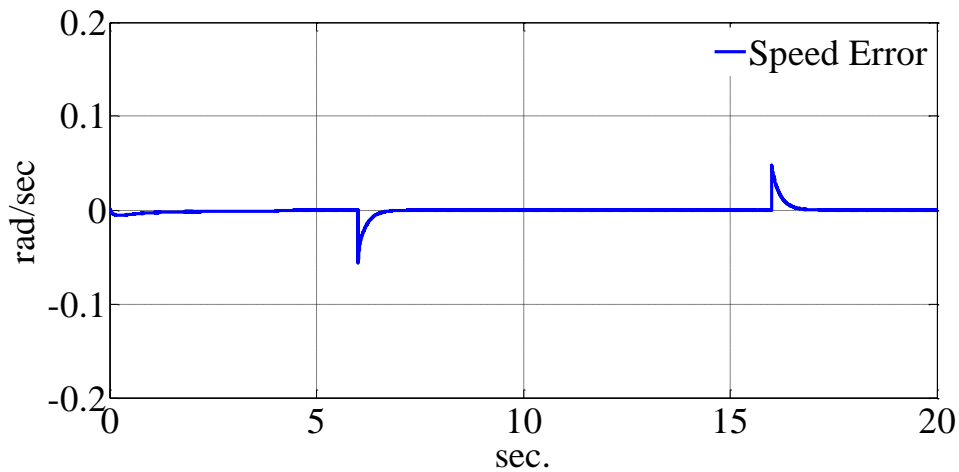
Figure 5.88: (a) The normalized currents of the third sequence (experimental results), (b) Actual and estimated rotor angle at the starting interval (experimental results).

5.6.4 Very Low Speed Run

The last test is the same controller in a very low speed. In this test the machine runs at the speed of 0.3 rad/sec and a step load is applied to the machine when it is in the steady state. The following figures show the simulation and experimental results. The speed reference starts from the zero and goes to a fixed speed at 0.3 (rad/sec) after drive settles down to the steady state conditions a step load torque is applied to the rotor for 10 seconds.

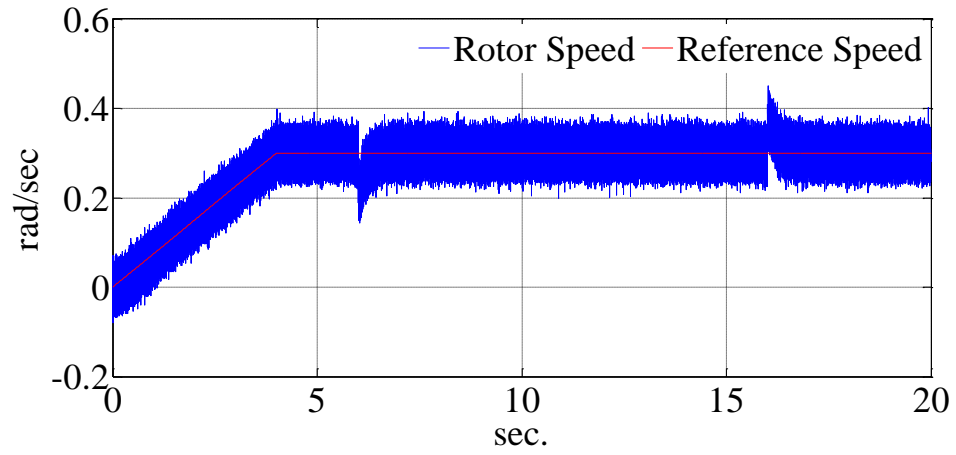


(a)

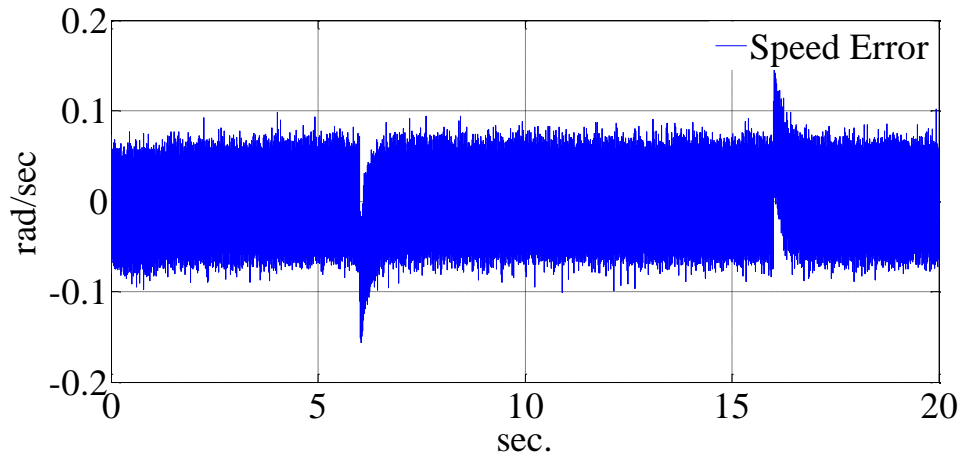


(b)

Figure 5.89: (a) The rotor speed and the reference speed (simulation results), (b) The speed error (simulation results).



(a)



(b)

Figure 5.90: (a) The reference and rotor speed (experimental results), (b) The speed error (experimental results).

Figures 5.89 (a) and 5.90 (a) show the reference and rotor speed for simulation and experimental results respectively. From these figures, it can be seen that the drive can track the rotor reference accurately. For better view, the speed errors are also presented in Figures 5.89 (b) and 5.90 (b) for simulation and experimental results respectively. Figure 5.91 shows the electromagnetic torque and the load torque for simulation. The electromagnetic torque of the machine for experimental result is also shown in the Figure 5.92. From these figures, it can be seen

that, the drive can react to the load torque and generate proper electromagnetic torque to keep the rotor speed constant.

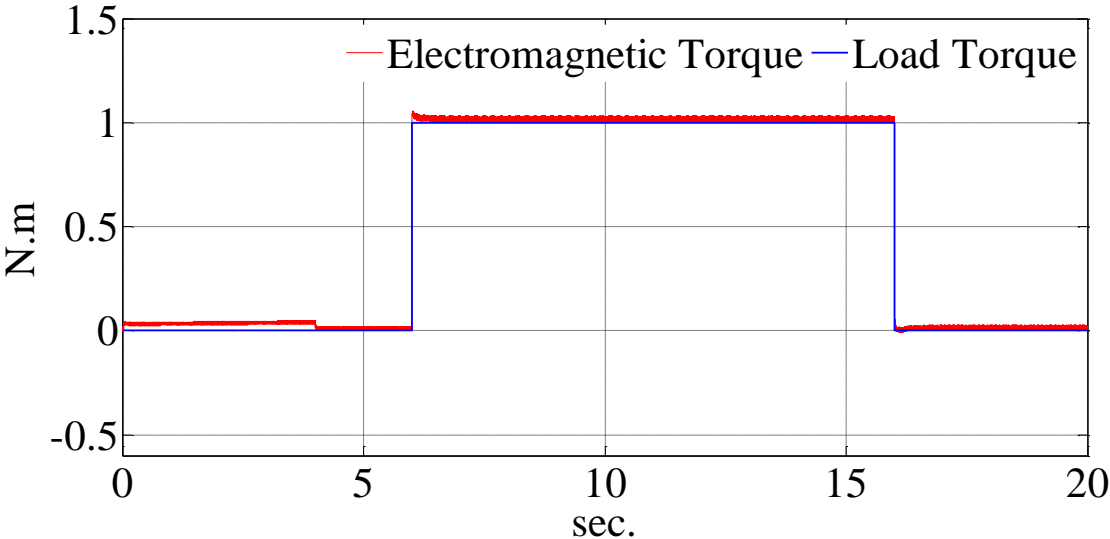


Figure 5.91: The load and electromagnetic torque (simulation results).

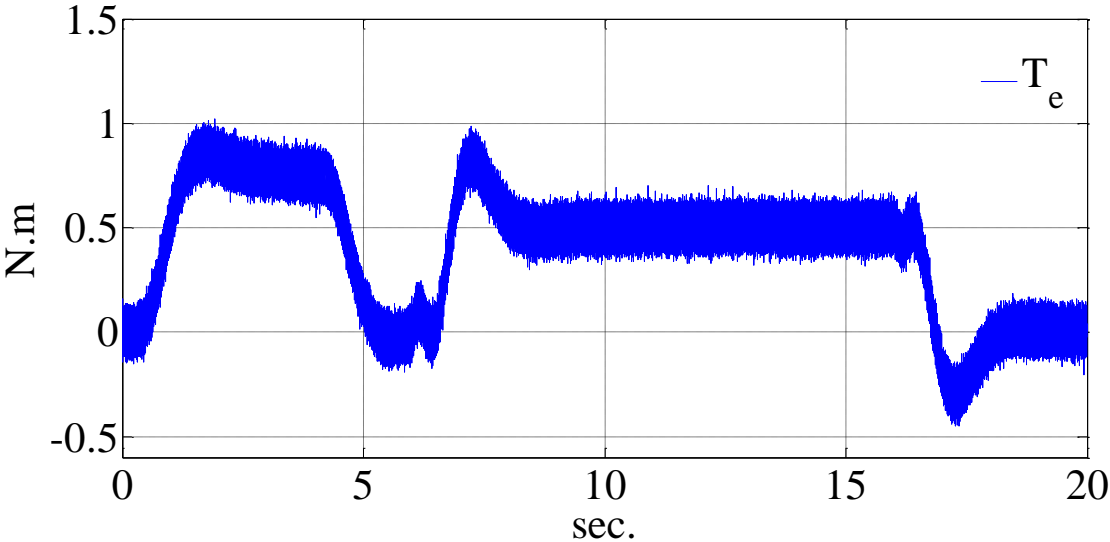


Figure 5.92: The electromagnetic torque of the machine (experimental results).

The voltages generated by machine controller in rotor reference frame are shown in the Figures 5.93 and 5.94 for simulation and experimental results respectively. Again from this Figures the reaction of the drive to the changes of the load on the motor shaft can be seen.

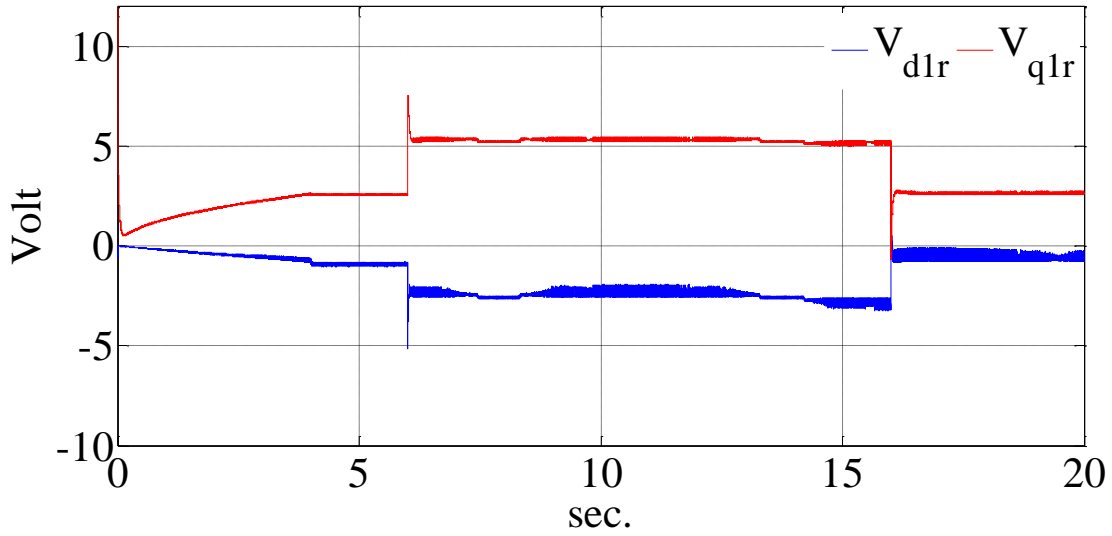


Figure 5.93: The q and d axis voltages in rotor reference frame generated by the controller (simulation results).

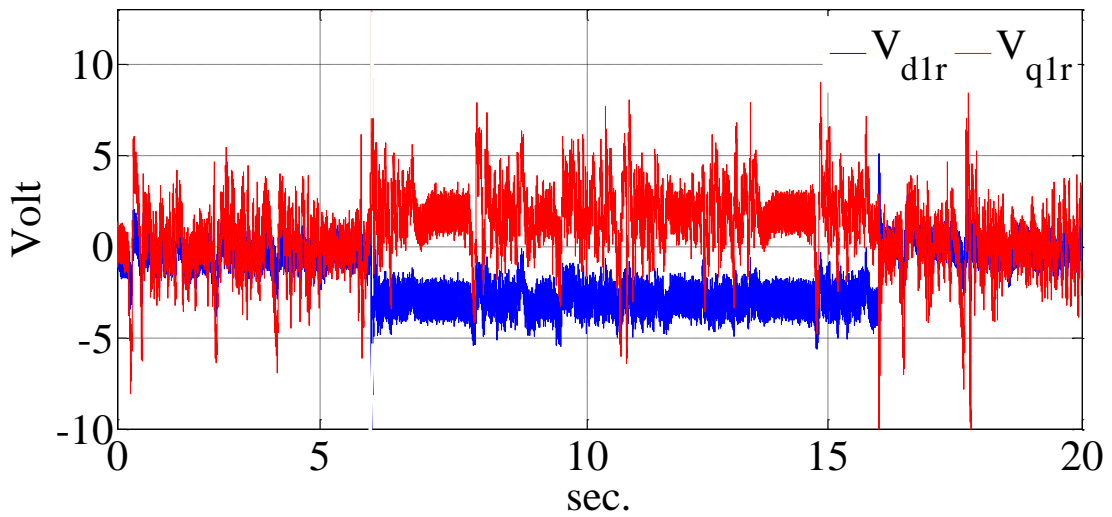


Figure 5.94: The q and d axis voltage of the machines in the rotor reference frame generated by the controller (experimental results).

The generated voltages are applied to the machine to inject the desired currents to the stator. Figures 5.95 and 5.96 show the reference and measured current of q axis reference frame for simulation and experiment respectively.

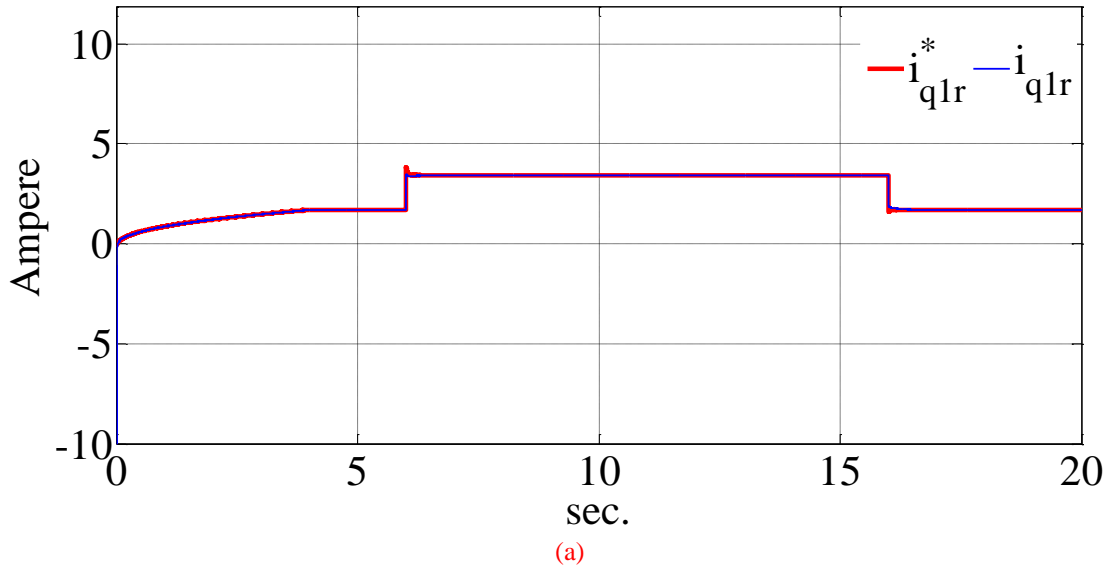


Figure 5.95: The reference and the feedback currents in rotor reference frame for q axis (simulation results).

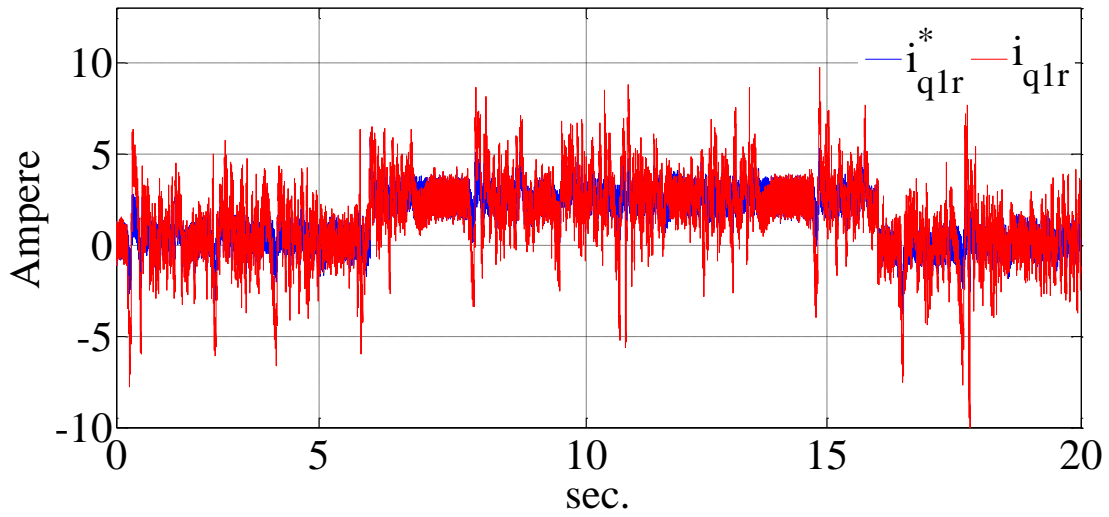


Figure 5.96: The reference and the feedback currents in rotor reference frame for q axis (experimental results).

Figures 5.97 and 5.98 also show the reference and measured current of d axis reference frame for simulation and experiment respectively.

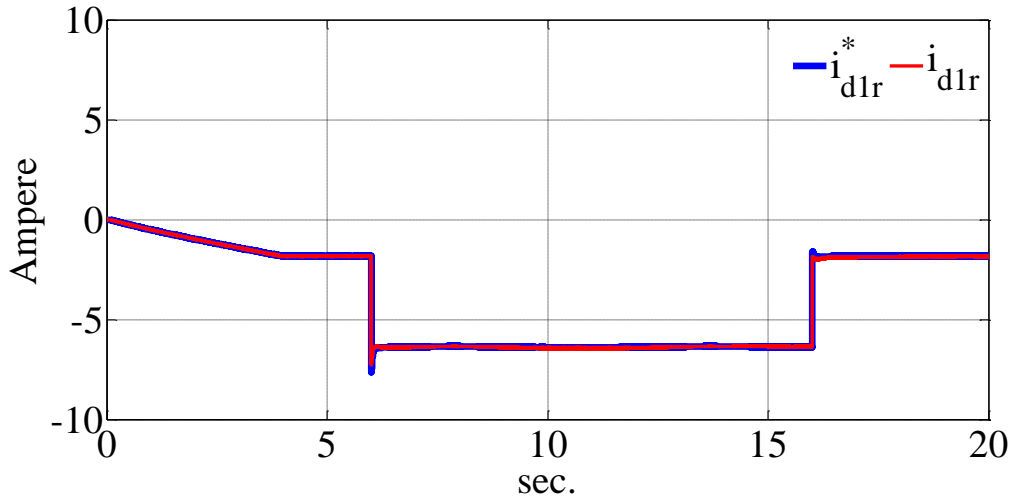


Figure 5.97: The reference and the feedback currents in rotor reference frame for d axis (simulation results).

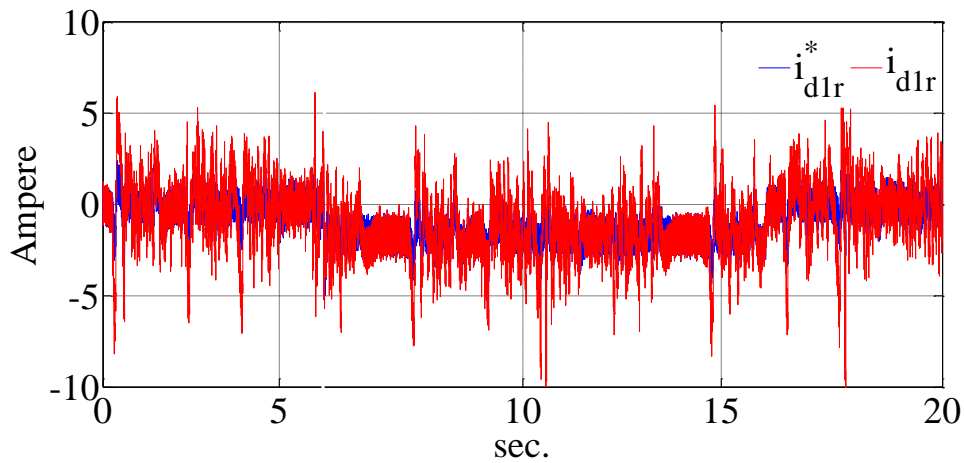
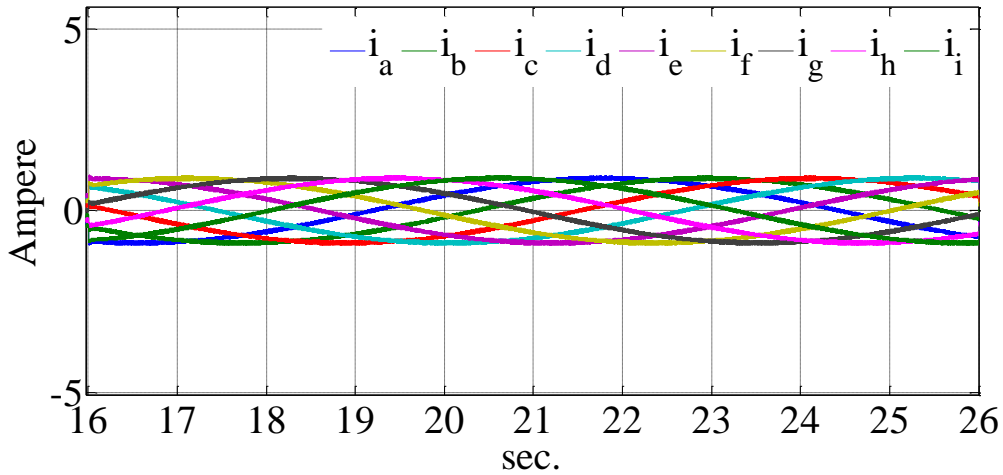
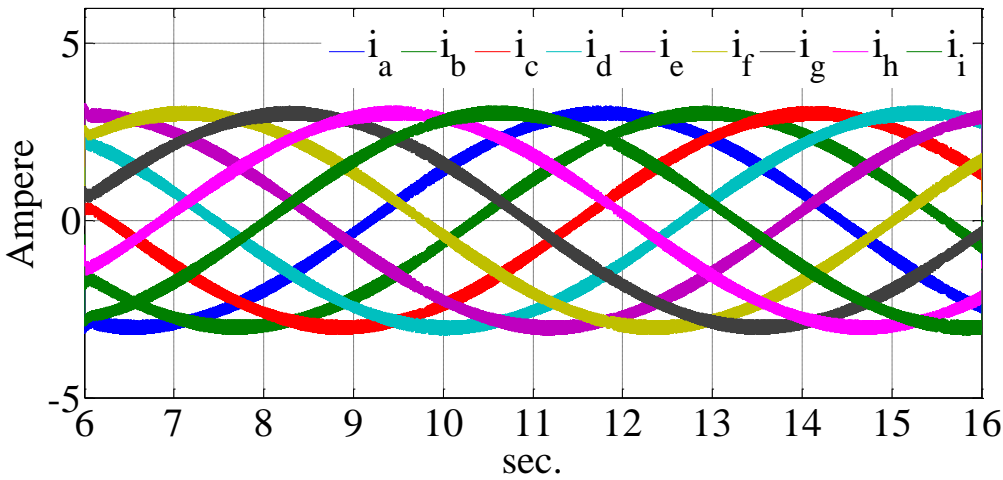


Figure 5.98: The reference and the feedback currents in rotor reference frame for d axis (experimental results).

Figure 5.99 shows the simulation results of the stator currents. From this figure it can be seen that, the magnitude of the stator current increases by applying the load torque to the machine. The stator currents of experimental results are also shown in Figures 5.100 and 5.101. Figure 5.100 shows the currents before applying load torque and Figure 5.101 shows the stator currents after applying load torque. The experimental current waveforms show some low frequency ripples which are due to some un-modeled nonlinearities of the machine such as magnetic saturation of the stator.



(a)



(b)

Figure 5.99: The simulation result of nine-phase stator currents, (a) Before applying load torque, (b) After applying load torque.

The currents of the third sequence of stationary reference frame are shown in the Figure 5.102 and 5.103 for simulation and experiment respectively. These currents are derived from the 9×9 transfer matrix in stationary reference frame. These currents can be used for signal processing and position estimation process. From these figures, it can be seen that, the third sequence currents have variable magnitudes. The ripples on the magnitudes are caused by the rotor saliency and they can be used for position estimation.

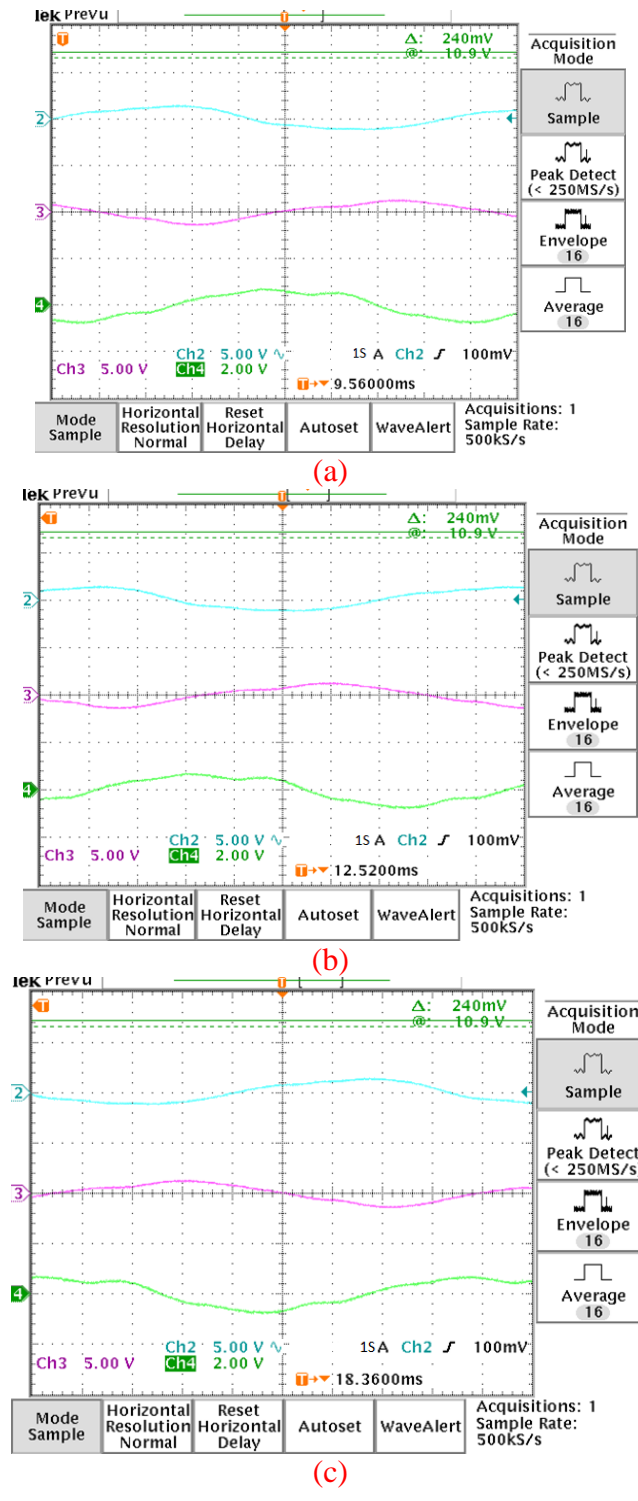
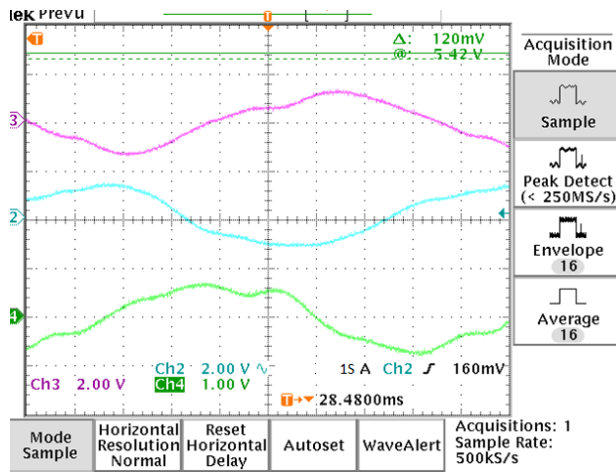
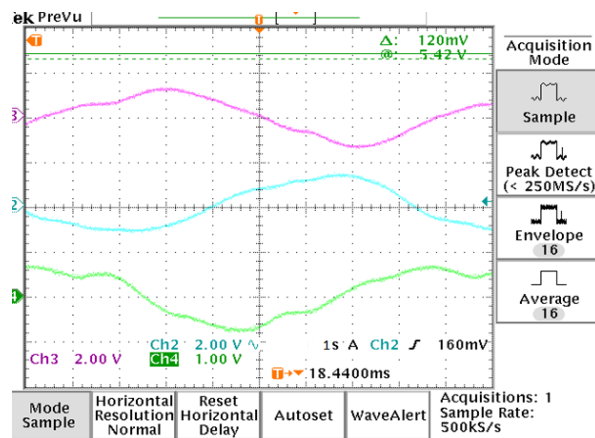


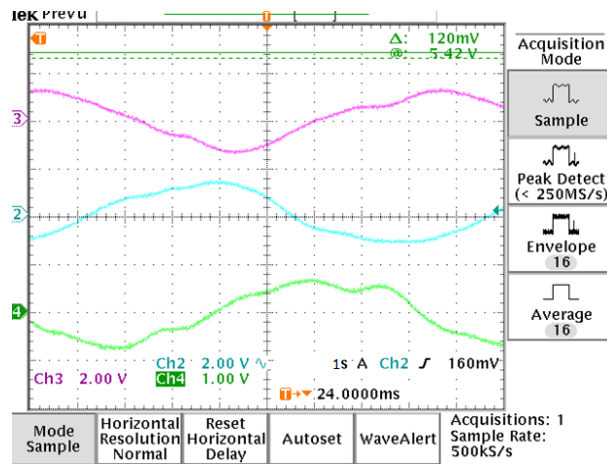
Figure 5.100: The nine-phase currents of the machine phases before applying load for phases, (a) ‘a’, ‘d’ and ‘g’, (b) ‘b’, ‘e’ and ‘h’, (c) ‘c’, ‘f’ and ‘i’ (experimental results) (5 A/ scale).



(a)



(b)



(c)

Figure 5.101: The nine-phase currents of the machine phases after applying load for phases for phases,

(a) 'a', 'd' and 'g', (b) 'b', 'e' and 'h', (c) 'c', 'f' and 'i' (experimental results) (5 A/ scale).

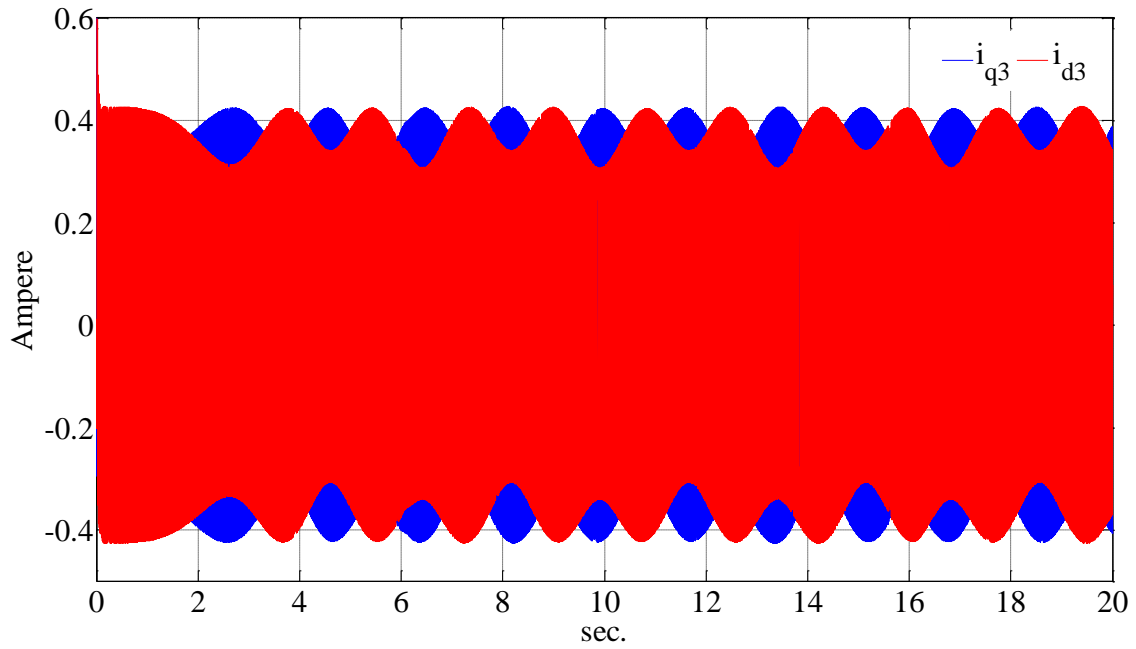


Figure 5.102: The dq_3 currents before heterodyning (simulation result).

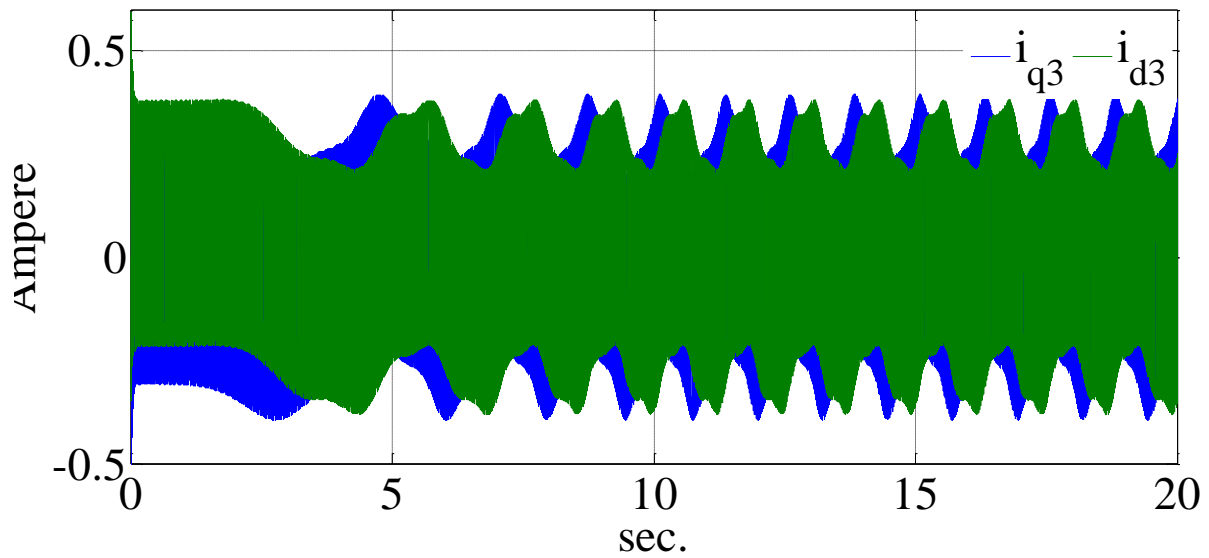


Figure 5.103: The dq_3 currents before heterodyning (experimental result).

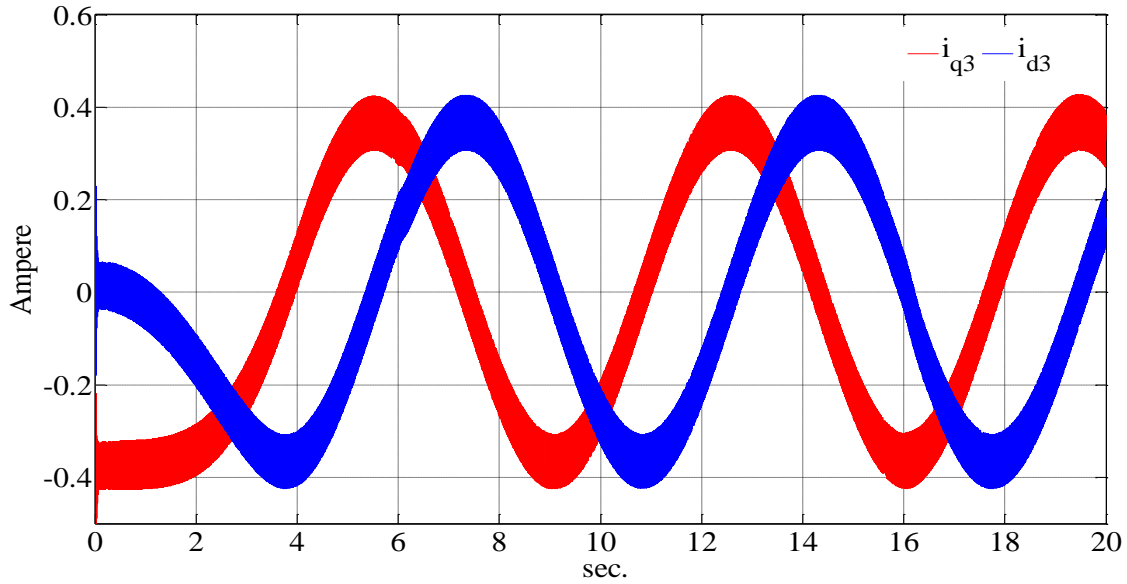


Figure 5.104: The dq_3 currents after heterodyning (simulation result).

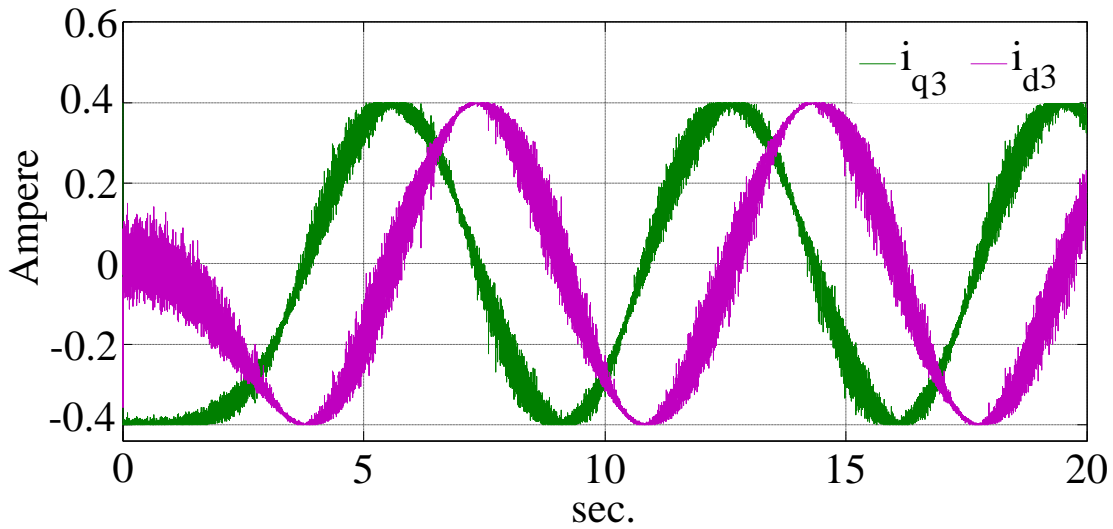


Figure 5.105: The dq_3 currents after heterodyning (experimental result).

Again to extract the low frequency content the signal needs to go through a heterodyning and filtering procedure. By multiplying the signals of the Figures 5.102 and 5.103 by $e^{-j\omega_s t}$ the signals change to signals of Figures 5.104 and 105 for simulation and experiment respectively. The signals of the Figures 5.104 and 105 pass through a low pass filter to shed their high frequency ripple. The experimental results waveforms show more ripples which are due to the sampling noise.

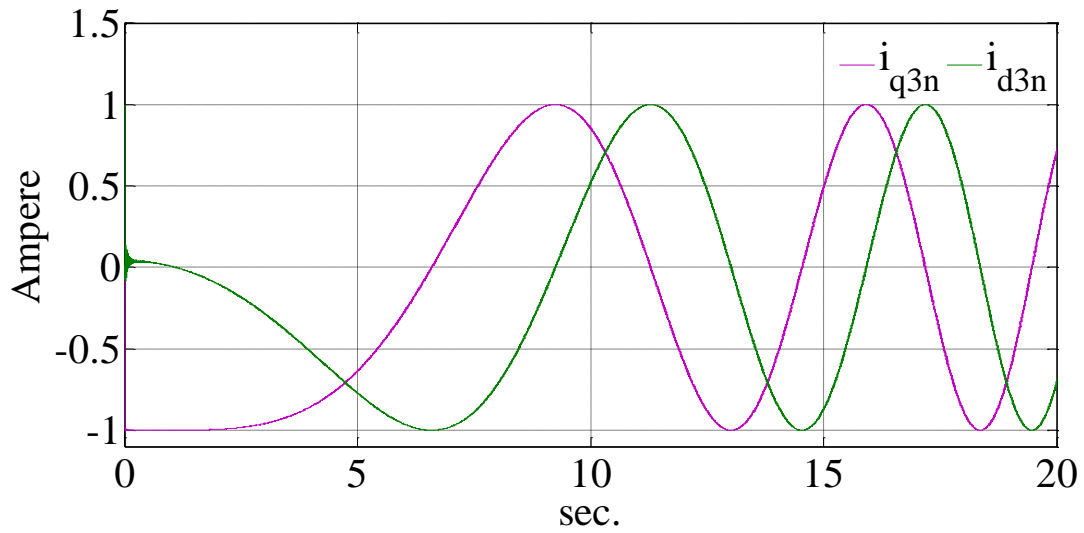


Figure 5.106: The dq_3 currents after filtering and normalizing (simulation result).

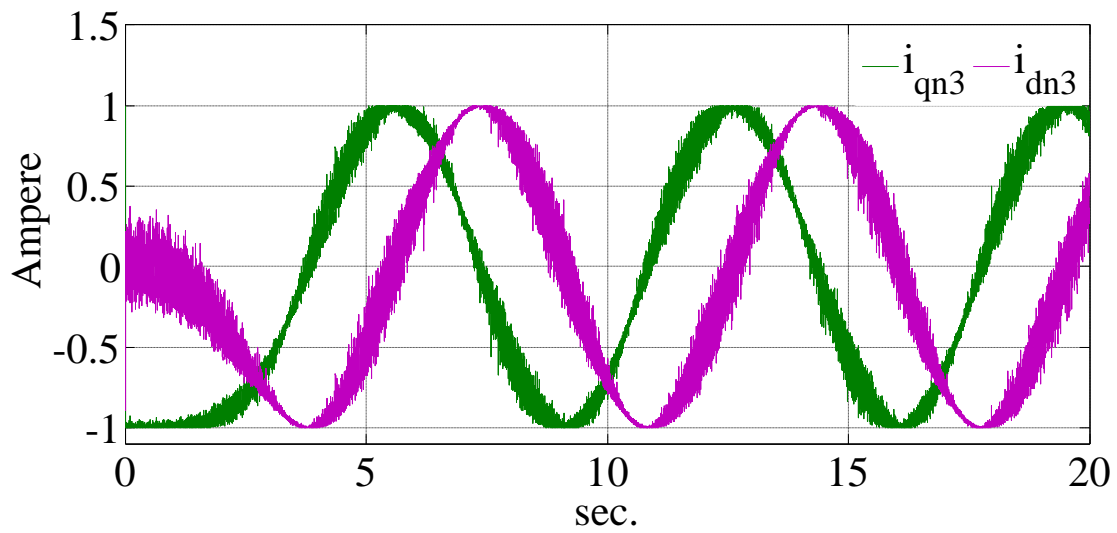


Figure 5.107: The dq_3 currents after filtering and normalizing (experimental result).

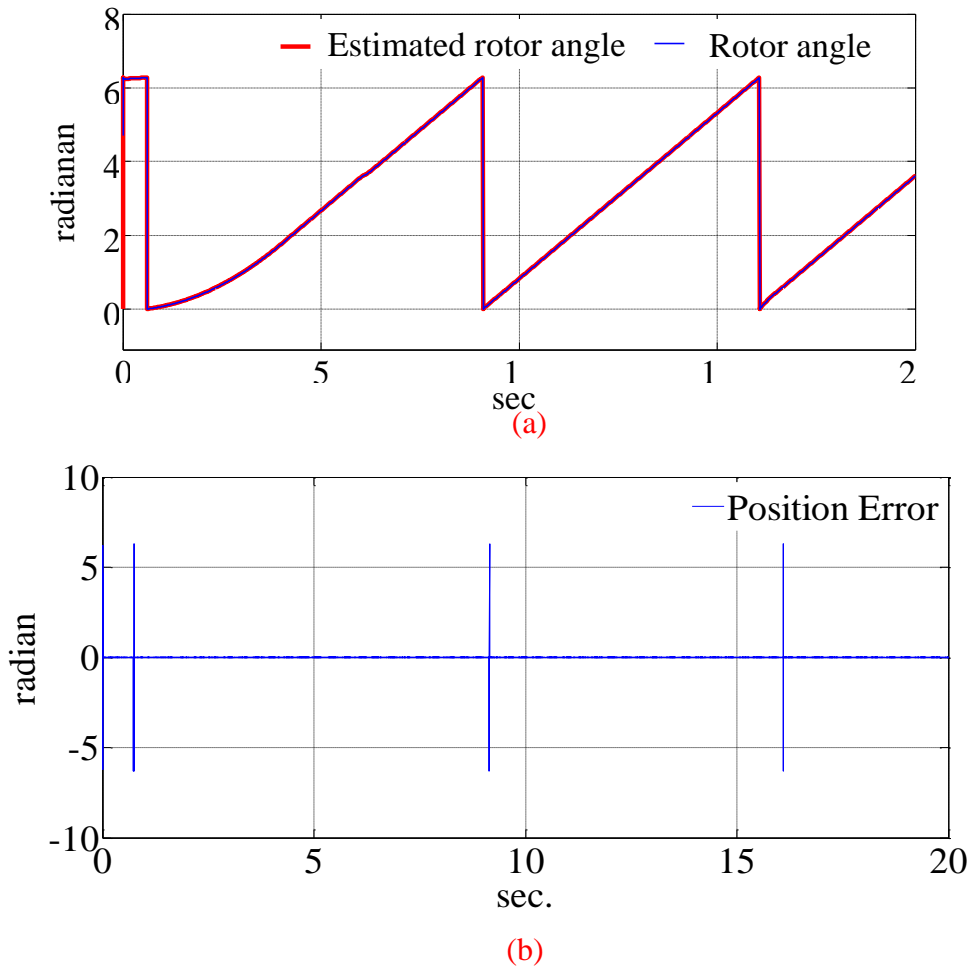
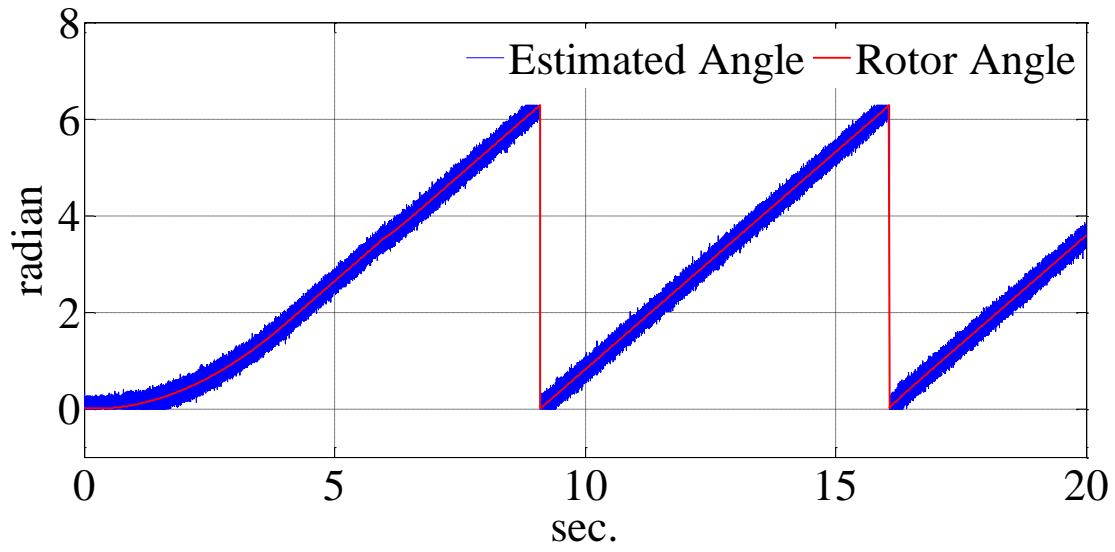
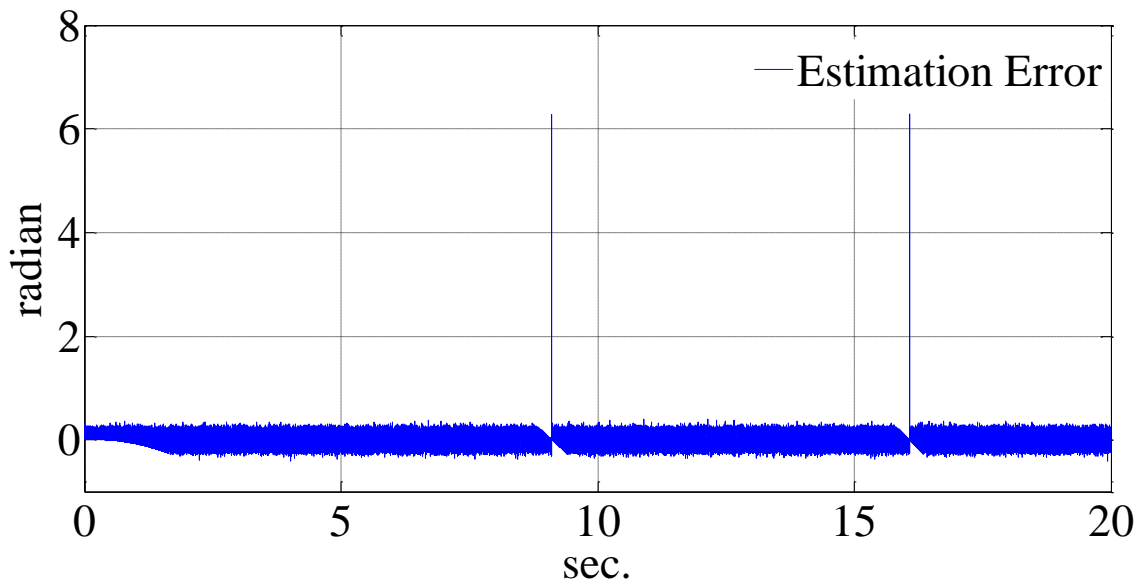


Figure 5.108: (a) Estimated and simulated rotor angle (simulation results), (b) The estimation error (simulation results).

Again since the currents after filtering have variable magnitudes which vary with the rotor speed they need to be normalized to make their magnitudes equal to unity. Figures 5.106 and 5.107 show the normalized currents after filtering and normalizing for simulation and experiment respectively. The signals of Figures 5.106 and 5.107 are fed to the Luenberger observer to generate the rotor angle. Figures 5.108 and 5.109 show the rotor angle along with estimated rotor angle and the estimation error for simulation and experiment respectively. It can be seen that the observer follows the rotor position in all steady state and transient intervals.



(a)



(b)

Figure 5.109: (a) Estimated and measured rotor angle (experimental results), (b) The estimation error (experimental results).

5.7 Steady State Performance of Nine the Phase IPM Using FEMM.

The inductances of the machine in q and d axis are generated in chapter 3. The machine inductances now can be used to obtain the steady state performance of the IPM machine using FEMM.

5.7.1 Steady State Performance of Nine the Phase IPM Below Base Speed

The equations (5.165) and (5.166) represent the steady state conditions for the machine operation when the rotor speed is less than the base speed.

$$i_q^2 + i_d^2 = I^2_{rated} \quad (5.165)$$

$$V_q^2 + V_d^2 < V^2_{rated} \Leftrightarrow (r_s i_q + \omega_r L_d i_d + \omega_r \lambda_{pm})^2 + (r_s i_d - \omega_r L_q i_q)^2 < V^2_{rated} \quad (5.166)$$

From the section 5.2 the relationship between the q and d axis currents for the minimum copper loss is expressed as:

$$i_d = -\frac{\lambda_{pm}}{2(L_d - L_q)} + \sqrt{\frac{\lambda_{pm}^2}{4(L_d - L_q)^2} + i_q^2} \quad (5.167)$$

At this region, machine operates under minimum copper loss strategy and rotor speed is below the base speed. The stator voltage is below the base value and stator current can be equal or smaller than the rated.

5.7.2 Steady State Performance of Nine the Phase IPM in Field Weakening Region I

When rotor speed exceeds the base speed, the machine constraints change to the equations (5.168) and (5.169) which are the field weakening region I.

$$i_q^2 + i_d^2 = I^2_{rated} \quad (5.168)$$

$$V_q^2 + V_d^2 = V_{rated}^2 \Leftrightarrow (r_s i_q + \omega_r L_d i_d + \omega_r \lambda_{pm})^2 + (r_s i_d - \omega_r L_q i_q)^2 = V_{rated}^2 \quad (5.169)$$

At this mode, the stator voltage and current are equal to the rated value and machine torque is less than the rated value.

5.7.3 Steady State Performance of Nine the Phase IPM in Field Weakening Region II

By increasing the rotor speed, the machine has to operate under new constrains which are presented in the equations (5.170) and (5.171) and represent field weakening region II. At this region, the stator current and voltage are below the rated values and the electromagnetic torque can increase to the maximum possible value.

$$i_q^2 + i_d^2 < I_{rated}^2 \quad (5.170)$$

$$V_q^2 + V_d^2 < V_{rated}^2 \Leftrightarrow (r_s i_q + \omega_r L_d i_d + \omega_r \lambda_{pm})^2 + (r_s i_d - \omega_r L_q i_q)^2 < V_{rated}^2 \quad (5.171)$$

Under these new constraints the Lagrange equations can be used to obtain the maximum possible torque which still satisfies the equations (5.170) and (5.171). Here it should be noted that, while solving the above equations to obtain the q and d axis currents of the machine in different operation modes the inductances which are corresponding to that values should be used. Using the chapter 3 results for the inductances, the steady state curves are plotted for the discussed machine. Figure 5.110 shows the maximum possible torque of the machine in different modes of operation it is clear that by increasing the speed after base value the maximum possible torque decreases in both of field weakening regions.

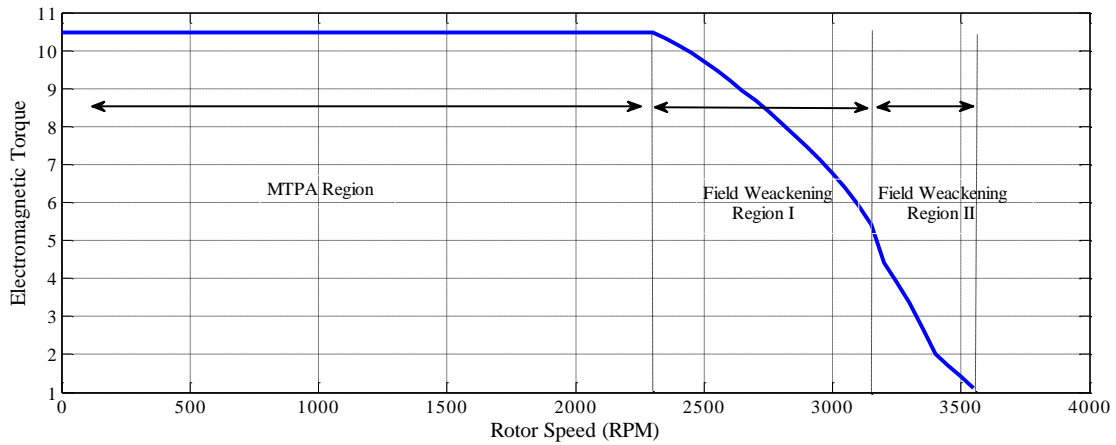


Figure 5.110: Maximum possible torque of the machine in different modes.

The i_d and peak value of the stator current of the machine are shown in the Figure 5.111 based on this figure the rated current can be injected to the stator of the machine until it is operating in the field weakening region II.

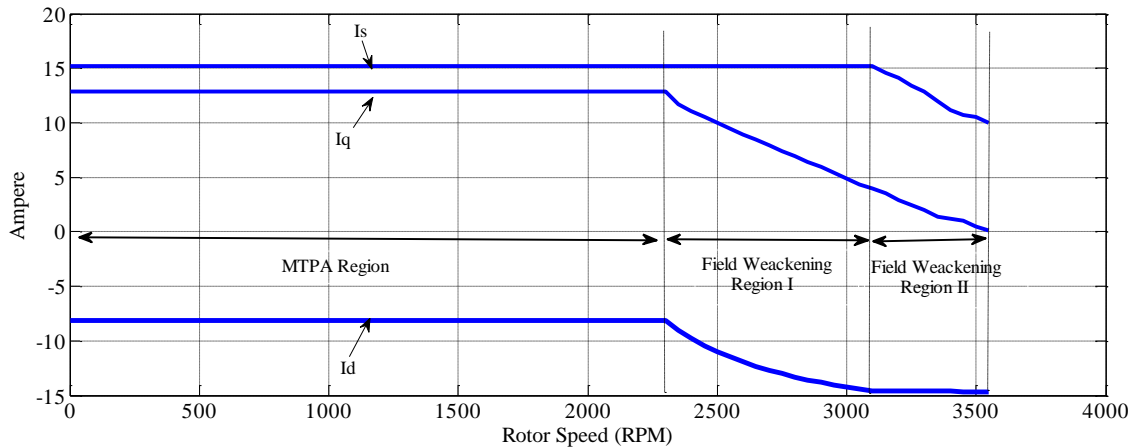


Figure 5.111: The q and d axis and stator currents.

Figure 5.112 shows the stator voltage of the machine. According to this figure, in the MTPA region, the stator voltage increases linearly with the rotor speed and beyond that it remains almost constant. Figures 5.113 and 5.114 show the copper loss and the total losses of the machine. The total loss of the machine includes the copper loss and hysteresis loss.

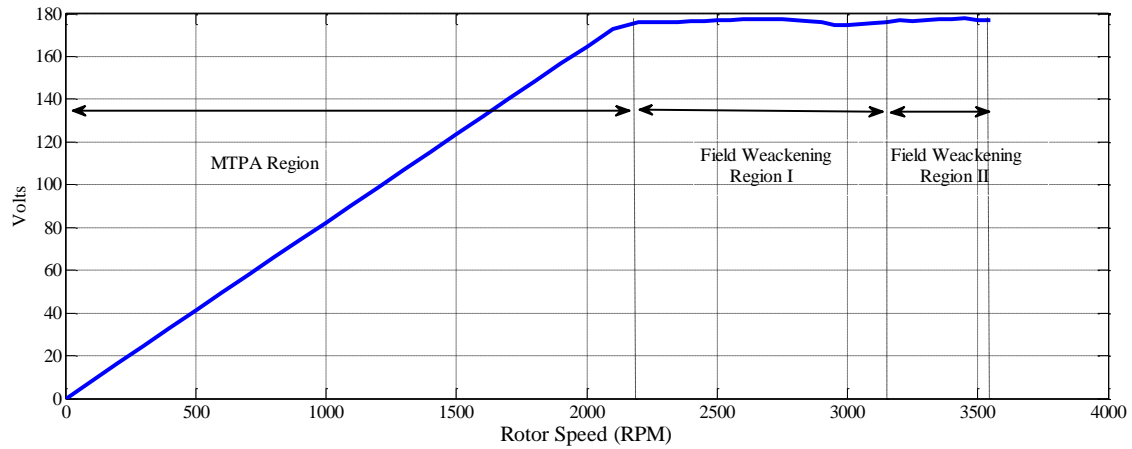


Figure 5.112: The stator phase voltage.

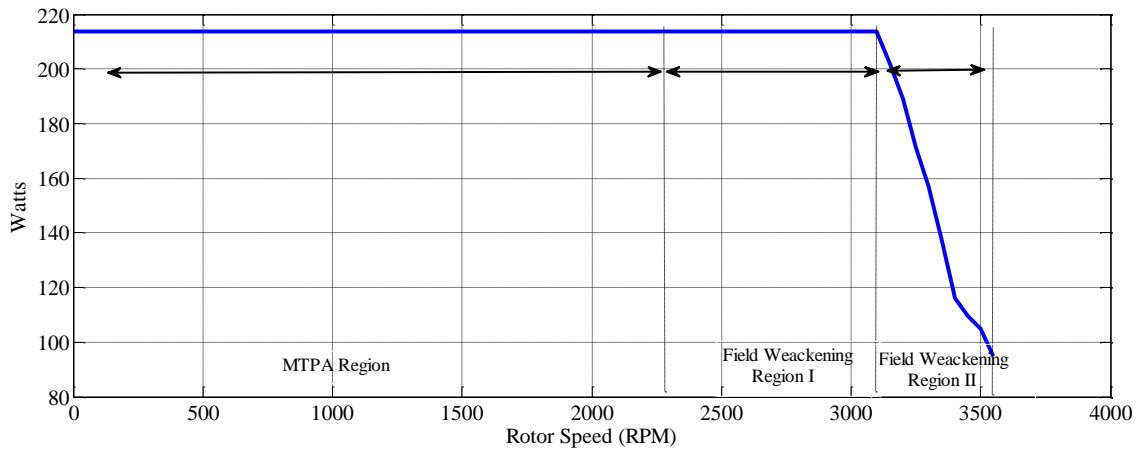


Figure 5.113: The copper loss of the machine.

Figure 5.113 shows the copper loss of the machine according to this figure in the field weakening region II, since the current is constant the copper loss would remain constant as well, beyond that speed since the stator current starts decreasing the copper loss also decreases. The total output power of the machine is shown in the Figure 5.115. It can be seen that below the base speed the machine power increases linearly by the rotor speed. While in the first region of the field weakening the output power is almost fixed and it is decreasing at the second field weakening region.

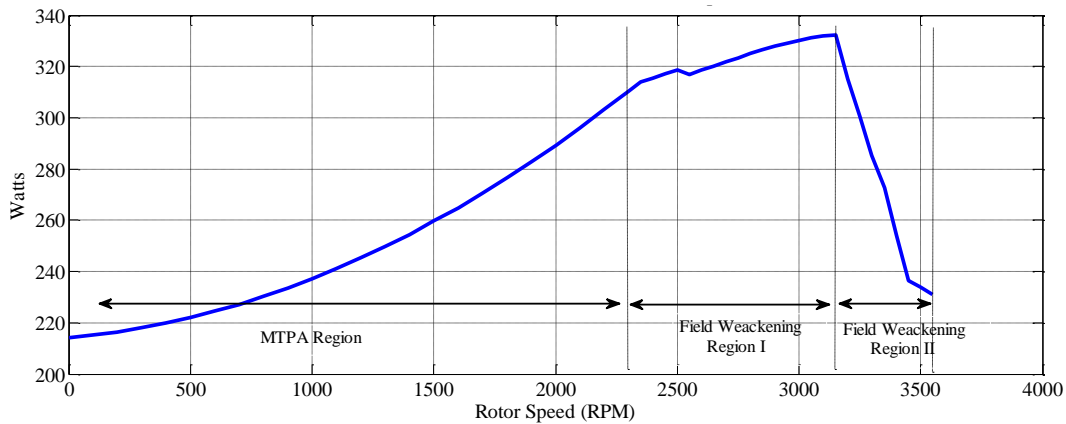


Figure 5.114: The total loss of the machine.

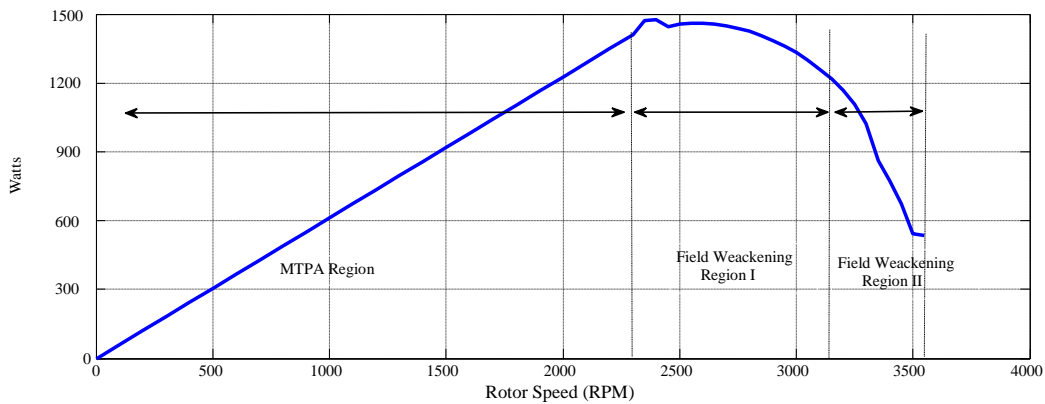


Figure 5.115: The output power of the machine.

5.8 Conclusion

In this chapter a nine-phase controller is designed for a single star nine phase machine using the main components of the machine circuit. The position observer is also presented in this chapter. The position observer uses high frequency injection in a non-torque producing channel. After high frequency analyses the essential signal processing method is presented and the position observer is designed. Finally, the performance of the drive and the observer is validated by simulation and experimental results. The major contribution of this chapter is designing a position observer that can observe the rotor position of the machine without producing extra torque pulsations. In the final

sections of this chapter the steady state performance of the machine is analyzed using FEMM for different stator current levels and operation modes of the controller.